National Library of Canada

Acquisitions and Bibliographic Services Branch

395 Wellington Street
Ottawa, Ontario
K1A 0N4

Bibliothèque nationale du Canada

Direction des acquisitions et des services bibliographiques

395, rue Wellington
Ottawa (Ontario)
K1A 0N4

Your file Votre référence

Our file Notre référence

NOTICE

The quality of this microform is heavily dependent upon the quality of the original thesis submitted for microfilming. Every effort has been made to ensure the highest quality of reproduction possible.

If pages are missing, contact the university which granted the degree.

Some pages may have indistinct print especially if the original pages were typed with a poor typewriter ribbon or if the university sent us an inferior photocopy.

AVIS

La qualité de cette microforme dépend grandement de la qualité de la thèse soumise au microfilmage. Nous avons tout fait pour assurer une qualité supérieure de reproduction.

S'il manque des pages, veuillez communiquer avec l'université qui a conféré le grade.

La qualité d'impression de certaines pages peut laisser à désirer, surtout si les pages originales ont été dactylographiées à l'aide d'un ruban usé ou si l'université nous a fait parvenir une photocopie de qualité inférieure.

Canada

Adaptive Equalization of Frequency Selective Indoor Wireless Channels

by

Xuan Chen, B.A.Sc.

A thesis submitted to
the School of Graduate Studies and Research
in partial fulfillment of
the requirements for the degree

Master of Applied Science

Ottawa-Carleton Institute for Electrical Engineering
Faculty of Engineering
Department of Electrical Engineering
University of Ottawa
Ottawa, Ontario, Canada, K1N 6N5

January, 1995

ISBN 0-612-04866-7

Canada

UNIVERSITÉ D'OTTAWA
UNIVERSITY OF OTTAWA

I hereby declare that I am the sole author of this thesis.

I authorize the University of Ottawa to lend this thesis to other institutions or individuals for the purpose of scholarly research.

Xuan Chen

I further authorize the University of Ottawa to reproduce this thesis by photocopying or by other means, in total or in part, at the request of other institutions or individuals for the purpose of scholarly research.

Xuan Chen

Abstract

In this thesis, we examine the performance of adaptive linear, $T/2$ fractionally spaced, and decision feedback equalizers (LE, FSE and DFE) for digital communication systems over indoor wireless channels affected by frequency selective fading. The channel is modeled as both fixed and time varying channels, and the data transmission rate is 10 $Mbits/s$. The simulation results show that, with differential encoding, the quadrature phase shift keying (DQPSK) modulation scheme outperforms 4-state and 8-state 8PSK-based trellis coded modulations (D8PTCM4 and D8PTCM8), when the DFE with the least-mean-square (LMS) algorithm (DFELMS) is used. While D8PTCM4 has better BER performance than D8PTCM8 with the DFELMS over time varying channels, the reverse conclusion can be obtained over fixed channels. When the recursive least-square (RLS) algorithm is applied instead of the LMS algorithm, the systems with the DFERLS can achieve slightly better bit error rate (BER) performance than those with the DFELMS.

Acknowledgements

I would like to thank my supervisor, Dr. Jean-Yves Chouinard, for his encouragement and numerous interesting discussions on the topic of this thesis. Thanks are also due to Dr. Tyseer Aboulnasr, who was my initial thesis supervisor. Dr David D. Falconer was also kind enough to provide me with some useful suggestions.

This thesis would not have been possible without the generosity of my parents. They have supported me throughout my education.

Many discussions with fellow graduate students in the Wireless Group improved the implementation of the design. I am also grateful both to James Emery for his help in editing and to Vojislav Radonjic for his assistance with software. Thanks are due to William Keays for his technical support on the computer system.

Contents

List of Figures

List of Tables

List of Acronyms

AWGN	Additive white gaussian noise
BER	Bit error rate
CDF	Cumulative distribution function
dB	Decibel
DFE	Decision feedback equalizer
DQPSK	Differential quadrature phase shift keyed
FSE	Fractionally spaced equalizer
IWC	Indoor wireless channel
LE	Linear equalizer
LMS	Least-mean-square
QPSK	Quadrature phase shift keyed
RF	Radio frequency
RLS	Recursive least-squares
SNR	Signal-to-noise ratio
TCM	Trellis coded modulation

List of Symbols

B_d	Doppler spread
f_c	Carrier frequency
$g(t)$	Shapped pulse
G	Power gain
G_r	Power gain of the receiving antenna
G_t	Power gain of the transmitting antenna
GHz	(10^9 Hertz)
$h(t)$	Complex lowpass channel impulse response
Hz	Hertz
I_n	The nth complex-valued information symbol; n=0,1,2,...
km/h	Kilometer per hour
MHz	Megahertz (10^6 Hertz)
$p(x)$	Probability of random variable x
rms	Root mean square
$r(t)$	Equivalent lowpass signal for a received signal
$s(t)$	Transmitted signal
t	Time
T_s	Symbol rate
T_l	The lth cluster arrival time of a channel
T_m	Multipath spread of a channel
$x(t)$	Received signal
$y(n)$	Equalizer output
$u(n)$	Equalizer input
$v(t)$	Equivalent lowpass signal for a transmitted signal
w_k	Coefficients of the equalizer
W	Signaling bandwidth
α	Distance-power law exponent

α_n	Attenuation factor of the nth path; n=0,1,2,...
β_{kl}	Amplitude gain of the kth ray within the lth cluster for a channel
$\overline{\beta^2(0,0)}$	Average power gain of the first ray of the first cluster
γ	Power-delay time constant for the cluters
Γ	Power-delay time constant for the rays
$\delta(t)$	Dirac delta function
Δf_c	Coherence bandwidth
Δt_c	Coherence time
θ_n	Phase shift of the nth path; n=0,1,2....
θ_{kl}	Phase shift of the kth ray within the lth cluster for a channel
λ_0	RF wavelength
λ	Ray arrival rate for the Poisson process
Λ	Cluster arrival rate for the Poisson process
π	Pi=3.1415926...
σ	Root mean square delay spread
$\overline{\tau}$	Average delay
τ_n	Propagation delay of the nth path; n=0,1,2,...
τ_{kl}	The kth ray arrival time within the lth cluster for a channel
$\phi_c(\tau;\Delta t)$	Multipath intensity profile
$\phi_C(\Delta f;\Delta t)$	Spaced-frequency spaced-time correlation function of the channel

Chapter 1

Introduction

1.1 Background

To meet the growing demand for mobile radio communications service, designers of these systems have two principal goals, namely to increase the capacity of the system and to provide simple operation. The current generation of cellular telephone systems permit mobile wireless access to the public telephone network [Good91]. For this purpose, a channel access technique, such as frequency division multiple access (FDMA), time division multiple access (TDMA), or code division multiple access (CDMA) is required. Currently, TDMA is being used for many digital cellular systems. One of the key challenges facing cellular system designers is the efficient use of the spectrum. With no new spectrum available to meet the demand for cellular services, research in the area of spectrally efficient digital modulation/demodulation techniques is very active.

Indoor wireless communications, which is an important form of mobile communication, allows information (eg. voice, data, etc.) to be transferred within a building. Since information signals are transmitted at higher frequencies (GHz) than those for cellular communications, indoor wireless systems have a greater available capacity. However, indoor wireless channels cause distortion similar to that found in mobile radio communication channels due to the time varying multipath propagation

of signals. This distortion, which causes the transmitted symbols to be spread and overlapped over successive time intervals, is referred to as intersymbol interference (ISI). Indoor wireless communication systems require adaptive equalization at the demodulator to combat the ISI. This form of equalization is particularly important in order to provide a quality wireless high speed data transmission service.

There exists two types of equalization techniques for combatting the ISI on bandlimited time dispersive channels, namely, linear and nonlinear equalization. A survey of adaptive equalization techniques is presented in [Proak91], which provides a thorough description of the performance characteristics and limitations for a wide range of equalizers. It is widely believed that nonlinear equalizers perform better than linear equalizers on channels with severe distortion, especially on channels with spectral nulls.

There are three types of effective nonlinear equalization methods. The first method is a symbol-by-symbol detection algorithm, developed by Abend and Fritchman in 1970 [Abend70]. The algorithm is optimum in the sense that it minimizes the probability of a symbol error. It is based on the computation of *a posteriori* probabilities. The second method is a sequence detection algorithm that is based on the maximum-likelihood sequence estimation (MLSE) criterion. It is efficiently implemented by means of the Viterbi algorithm [For73]. The symbol error rate of the Viterbi algorithm is often much lower than those of the symbol-by-symbol detectors, and thus the sequence detection algorithm gives quite good performance. However, the total storage (complexity) of the algorithm is proportional to the number of states of the trellis which grows exponentially with the channel memory length. Various approaches are described in [Verm74][Eyu88][Duel89] to reduce the complexity of the Viterbi algorithm by "shortening" the memory of the channel. These approaches demonstrate the direct tradeoff between complexity and performance in digital communications over ISI channels.

In this thesis, the performance of the decision feedback equalizer (DFE), which

is the third of three effective nonlinear equalization methods mentioned in [Good91], is investigated. The influence of the DFE collaborating with both differential quadrature-phase-shift keying (DQPSK) modulation and 8PSK-based trellis coded modulation (D8PTCM) to combat the ISI is explored.

The DFE requires a "desired sequence" that can be obtained with a decision device at the output of the DFE. When the DFE operates over a channel with severe ISI, the "desired sequence" is not accurate and subsequently the feedback filter of the DFE causes significant performance degradation. An improved DFE, which is presented in [Eyu88], can be used in coded modulation systems. An interleaver/deinterleaver pair rearranges the order of received signals prior to decoding, in a manner such that delayed reliable decisions ("desired sequence") are used for the DFE.

1.2 Motivation

[Zig92] analyses the performance of the DFE combined with the 4-QAM modulation scheme over an indoor wireless channel. [Pai91] investigates the performance of DQPSK and D8PTCM over an indoor wireless channel. Both [Zig92] and [Pai91] used a time invariant tapped delay line channel model. This channel model is a tapped delay line model [Proak89] formed by a channel impulse response generated according to Saleh & Valenzuela's channel model for indoor wireless channels [Sal87(2)]. However, this model could only be used by ignoring the Doppler frequency effect caused by the slow movement of a person in a building. In this thesis, we introduce a time varying channel model, whose taps are based on the tapped delay line model and thus they change with time. We suggest that this time varying model better represents the indoor wireless transmission medium. Communication system performances with both DQPSK and D8PTCM modulations combined with various adaptive equalizers are presented by means of computer simulation results. Simulations were performed on both channel models to provide a comparison of the performance of different communication systems in both operating environments. Higher bit error rates are normally

found when operating over a time varying channel.

1.3 Outline

Chapter 2 of this thesis provides a description of indoor wireless channel models. This chapter includes a review of the time invariant channel model presented by [Sal87(2)]. Next, the time variant channel model that we developed, which is based on the channel impulse response of [Sal87(2)], is described. Three different time varying channels, which are used for the simulations, are presented.

In Chapter 3, we present an overview of three types of adaptive equalizers that are used to combat intersymbol interference in indoor wireless channels. Two algorithms, namely least-mean-square (LMS) and recursive least-squares (RLS), are described. These algorithms are used in this thesis to optimize the performance of the equalizers.

Chapter 4 provides a general description of the indoor wireless communication systems that are analyzed in this thesis. The characteristics of the shaping filters are detailed. The remainder of the chapter reviews two modulation schemes: differential quadrature-phase-shift keying (DQPSK) modulation and differential trellis coded modulation (D8PTCM).

In Chapter 5, the simulation results are presented and discussed. First, the performance of adaptive equalizers used with DQPSK modulation is presented. Then the adaptive equalizers are evaluated for both 4-state and 8-state D8PTCM modulation schemes. The convergence properties of decision feedback equalizers are analyzed for least-mean-square and recursive least-squares algorithms.

Finally, conclusions and suggestions for further research are provided in Chapter 6.

Chapter 2

Indoor Wireless Channel

The indoor wireless channel (IWC) model is a mathematical model used to represent the multipath propagation characteristics, such as the fading behavior of an actual indoor channel. This channel model can be used to analyze the performance of a communication system operating in a wireless environment.

2.1 Indoor Wireless Channel Model

In radio communications a phenomena called multipath transmission is caused by reflections on surrounding scatterers such as doors, walls, and buildings. A channel model is required for examining the effects of the multipath channel on a transmitted signal.

A transmitted signal can be expressed [Proak89] as

$$s(t) = Re\left\{v(t)e^{j2\pi f_c t}\right\}, \tag{2.1}$$

where f_c is the carrier frequency and $v(t)$ is the equivalent lowpass information-bearing signal in the form

$$v(t) = \sum_{n=-\infty}^{\infty} I_n g(t - nT_s), \tag{2.2}$$

where I_n represents the nth complex-valued information symbol with rate T_s, and $g(t)$ represents the shaped pulse. After transmitting $s(t)$, the received bandpass signal may be given as

$$x(t) = \sum_n \alpha_n(t) s[t - \tau_n(t)], \tag{2.3}$$

where $\alpha_n(t)$ and $\tau_n(t)$ are the attenuation factor and the propagation delay for the signal received on the nth path, respectively. Substituting $s(t)$ from Equation(2.1) into Equation(2.3), we can obtain the equivalent lowpass received signal as

$$r(t) = \sum_n \alpha_n(t) e^{-j2\pi f_c \tau_n(t)} v[t - \tau_n(t)], \tag{2.4}$$

and the equivalent lowpass channel described by the time variant impulse response

$$\begin{aligned} h(t) &= \textstyle\sum_n \alpha_n(t) e^{-j2\pi f_c \tau_n(t)} \delta[t - \tau_n(t)] \\ &= \textstyle\sum_n \alpha_n(t) e^{j\theta_n(t)} \delta[t - \tau_n(t)], \end{aligned} \tag{2.5}$$

where $\delta(\cdot)$ is the Dirac delta function, and $\theta_n(t) = -2\pi f_c \tau_n(t)$. Because of dynamic changes in the transmission medium, the parameters $\alpha_n(t)$, $\theta_n(t)$ and $\tau_n(t)$ are randomly time varying functions. That is, $h(t)$ can be modeled as a random process. In particular, when there is a large number of paths, $h(t)$ can be modeled as a complex-valued Gaussian random process by using the Central Limit Theorem.

In this thesis, Saleh & Valenzuela's channel model is chosen to evaluate the performance of the communication system. The indoor multipath channel is described by multiple paths having different real positive gains, propagation delays and phase shifts, caused by building walls, doors, etc. The complex, low-pass impulse response of the indoor wireless channel is represented [Sal87(2)] by

$$h(t) = \sum_{l=0}^{\infty} \sum_{k=0}^{\infty} \beta_{kl}\, e^{j\theta_{kl}}\, \delta(t - T_l - \tau_{kl}), \tag{2.6}$$

where $\{\beta_{kl}\}$ represents amplitude gains which are statistically independent positive random variables described by a Rayleigh distribution:

$$p(\beta_{kl}) = (2\beta_{kl}/\overline{\beta_{kl}^2})\, exp(-\beta_{kl}^2/\overline{\beta_{kl}^2}), \tag{2.7}$$

where the phase shifts $\{\theta_{kl}\}$ are statistically independent uniform random variables over $[0, 2\pi)$. T_l and τ_{kl} represent the cluster arrival times and the ray arrival times within each cluster, respectively.

The cluster arrival times and the ray arrival times are modeled as two Poisson arrival processes with fixed rates Λ and λ, respectively. The arrival times for clusters and rays can be expressed by the "interarrival" exponential probability density functions, individually

$$p(T_l|T_{l-1}) = \Lambda\, exp[-\Lambda(T_l - T_{l-1})] \qquad \text{for } l > 0 \quad \text{and,} \tag{2.8}$$

$$p(\tau_{kl}|\tau_{(k-1)l}) = \lambda\, exp[-\lambda(\tau_{kl} - \tau_{(k-1)l})] \qquad \text{for } k > 0. \tag{2.9}$$

The mean square values of the individual path gains $\{\overline{\beta_{kl}^2} \equiv \overline{\beta^2(T_l, \tau_{kl})}\}$ monotonically decrease according to the power-delay time constants Γ and γ for clusters and rays, respectively, as shown by the following:

$$\overline{\beta_{kl}^2} = \overline{\beta^2(0,0)}\, e^{-T_l/\Gamma} e^{\tau_{kl}/\gamma} \tag{2.10}$$

with $\overline{\beta^2(0,0)}$ being the average power gain of the first ray in the first cluster. The average power gain of the first path $\overline{\beta^2(0.0)}$ can be computed [Sal87(2)] by

$$\overline{\beta^2(0,0)} \approx (\gamma\lambda)^{-1} G(1m) r^{-\alpha}, \tag{2.11}$$

where α is a distance-power law exponent and $G(1m)$ is the multipath power gain when the antenna separation r equal to 1 m. $G(1m)$ can be approximated by the following

$$G(1m) \approx GtGr(\lambda_0/4\pi)^2, \tag{2.12}$$

where Gt and Gr are the gains of the transmitting and receiving antennas respectively, and λ_0 is the radio frequency (RF) wavelength. The discrete channel model is sketched in Figure 2.1. The indoor wireless channel considered here is a time varying channel, whose parameters change very slowly compared to the signaling rate considered here, i.e. 5 $Mbauds/s$.

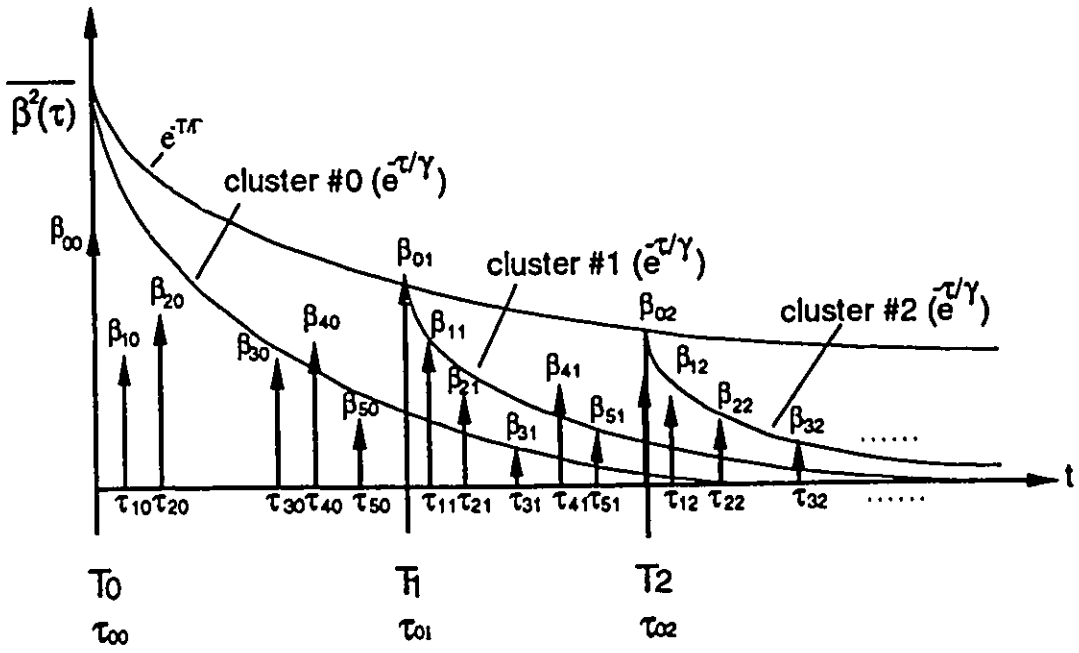

Figure 2.1: The Saleh & Valenzuela discrete indoor wireless channel model.

2.2 Modeling of the Channel

The channel model is expressed mathematically in the last section. In this section, a set of impulse responses of the IWC is presented by selecting different indoor channel model parameters.

2.2.1 Channel Impulse Response

According to the model in [Sal87(2)], the channel impulse response is generated with the following parameter values:

Table 2.1: The IWC parameters

α	r (m)	λ_0 (m)	Gt	Gr	$1/\lambda$ (ns)	$1/\Lambda$ (ns)	γ (ns)	Γ (ns)
3.5	10	0.2	1.0	1.0	5	200	20	60

The parameter values in Table 2.1 were chosen so that the IWC model cor-

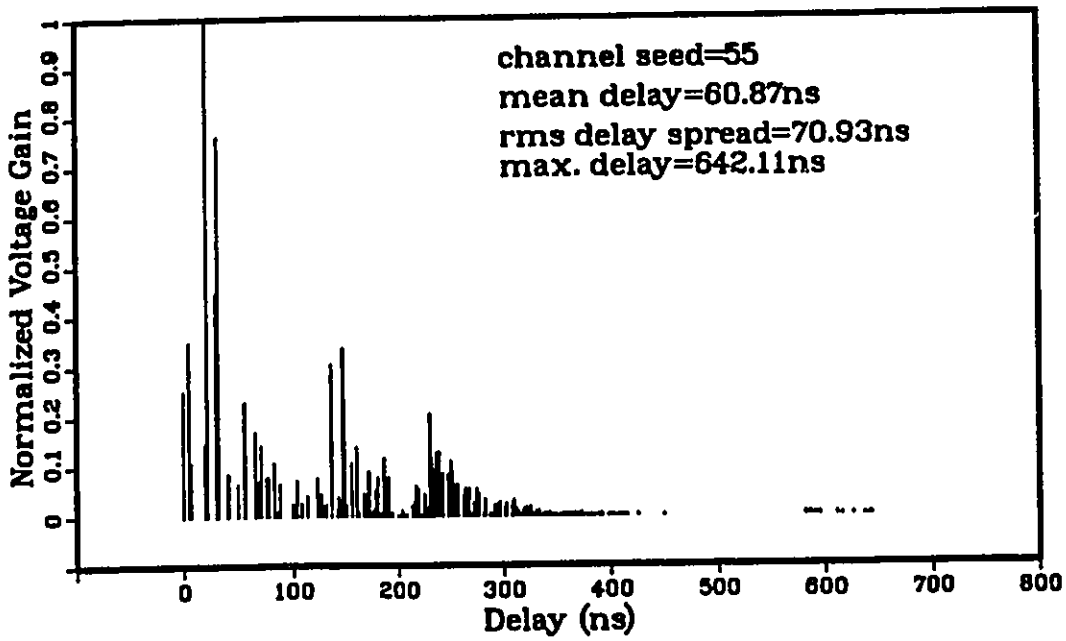

Figure 2.2: Simulated IWC impulse response (rms delay-spread $\sigma = 70.93\ ns$).

responds to impulse response measurements taken inside a medium size two-story office building. The RF used here is 1.5 GHz. Parameter r is the maximum distance between the transmitting and the receiving antennas. According to [Sal87(2)], the cluster interarrival time $(1/\Lambda)$ is roughly in the range from 200 ns to 300 ns. If a cluster interarrival time $(1/\Lambda)$ of 200 ns is used instead of 300 ns, the rms delay spread is larger. The comparison of corresponding cumulative distribution of their rms delay spreads will be given in next section. An impulse response of the channel (Figure 2.2), is normalized by the maximum value of the set of voltage gains $\{\beta_{kl}\}$. The impulse response of the channel (random number generator seed 55) has been generated with 6 clusters and 500 rays within each cluster. When all rays that are 60 dB less than the ray with the maximum power gain are truncated, the resulting multipath spread T_m of the channel is 642.11 ns and the rms delay-spread σ of the channel is 70.93 ns. However, by using a cutoff of 100 dB instead of 60 dB, the rms delay-spread σ and maximum multipath spread T_m are 70.94 ns and 844.43 ns, respectively. Hence there is very little difference in the two rms delay-spread values

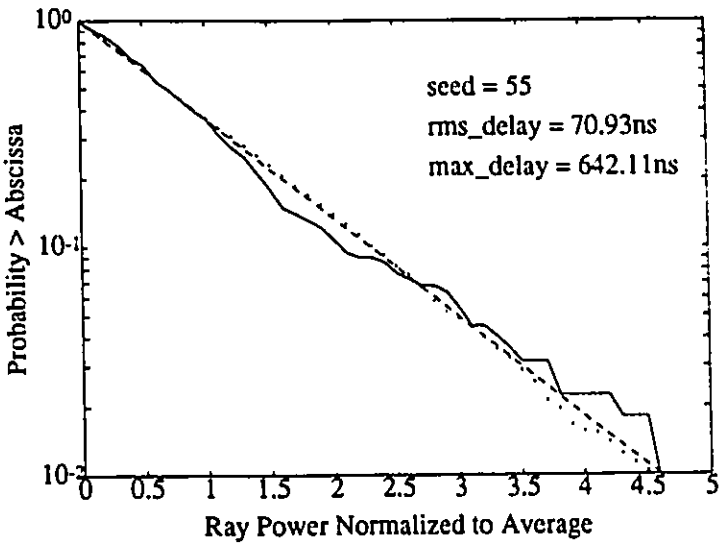

Figure 2.3: The cumulative distribution function (CDF) of the normalized power gain.

when truncating the impulse response $h(t)$ at 100 dB and 60 dB. Since it has been shown [Cox75] that the rms delay-spread is the dominant factor effecting the communication system performance, therefore, the impulse response of the channel with 60 dB truncation is suitable for system analysis and it is used in all simulation processes. A detailed discussion of rms delay spread is provided in the next section.

The cumulative distribution functions (CDF) of the normalized channel power gain $\beta_{kl}^2/\overline{\beta_{kl}^2}$ with 60 dB truncation or without truncation are respectively shown as a solid line and a dotted line in Figure 2.3. The impulse response of the channel has been given in Figure 2.2. The dashed line in Figure 2.3 represents the unity-mean exponential cumulative distribution, which is expressed as

$$P[\beta_{kl}^2/\overline{\beta_{kl}^2} > X] = exp(-X). \tag{2.13}$$

It is shown that the solid line fits the dashed line quite well. Furthermore, the exponential cumulative distribution for the path power gain is equivalent to a Rayleigh distribution for the path voltage gain, as shown in Equation(2.7).

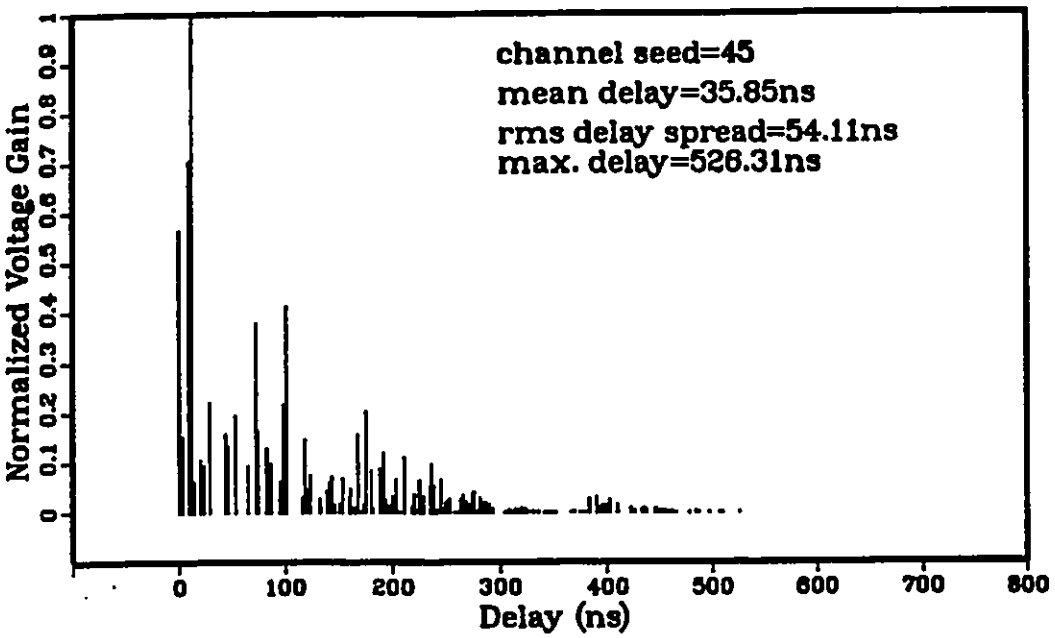

Figure 2.4: Simulated impulse response of the IWC (rms delay spread $\sigma = 54.11\ ns$).

Figure 2.4 and Figure 2.5 respectively show the simulated impulse response and the cumulative distribution function of the normalized power gain of a channel (seed 45). Both the rms delay spread (54.11 ns) and multipath spread (526.31 ns) values of the channel are smaller than those of the channel obtained with seed 55. But simulation results will show that the channel with seed 45 degrades communication system performances more than the channel of seed 55. The dispersive path rays with delay of about 600 ns Figure 2.2 cause the channel to have a larger rms delay spread than that of Figure 2.4. As before, the solid line representing the CDF of the normalized channel power gain with 60 dB truncation in Figure 2.5 closely fits the exponential cumulative distribution (dashed line). The dotted line is the CDF of the normalized channel power gain without truncation. The impulse response of a channel (seed 52) experiencing a small multipath delay T_m of 404.45 ns is shown in Figure 2.6, and this channel is considered to have relatively little multipath corruption. All three channel impulse responses, which have been discussed in this section, will be used to analyze communication systems in later chapters.

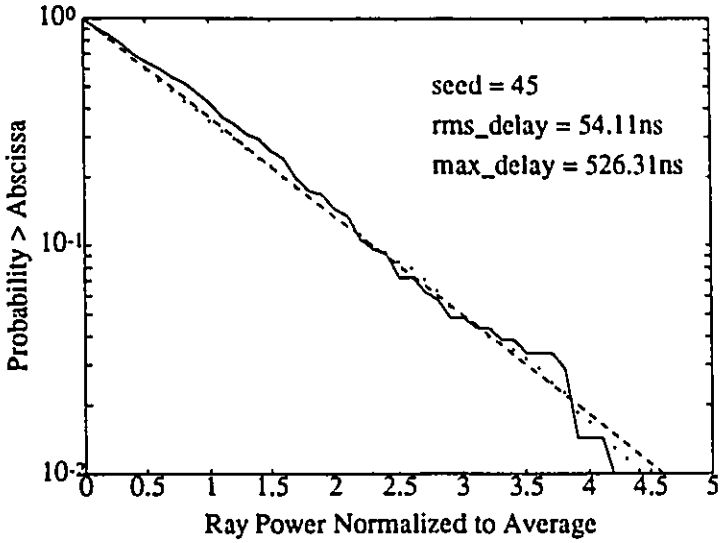

Figure 2.5: CDF of the normalized power gain for the IWC (rms delay-spread σ = 54.11 ns).

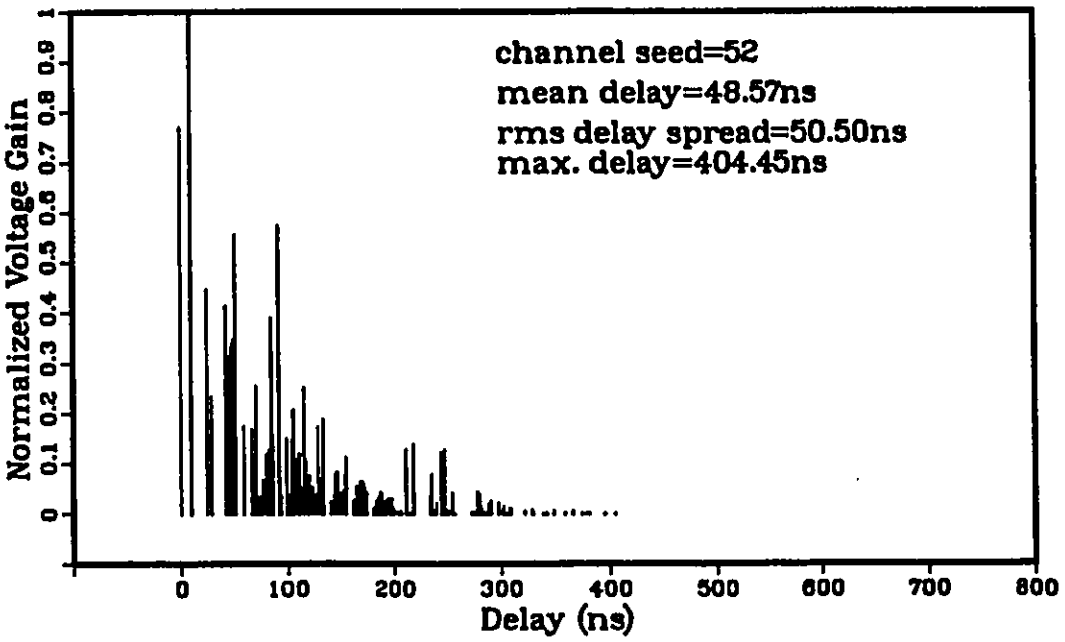

Figure 2.6: The impulse response of a channel with seed 52 (rms delay spread σ = 50.50 ns).

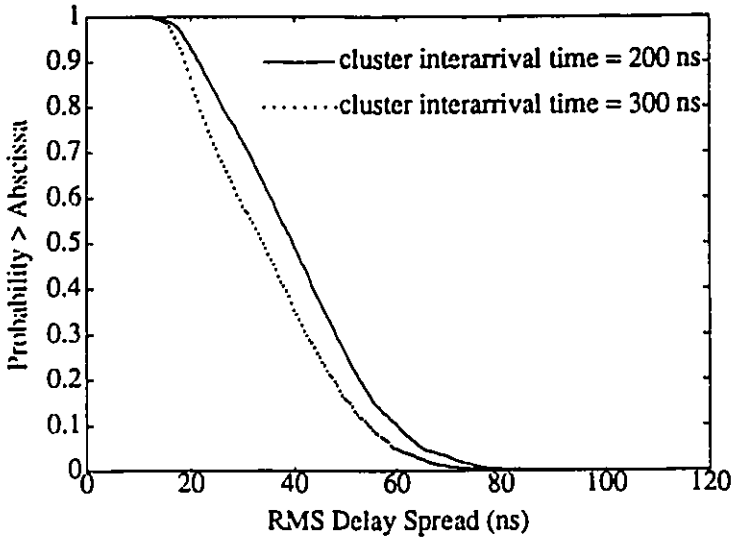

Figure 2.7: CDF of the rms delay spread (2000 impulse responses).

2.2.2 RMS Delay Spread

Statistical characteristics, such as the cumulative distribution of the rms delay spread of indoor wireless channels will now be discussed. Firstly, we introduce definitions for the average delay and the root mean square (rms) delay spread. According to [Cox72], the average delay $\overline{\tau}$ for the rays within clusters can be defined by

$$\overline{\tau} = \frac{\sum_l \sum_k (T_l + \tau_{kl}) G(T_l + \tau_{kl})}{\sum_l \sum_k G(T_l + \tau_{kl})}, \tag{2.14}$$

where $G(T_l + \tau_{kl})$ is the power delay profile of the kth ray of the lth cluster. The rms delay spread is defined as

$$\sigma = \sqrt{\frac{\sum_l \sum_k (T_l + \tau_{kl} - \overline{\tau})^2 G(T_l + \tau_{kl})}{\sum_l \sum_k G(T_l + \tau_{kl})}}. \tag{2.15}$$

A set of 2,000 impulse responses has been generated with the parameter values given in Table 2.1. A second set of impulse responses was created for a cluster interarrival time $1/\Lambda$ of 300 ns. The cumulative distributions of the rms delay spread of the two channel impulse response sets are presented in Figure 2.7. The values of the rms delay spread range from 7.78 to 87.53 ns for the set of impulse responses

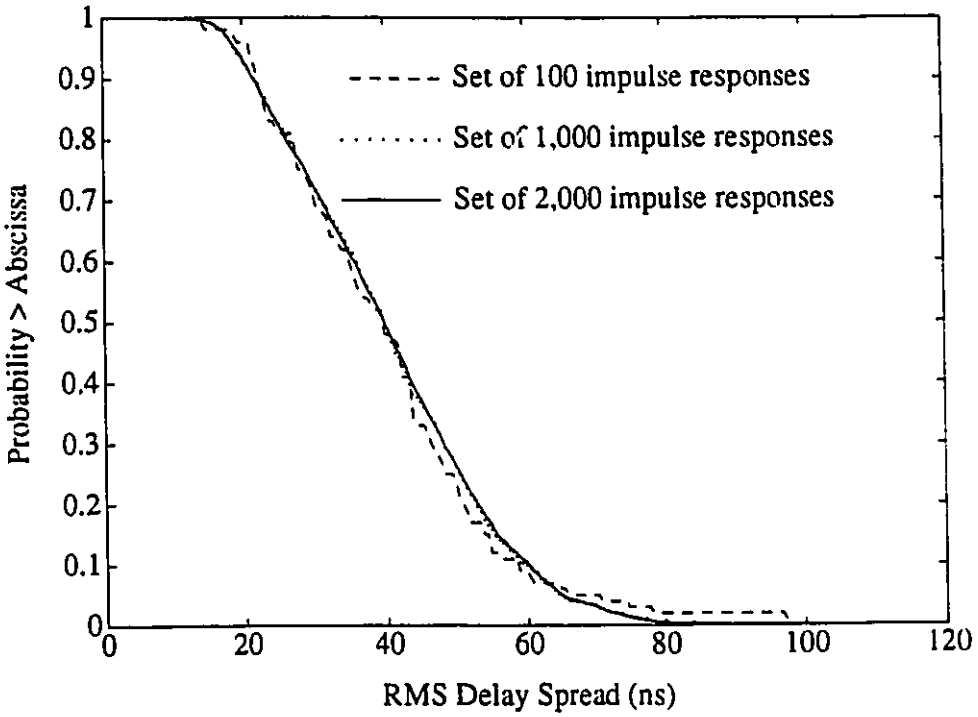

Figure 2.8: CDF of the rms delay spread (with three sets of impulse responses).

generated with $1/\Lambda = 300ns$ (dotted line). For the set of impulse responses generated with $1/\Lambda = 200ns$, the rms delay spread values are from 8.29 to 101.10 ns (solid line). The figure shows clearly that the rms delay spread for the channels with $1/\Lambda = 200ns$ is consistently larger than those of the channels with $1/\Lambda = 300ns$. Since channels with larger rms delay values statistically cause worse system performance, therefore all the impulse responses, used for analysis of communication system performance in this thesis, are generated with $1/\Lambda = 200ns$. This will help to provide performance results which reflect how the communication systems perform under very difficult channel conditions.

Figure 2.8 shows that the cumulative distribution of the rms delay spread changes only slightly, if a set of 1,000 channel impulse responses (dotted line) is used instead of a set of 2,000 channel impulse responses (solid line). Although the cumulative distribution of the rms delay spread for a set of 100 channel impulse responses

(dashed line) deviates slightly from that for a set of 2,000 channel impulse responses, it consistently follows the same distribution as a set of 2,000 channel impulse responses. Since this set of 100 channel impulse responses can accurately represent the second-order statistical characteristics of the indoor wireless channel, it is used for later simulations.

2.2.3 Tapped Delay Line Time Varying and Time invariant Channel Models

Multipath propagation causes fading of the received signal given in Equation (2.4). This fading phenomenon can be seen when the vector $\alpha_n(t)e^{j\theta_n(t)}$ with randomly time variant phases $\theta_n(t) = -2\pi f_c \tau_n(t)$ add destructively yielding very small received signals. At other times the received signal is large, since the vectors $\alpha_n(t)e^{j\theta_n(t)}$ add constructively. This kind of amplitude variation in the received signal is called signal fading, and it is caused by the time variant multipath characteristics of the channel.

The coherence bandwidth Δf_c and the coherence time Δt_c can be used to analyze the effects of signal characteristics on the choice of a channel model. The spaced-frequency spaced-time correlation function $\phi_C(\Delta f; \Delta t)$ of the channel, which is the Fourier transform of the multipath intensity profile (also called the delay power spectrum), is used to characterize time variant multipath channels. By assuming indoor wireless channels are both uncorrelated scattering and wide sense stationary (i.e. USWSS), $\phi_C(\Delta f; \Delta t)$ is dependent on frequency and observation time differences. By setting Δt to zero, the coherence bandwidth $|\Delta f_c|$ of the channel can be measured by [Proak89]

$$|\Delta f_c| \approx \frac{1}{T_m}, \tag{2.16}$$

where T_m is the multipath spread (also called the maximum delay spread) of the channel. A data rate of 10 $Mbits/s$ (corresponding to a symbol rate of 5 $Msymbols/s$ for QPSK modulation scheme), with $T_m = 400\ ns$ for the IWC, yields $|\Delta f_c| = 2.5$ MHz. This means that the bandwidth of the transmitted signal is large in comparison

with the coherence bandwidth of the channel. Indoor wireless channels are thus said to be frequency selective. Frequency selective channels can be modeled with the tapped delay line model.

With Δf of the correlation function set to zero, the Doppler spread B_d of the channel can be used to give the coherence time $|\Delta t_c|$ of the channel. That is

$$|\Delta t_c| \approx \frac{1}{B_d}. \tag{2.17}$$

$|\Delta t_c|$ or B_d can be used to characterize the rapidity of the channel fading, which is another type of distortion evidenced as a variation in the received signal strength. When the signaling interval T_s is smaller than the coherence time $|\Delta t_c|$ of a channel, the channel is considered a slowly fading channel. The Doppler spread of indoor wireless channels is found to be approximately 4 Hz in any fixed receiving location, and the cumulative distribution of envelope fading corresponds to a Rician curve. However, exceptions were found in some buildings where the envelope fading had a Rayleigh distribution [Bult87]. For IWCs, the Doppler spread of the signal is about 7 Hz when a user walks at a speed of 5 km/h. Thus the IWCs are slowly fading channels.

When the signaling bandwidth W is larger than the coherent bandwidth $|\Delta f_c|$, and the signaling interval T_s is smaller than the coherent time $|\Delta t_c|$ for the IWC, the channel can be modeled using a tapped delay line model. The lowpass impulse response for the channel can be described as

$$h(\tau; t) = \sum_{n=0}^{L-1} h_n(t)\delta(\tau - nT_s). \tag{2.18}$$

$\{h_n(t)\}$ represent the tap-coefficients which are spaced by T_s. The total number of paths L is equal to $(\lfloor T_m/T_s \rfloor + 1)$. Figure 2.9 gives the tapped delay line model for frequency selective channels.

An indoor wireless channel can be truncated at L paths. Figure 2.10 shows how the channel time delay spread can be divided into L periods for a signaling rate of 5

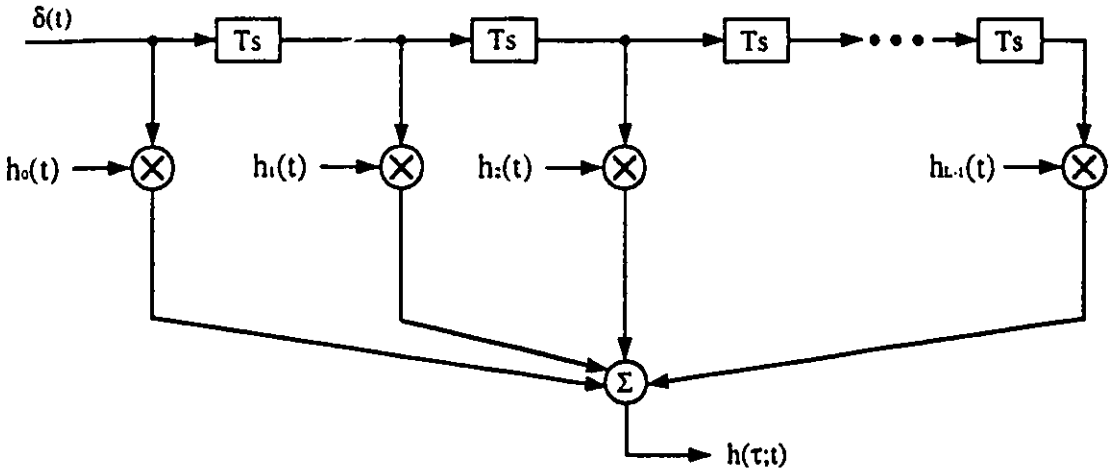

Figure 2.9: Tapped delay line model of frequency selective channel.

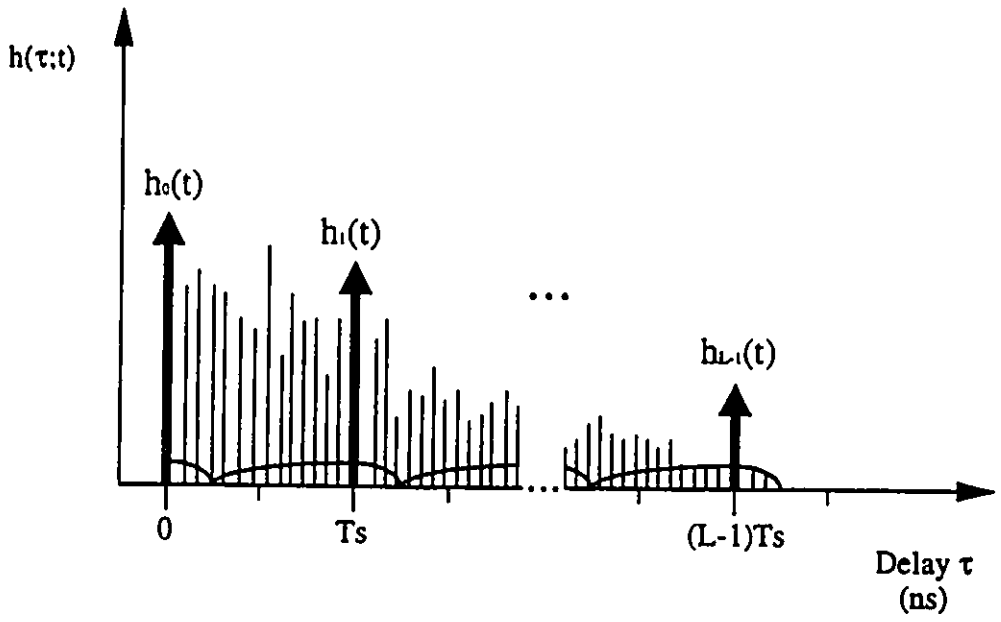

Figure 2.10: Divisions of time periods for the tap-coefficients.

Msymbol/s. The tap-coefficients for each path are created by vectorially adding the channel responses over the fixed time periods which are 200 *ns* in duration (except for the first path which represents the first 50 *ns* duration). For a time invariant IWC (also called fixed IWC), all tap-coefficients do not change with time in the simulations. Since an IWC is a slow fading channel, it can be considered a fixed IWC. Thus some simulations [Pai91] [Zig92] use the fixed IWC model.

However, in order to provide a more realistic transmission channel model for the communication system simulations, each tap of a tapped delay line channel model should be time variant. The amplitudes of those complex tap-coefficients $\{h_n(t)\}$ in the IWC model are functions of time, following a Rayleigh distribution, and the corresponding phases are uniformly distributed over $[0, 2\pi)$. Figure 2.11 shows the amplitude and phase of a Rayleigh fading signal created by [Jakes74]. When a user walks at a regular pace of 5 km/h through a medium-size office building [Sal87(1)], the Doppler spread of this Rayleigh signal is about 7 Hz for a carrier frequency of 1.5 GHz.

Figure 2.12 shows a slow time varying IWC (with four paths). In the figure, a set of $h_n(t)$ for $n = 0, ..., L$ at time t=0 correspond to the impulse response of the IWC (with a random generator seed 45) generated by [Sal87(2)]. Afterwards ($t > 0$), $\{h_n(t)\}$ changes with time, and each $h_n(t)$ for $n = 0, ..., L$ is characterized both by a different Rayleigh distributed amplitude and a distinct phase with a uniform distribution over the interval $[0, 2\pi)$. On the other hand, $\{h_n(t)\}$ for a fixed IWC remain constant with time. In other words, $\{h_n(t)\}$ values are equal to $\{h_n(0)\}$ for $t \geq 0$.

Two other time varying channel impulse responses at $t = 0$ for seed 55 and seed 52 were presented earlier. The tap-coefficients for those two channels are shown in Figure 2.13 and Figure 2.14, respectively. At $t = 0$, the amplitude of the first tap-coefficient is smaller than that of the second tap-coefficient in Figure 2.13. However in Figure 2.12, the amplitude value for the first tap-coefficient is almost the same as that

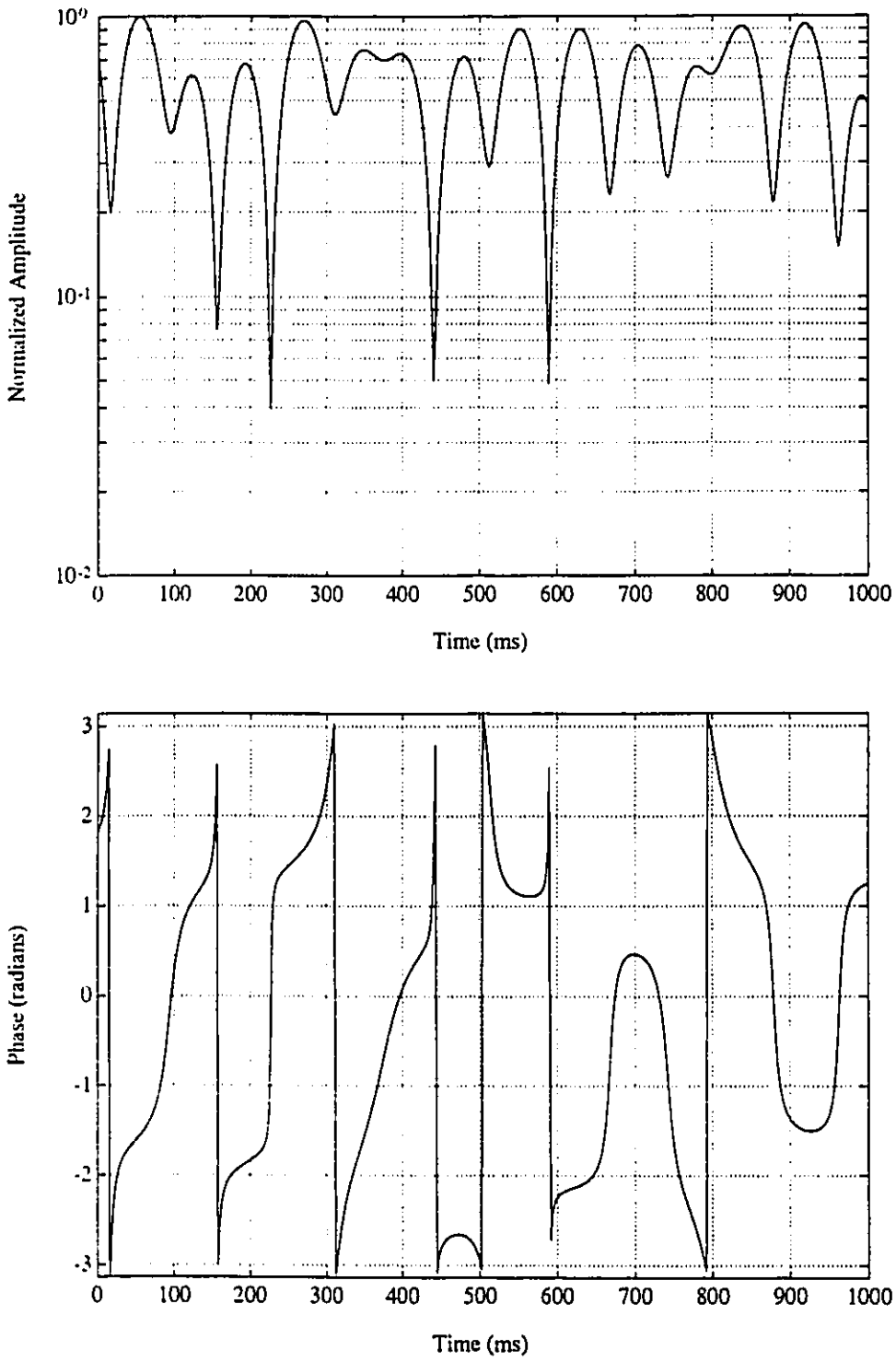

Figure 2.11: A Rayleigh fading signal.

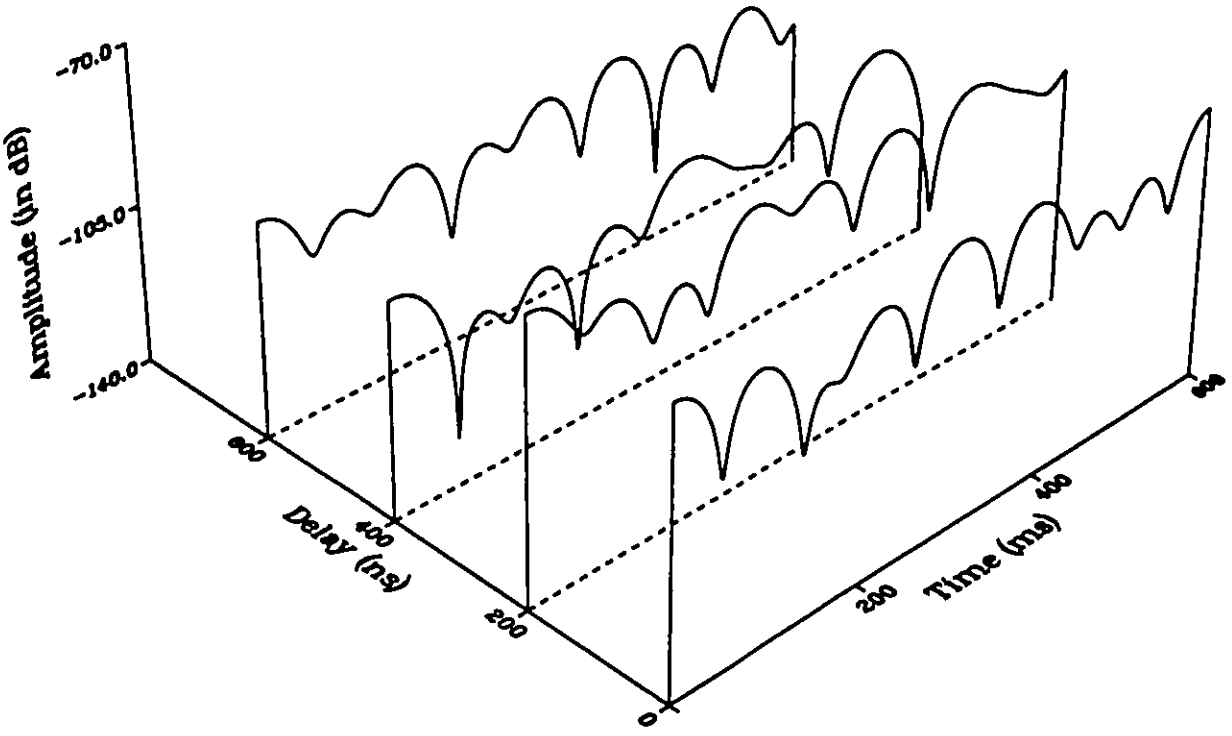

Figure 2.12: A slow time varying indoor wireless channel (random generator seed 45)

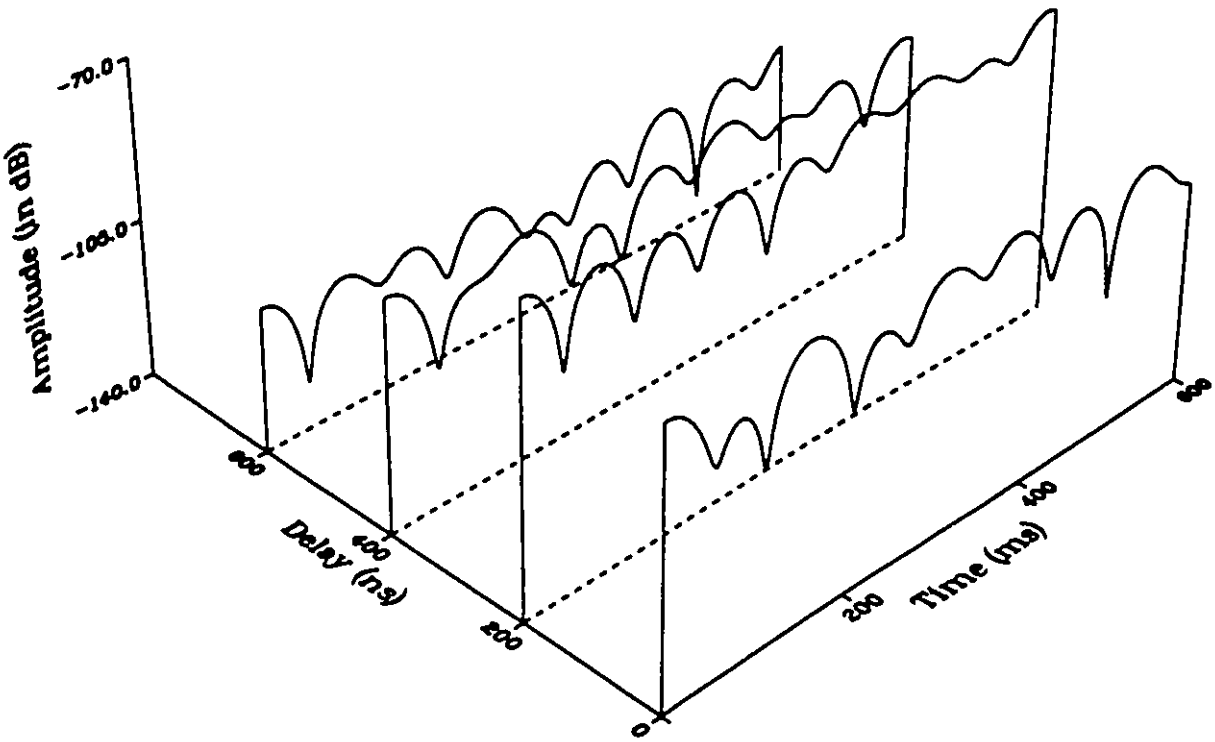

Figure 2.13: A slow time varying indoor wireless channel (random generator seed 55)

of the second tap-coefficient. The time varying channel with seed 52 (in Figure 2.13), has only three taps, and the amplitude of the first tap-coefficient is larger than that of the second tap-coefficient. Three different realizations of the time varying channel (identified as "CHNL1", "CHNL2", and "CHNL3"), with different levels of intersymbol interference (ISI), are considered here: channel "CHNL2" represents a typical time varying wireless channel with moderate ISI and "CHNL1" is a "better" channel experiencing low ISI. Channel "CHNL3", which consists of four taps, is considered the worst channel experiencing high ISI. Its free-delay tap (i.e., first delay-line model tap) and one-symbol-delay tap have almost identical amplitudes. Thus it has been shown that the time variant channel model represents the frequency-selective slow Rayleigh fading channel. The three channels (CHNL1, CHNL2 and CHNL3) that were introduced are useful transmission medium models for indoor wireless communication system and they are expected to provide realistic simulation results.

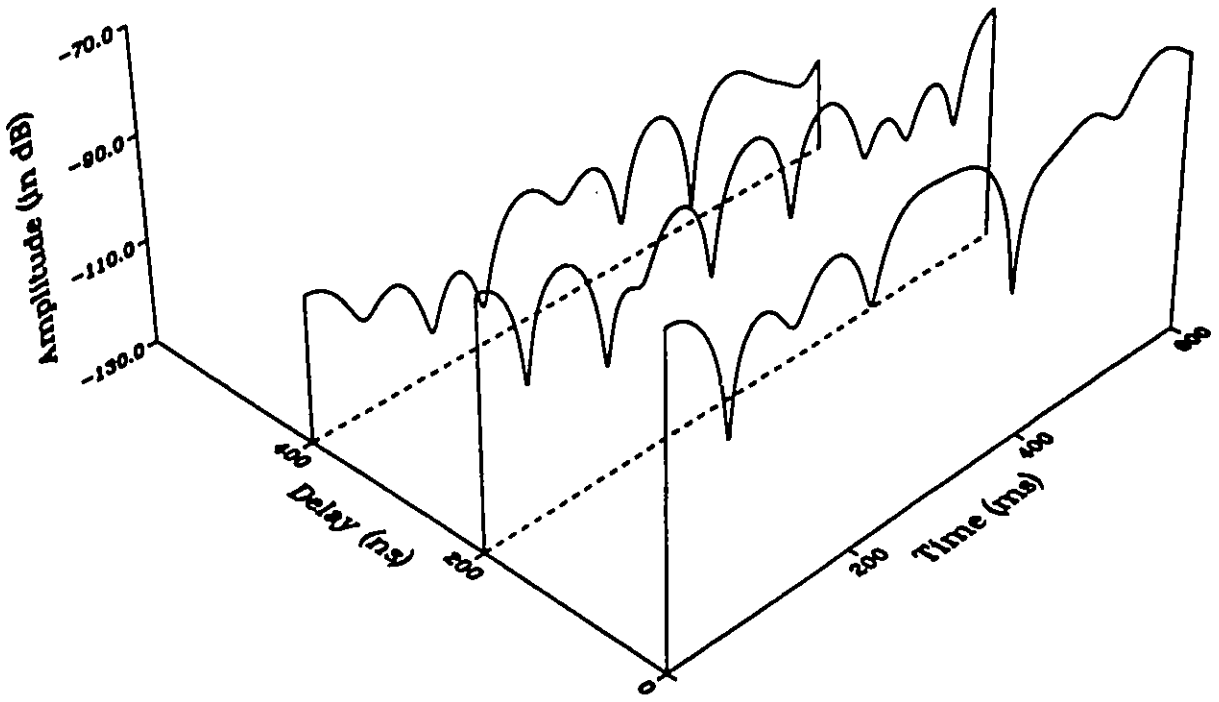

Figure 2.14: A slow time varying indoor wireless channel (random generator seed 52)

Chapter 3

Equalization Techniques for Indoor Wireless Channel

Adaptive equalization constitutes a useful method to combat the time varying inter-symbol interference (ISI) caused by dispersion in the transmit filter, the transmission medium, and the receive filter in an indoor wireless communication system. Adaptive equalizers can provide precise control over the time response of time varying channels. The objective of this chapter is to study three adaptive equalizers, whose structures are transversal. These are linear, fractionally spaced and decision feedback equalizers. Two algorithms are considered to optimize the design of these equalizers. They are the least-mean-square (LMS) algorithm and the recursive least-squares (RLS) algorithm. The LMS algorithm is related to the stochastic gradient method which is derived from the steepest descent algorithm, and the RLS algorithm is a special case of the Kalman filter.

3.1 Linear Adaptive Equalizer with Algorithms

An adaptive linear equalizer can be implemented as a finite-duration impulse response (FIR) filter with adjustable tap-weights. The $(2M + 1)$ equalizer tap-weights can adaptively be adjusted during the transmission of information by using the deci-

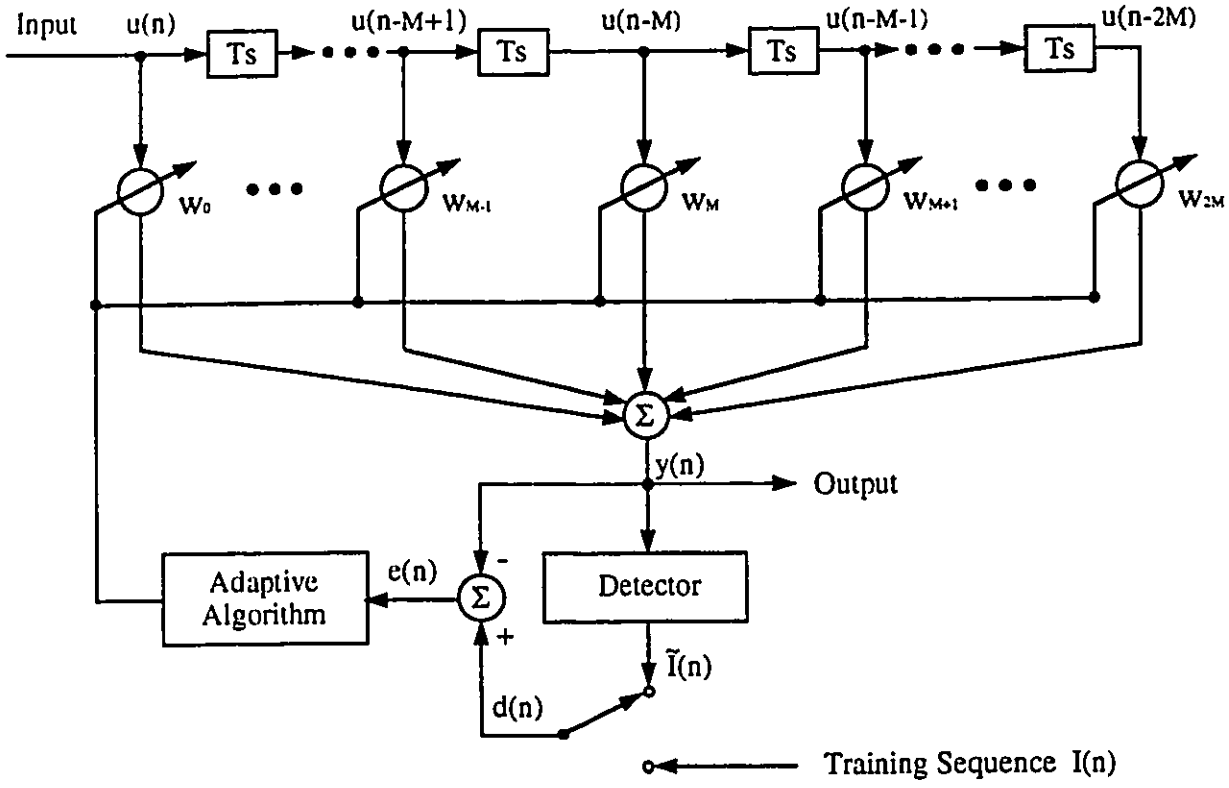

Figure 3.1: An adaptive linear equalizer.

sions made at the output of the detector to form the error signal for adaptation, as shown in Figure 3.1. A training sequence (i.e., a short known sequence of symbols) is transmitted for the purpose of initial adjustment of the equalizer tap-weights. When the average probability of symbol error is below 10 percent, the decisions made by the receiver are accurate enough for estimating the error signal (see [Hay91]). The linear equalizer has a tapped-delay-line structure, and thus it is called the transversal filter. The algorithms, which are employed to adaptively adjust the equalizer parameters according to some specified performance criterion, will be discussed in next three sections.

3.1.1 Steepest Descent Algorithm

The steepest descent algorithm is an iterative method of optimization which provides a means for searching a multi-dimensional performance surface. The equalizer output $y(n)$ at discrete time instant n, shown in Figure 3.1, is represented by the linear convolution sum:

$$y(n) = \sum_{k=0}^{2M} w_k^* \, u(n-k), \qquad n = 0, 1, 2, \ldots, \tag{3.1}$$

where the received sequence is $u(n-k)$, and w_k is the coefficient of the equalizer. The asterisk $*$ denotes complex conjugation. The estimation error $e(n)$ is given by

$$e(n) = d(n) - y(n). \tag{3.2}$$

The desired response $d(n)$ can be obtained from the output $\tilde{I}(n)$ of the decision device at the receiving end. This method is referred to as the decision-directed method. For symbol error rates below 10^{-1}, the occasional errors made by the detector usually have a negligible effect on the performance of the equalizer. For channels affected with higher BERs, a training method will be used at the beginning period of the adaptive process to obtain the desired response $d(n)$, which is actually the known transmitted sequence $I(n)$ stored in the receiver. After this training period, a switch is shifted so that $d(n)$ is connected to the output of the detector which creates the estimated transmission sequence $\tilde{I}(n)$, as shown in Figure 3.1. The estimation error is used to adjust the equalizer's coefficients to make an accurate decision at the receiving end.

One popular method, for optimizing the design of the equalizer, is to minimize the mean-square value of the estimation error, defined by

$$\begin{aligned} J(\mathbf{w}) &= E[|e(n)|^2] \\ &= E[|d(n) - \mathbf{w}^H \mathbf{u}(n)|^2], \end{aligned} \tag{3.3}$$

where the superscript H denotes Hermitian transposition, $\mathbf{w}$ is the tap-weight column vector of the equalizer, and $\mathbf{u}(n)$ is the tap input column vector. Another method is

to minimize the sum of error squares, called the method of least squares, defined by

$$\begin{aligned} \mathcal{J}(\mathbf{w}, n) &= \sum_{i=1}^{n} |e(i)|^2 \\ &= \sum_{i=1}^{n} |d(i) - \mathbf{w}^H \mathbf{u}(i)|^2. \end{aligned} \tag{3.4}$$

Equation(3.3) relies on ensemble averaging operations and Equation (3.4) depends on time averaging operations.

The optimum equalization design consists therefore in determining the operating conditions for which J or $\mathcal{J}$ attains its minimum value. In this section, we only discuss the minimization of J: $\mathcal{J}$ will be explored in section 3.1.3.

To minimize J (also called the cost function), all the elements of the gradient vector $\nabla(\mathbf{J})$ must be simultaneously equal to zero, as shown by

$$\nabla (\mathbf{J}) = 0. \tag{3.5}$$

Consequently, the optimum tap-weight vector $\mathbf{w}_o$ can be obtained by

$$\mathbf{w}_o = \mathbf{R}^{-1}\mathbf{p}. \tag{3.6}$$

This tap weight vector $\mathbf{w}_o$ is known as the optimum Wiener solution. $\mathbf{R}$ denotes the correlation matrix of the tap inputs of the equalizer, and $\mathbf{p}$ denotes the cross correlation vector between the tap inputs of the equalizer and the desired response, shown respectively by

$$\mathbf{R} = E[\mathbf{u}(n)\mathbf{u}^H(n)] \tag{3.7}$$

and

$$\mathbf{p} = E[\mathbf{u}(n)d^*(n)]. \tag{3.8}$$

When the tap inputs of the transversal filter and the desired response are jointly stationary, the cost function J is precisely a second-order function of the tap weights in the filter. Therefore, J can be viewed as a bowl-shaped surface with $(2M + 1)$ degrees of freedom represented by the tap weights of the filter. This surface, called the error performance surface, is characterized by a unique minimum, defined as

$$J_{min} = \sigma_d^2 - \mathbf{p}^H \mathbf{w}_o, \tag{3.9}$$

where σ_d^2 is the variance of the desired response $d(n)$.

However, the computation required for inverting $\mathbf{R}$ to the Wiener solution can be quite difficult, especially when the input data rate is high and when the equalizer has a large number of tap weights. Alternatively, the method of steepest descent, which involves significantly less computation, can be used. It is an optimization technique which is iterative in the sense that starting arbitrarily from some initial value for the tap-weight vector, it improves with increased number of iterations. The reduction in computational complexity is achieved by computing the gradient vector $\nabla(\mathbf{J}(n))$ to successivelly correct the tap-weight vector in the direction of the steepest descent of the error performance surface. The final value being computed for the tap-weight vector converges to the Wiener solution, and the cost function J approaches the minimum mean-squared error J_{min}. The tap-weight vector is recursively computed by

$$\mathbf{w}(n+1) = \mathbf{w}(n) + \frac{1}{2}\mu[-\nabla(\mathbf{J}(n))], \tag{3.10}$$

where μ is the step size parameter which controls the incremental correction for the tap-weight vector. The gradient vector $\nabla(\mathbf{J}(n))$ is given by

$$\nabla(\mathbf{J}(n)) = -2\mathbf{p} + 2\mathbf{R}\mathbf{w}(n). \tag{3.11}$$

The stability of the steepest descent algorithm is highly sensitive to the step size parameter μ and the correlation matrix $\mathbf{R}$ of the tap inputs.

The method of steepest descent is a multiparameter closed-loop deterministic control system that finds the minimum point of the ensemble averaged error performance surface without knowledge of the surface itself. This method provides a quantitative measure of the amount by which the final value of the mean-squared error, averaged over an ensemble of equalizer data, deviates from the minimum mean-squared error produced by the Wiener filter, to make the parameters converge to the optimum Wiener solution for a stationary environment in some statistical sense, and

to track time variations in the statistics of the input data for a nonstationary environment. In the next section, the least-mean-square (LMS) algorithm, which can be used to estimate the gradient vector $\nabla(\mathbf{J}(n))$ instead of computing it, will be introduced.

3.1.2 Least-Mean-Square Algorithm

LMS Adaptation Algorithm

The least-mean-square (LMS) algorithm, devised by Widrow and Hoff [Wid60], is a stochastic gradient-based algorithm. The LMS algorithm can be used to estimate the gradient vector for the operation of an adaptive equalizer instead of computing it as in the steepest descent algorithm. Accordingly, the calculation of the correlation matrix $\mathbf{R}$ of the tap input vector $\mathbf{u}(n)$ and the cross correlation vector $\mathbf{p}$ between the tap input vector $\mathbf{u}(n)$ and the desired response $d(n)$ are simplified to estimate them for LMS instead of computing expectation values for the steepest descent algorithm, as defined by, respectively,

$$\mathbf{R} = E[\mathbf{u}(n)\mathbf{u}^H(n)] \qquad \Longrightarrow \qquad \hat{\mathbf{R}}(n) = \mathbf{u}(n)\mathbf{u}^H(n) \tag{3.12}$$

and

$$\mathbf{p} = E[\mathbf{u}(n)d^*(n)] \qquad \Longrightarrow \qquad \hat{\mathbf{p}}(n) = \mathbf{u}(n)d^*(n). \tag{3.13}$$

The estimate $\hat{\nabla}(\mathbf{J}(n))$ of the gradient vector from Equation (3.11) is simplified as [Hay91]

$$\hat{\nabla}(\mathbf{J}(n)) = -2\mathbf{u}(n)d^*(n) + 2\mathbf{u}(n)\mathbf{u}^H(n)\hat{\mathbf{w}}(n). \tag{3.14}$$

Therefore, from Equation (3.10), the updated tap-weight vector becomes

$$\begin{aligned} \hat{\mathbf{w}}(n+1) &= \hat{\mathbf{w}}(n) + \mu\mathbf{u}(n)[d^*(n) - \mathbf{u}^H(n)\hat{\mathbf{w}}(n)] \\ &= \hat{\mathbf{w}}(n) + \mu\mathbf{u}(n)e^*(n). \end{aligned} \tag{3.15}$$

The tap weights $\hat{w}_0(n)$, $\hat{w}_1(n)$, ..., $\hat{w}_{2M}(n)$ form the elements of the $(2M+1)$-by-1 tap-weight vector $\hat{\mathbf{w}}(n)$.

The necessary and sufficient condition for convergence of the LMS algorithm, is given [Wid71] by

$$0 < \mu < \frac{1}{\lambda_{max}}, \tag{3.16}$$

where λ_{max} is the largest eigenvalue of the correlation matrix $\mathbf{R}$. However, the eigenvalues λ_i are rarely known in practice, so $tr[\mathbf{R}]$ which is the trace of the correlation matrix $\mathbf{R}$ is used instead of λ_{max}. $tr[\mathbf{R}]$ is equal to $\sum_{i=0}^{2M} \lambda_i$ (the total of input powers), and greater than λ_{max}. Thus, Equation (3.16) can be simplified into

$$0 < \mu < \frac{1}{\sum_{i=0}^{2M} \lambda_i}. \tag{3.17}$$

In Equation (3.15), the step size μ which is the only adjustable parameter, controls both the stability and the adaptation rate of the equalizer. The existence of only a single adjustable parameter is a fundamental limitation which causes the convergence rate of the LMS algorithm to be slow.

If the step size μ is chosen using Equation (3.17), the tap-weights will relax from their initial condition to the Wiener solution $\mathbf{w}_o$. Then the time constant $\tau_{i,LMS}$ for the relaxation process can be determined [Wid76] as follows

$$\tau_{i,LMS} \approx \frac{1}{2\mu\lambda_i}, \qquad 0 \leq i \leq 2M. \tag{3.18}$$

When the adaptive process is convergent, the mean square error J undergoes a geometric progression toward the minimum mean square error J_{min}. The learning curve is a plot of the mean square error versus the number of iterations. The mean square error learning curve time constant is given [Wid76] by

$$\tau_{i,mse} \approx \frac{1}{4\mu\lambda_i}, \qquad 0 \leq i \leq 2M. \tag{3.19}$$

Clearly, the convergence time is inversely proportional to the step size parameter μ.

This simple LMS algorithm, which is highly popular and widely used in a variety of applications, achieves satisfactory performance in most cases. The value of the tap-weight vector $\mathbf{w}(n)$ calculated by the LMS algorithm is around the optimum

solution since $\mathbf{w}(n)$ executes a random motion around the minimum point of the error performance surface. Furthermore, the primary limitation of the LMS algorithm is the relatively long convergence times for those modes of the input data sequence which have small eigenvalues [Fri82], [Hay91].

Stability of the LMS Algorithm

An analysis of the performance of LMS algorithm should consider both the convergence and misadjustment due to noise and parameter variation (also called lag). Although the LMS algorithm is simple in implementation, particular attention must be paid in carefully choosing the step-size parameter μ. When the step-size parameter μ is chosen properly, the LMS algorithm converges in the mean (i.e. the expectation of the tap-weight vector $E[\hat{\mathbf{w}}(n)]$ approaches the Wiener solution $\mathbf{w}_o$ as the number of iterations n approaches infinity). The LMS algorithm also exhibits another form of convergence, called convergence in the mean square, where the final value $J(\infty)$ of the mean-squared error is finite and always greater than the minimum mean-squared error J_{min} that corresponds to the Wiener solution, as the number of iterations n tends towards infinity. Since the LMS algorithm exhibits both of forms of convergence, it is stable. The simplified necessary and sufficient conditions for convergence of the LMS algorithm in the mean square can be given in Equation (3.17).

When an adaptive equalizer operates in a nonstationary environment, the LMS algorithm has the task of not only producing tap-weight vector estimates $\hat{\mathbf{w}}(n)$ that closely match the unknown value $\mathbf{w}_o(n)$, but also of tracking the moving minimum point of the error performance surface. The tap-weight error vector at the nth instant may be expressed as

$$\begin{aligned} \mathbf{e}(n) &= \hat{\mathbf{w}}(n) - \mathbf{w}_o(n) \\ &= (\hat{\mathbf{w}}(n) - E[\hat{\mathbf{w}}(n)]) + (E[\hat{\mathbf{w}}(n)] - \mathbf{w}_o(n)) \\ &= \mathbf{e}_1(n) + \mathbf{e}_2(n). \end{aligned} \tag{3.20}$$

The weight vector noise $\mathbf{e}_1(n)$ is the difference between the individual tap-weight vec-

tors of the equalizer and their ensemble. The weight vector lag $\mathbf{e}_2(n)$ is the difference between the ensemble mean of the tap-weight vector and $\mathbf{w}_o(n)$. The weight vector lag is zero when the LMS algorithm is applied to a stationary environment, since $\mathbf{w}_o(n)$ assumes a constant value that equals $E[\hat{\mathbf{w}}(n)]$. The excess mean-squared error can also be expressed as the following

$$\begin{aligned} J_{ex}(n) &= J(n) - J_{min} \\ &= tr[\mathbf{R}\mathbf{K}_1(n)] + tr[\mathbf{R}\mathbf{K}_2(n)], \end{aligned} \tag{3.21}$$

where $\mathbf{K}_1$ and $\mathbf{K}_2$ are the correlation matrices of the weight vector noise $\mathbf{e}_1(n)$ and the weight vector lag $\mathbf{e}_2(n)$, respectively. The total excess mean-squared error of the LMS adaptive equalizer, defined by Equation (3.21), is the sum of two components. The two terms are respectively related to the weight vector noise $\mathbf{e}_1$ and weight vector lag $\mathbf{e}_2$. The misadjustment $\mathcal{M}$ can be used to provide a quantitative measure of the deviation between the final mean-squared error value and the minimum mean-squared error. The misadjustment $\mathcal{M}$ is defined as

$$\mathcal{M} \triangleq \frac{J_{ex}(\infty)}{J_{min}}, \tag{3.22}$$

where $J_{ex}(\infty) = J(\infty) - J_{min}$. Assuming that; (1): the tap input vector is uncorrelated over time (i.e., $E[\mathbf{u}_j\mathbf{u}_k] = 0$, $j \neq k$). and (2): the step size μ is small compared to $1/\lambda_{max}$, if the weight vector $\mathbf{w}$ converges to the Wiener solution for the stationary environment, then $\mathcal{M}$ can be expressed [Wid76] by

$$\begin{aligned} \mathcal{M} &= \mu \textstyle\sum_0^{2M} \lambda_i \\ &= (2M+1)\mu\lambda_{avg}, \end{aligned} \tag{3.23}$$

where λ_{avg} is the average of the eigenvalues.

When a LMS adaptive equalizer operates in a nonstationary environment, the misadjustment $\mathcal{M}_{\mathbf{e}_1}$ due to the weight vector noise is equal to the value in Equation (3.23), and the excess mean-squared error $J_{ex,\mathbf{e}_1} = \mu J_{min} tr[\mathbf{R}]$. If the time constant

τ_{w_o} of the nonstationary environment is assumed to be large, then the excess mean-squared error due to the weight vector lag can be expressed [Wid76] by

$$J_{ex,e_2} = \frac{(2M+1)\sigma_W^2}{4\mu}. \tag{3.24}$$

The misadjustment $\mathcal{M}_{e_2}$ due to the lag is represented by

$$\mathcal{M}_{e_2} \approx \frac{1}{\mu}\left(\frac{(2M+1)\sigma_W^2}{4J_{min}}\right), \qquad \tau_{w_o} \gg \tau_{i,LMS}, \tag{3.25}$$

where σ_W^2 is the variance of the white noise. The total misadjustment is the sum of the two misadjustment components $\mathcal{M}_{e_1}$ and $\mathcal{M}_{e_2}$. The misadjustment caused by the weight vector noise is proportional to the step size parameter μ and the number of tap weights. The misadjustment arising from the weight vector lag is proportional to the number of tap weights but inversely proportional to the step size parameter μ. In order to minimize the total misadjustment, a value of μ must be chosen so that $\mathcal{M}_{e_1} = \mathcal{M}_{e_2}$ [Wid76].

3.1.3 Recursive Least-Squares Algorithm

RLS Algorithm

The recursive least-squares (RLS) algorithm is different from the LMS algorithm, since it involves the use of time averages instead of statistical averages in order to minimize the square of the estimation error. The algorithm is commonly considered to have a fast convergence speed and perform well in a time varying environment. In the RLS algorithm, the estimation error at time i is defined as

$$e(i) = d(i) - \mathbf{w}^H(n)\mathbf{u}(i), \tag{3.26}$$

where $d(i)$ and $\mathbf{u}(i)$ are the desired response and the tap-input vector at time i, respectively. $\mathbf{w}(n)$ is the tap-weight vector at time n. The cost function to be minimized for the RLS algorithm is represented as

$$\mathcal{J}(n) = \sum_{i=1}^{n} \rho^{n-i}|e(i)|^2, \tag{3.27}$$

where ρ^{n-i} is an exponential weighting factor which has to satisfy the following inequalities:

$$0 < \rho^{n-i} \leq 1, \qquad i = 1, 2, \ldots, n. \tag{3.28}$$

The inverse of $1-\rho$ is a measure of the memory of the algorithm. By using the matrix inversion lemma, the RLS algorithm can be implemented according to the following equations:

$$\mathrm{k}(n) = \frac{\mathbf{P}(n-1)\mathrm{u}(n)}{\rho + \mathrm{u}^H(n)\mathbf{P}(n-1)\mathrm{u}(n)}, \tag{3.29}$$

$$\mathbf{P}(n) = \rho^{-1}[\mathbf{P}(n-1) - \mathrm{k}(n)\mathrm{u}^H(n)\mathbf{P}(n-1)]. \tag{3.30}$$

$$\alpha(n) = d(n) - \hat{\mathbf{w}}^H(n-1)\mathrm{u}(n), \tag{3.31}$$

$$\hat{\mathbf{w}}(n) = \hat{\mathbf{w}}(n-1) + \mathrm{k}(n)\alpha^*(n), \tag{3.32}$$

where $\mathrm{k}(n)$ is a gain vector. $\alpha(n)$ is an *a priori* estimation error, and $\mathbf{P}(n)$ is the inverse of the correlation matrix $\mathbf{\Phi}(n) = \sum_{i=1}^{n} \rho^{n-i}\mathrm{u}(i)\mathrm{u}^H(i)$.

The application of the RLS algorithm first requires an initialization of the recursion in Equation (3.30) by setting the starting value $\mathbf{P}(0)$ as follows

$$\mathbf{P}(0) = \delta^{-1}\mathrm{I}, \tag{3.33}$$

where the positive constant δ should satisfy the following inequality:

$$\delta < 0.01\{\text{variance of an input sample}\}. \tag{3.34}$$

Secondly, the algorithm requires that the initial value of the tap-weight vector be set to zero (i.e., $\hat{\mathbf{w}}(0) = \mathbf{0}$).

Stability Analysis of RLS Algorithm

It was demonstrated in [Hay91] that the estimated tap-weight vector is convergent in the mean, and that both the tap-weight error vector and the *a priori* estimation error are convergent in the mean square.

An exponential weighting factor of $\rho = 1$ is well suited for the RLS algorithm when operating in a stationary environment. However, when the RLS algorithm is used in a nonstationary environment, the value of ρ is chosen to be less than unity. As in the LMS algorithm shown early, the excess mean-squared error for the RLS algorithm can also be expressed by two main sources of error. The first source of error, called the weight vector noise $\mathbf{e}_1$, occurs when the estimated tap-weight vector of an adaptive equalizer does not converge to its optimal setting. The second source of error, called the weight vector lag $\mathbf{e}_2$, results from an inability to track time varying input signals.

[Ele86] derived the following formulas to investigate the tracking properties and steady-state performance of the RLS algorithm. When the value of ρ is approximately 1, the steady-state excess mean-squared error due to the tap-weight vector error can be expressed as

$$\mathcal{J}_{ex,\mathbf{e}_1} \approx \frac{1-\rho}{1+\rho}(2M+1)\mathcal{J}_{min}, \tag{3.35}$$

and the corresponding misadjustment is

$$\mathcal{M}_{\mathbf{e}_1} = \frac{1-\rho}{1+\rho}(2M+1). \tag{3.36}$$

Equation (3.36) shows that decreasing ρ or increasing the number of tap-weights results in a more noisy adaptation process. Assuming that the unknown tap-weights obey a first-order Markov process, the excess mean-squared error due to the weight vector lag is derived as

$$\mathcal{J}_{ex,\mathbf{e}_2} \approx \frac{\sigma_W^2}{2(1-\rho)} tr[\mathbf{R}]. \tag{3.37}$$

where σ_W^2 is the variance of white noise. Thus, $\mathcal{J}_{ex,\mathbf{e}_2}$ is proportional to both the white noise power and the tap input powers. The weight vector lag error is a geometric converging process whose time constant is given by

$$\tau_{i,RLS} = \frac{1}{1-\rho}, \qquad 0 \le i \le 2M. \tag{3.38}$$

We note that the time constant is independent of the spread of eigenvalues from input vector's autocorrelation matrix. Furthermore, the time constant value is smaller than

that of the LMS algorithm. Hence, the tracking ability of the RLS algorithm is always at least as good as that of the LMS algorithm. The total excess mean-squared error is computed by

$$\mathcal{J}_{ex,RLS} = \frac{1-\rho}{1+\rho}(2M+1)\mathcal{J}_{min} + \frac{1}{2(1-\rho)}tr[\mathbf{R}]\sigma_W^2. \tag{3.39}$$

The optimum exponential weighting factor for minimizing $\mathcal{J}_{ex,RLS}$ is

$$\rho_{opt} = \frac{1-\zeta}{1+\zeta} \tag{3.40}$$

where

$$\zeta = \left(\frac{\sigma_u^2\sigma_W^2}{4\,\mathcal{J}_{min}}\right)^{1/2} \tag{3.41}$$

with the constraint $\zeta < 1$. From Equations (3.40) and (3.41), we can see that ρ_{opt} is independent of the length $(2M+1)$ of the adaptive equalizer.

The time constant of the geometrical converging tracking process of the RLS algorithm is independent of the eigenvalues of the autocorrelation matrix $\mathbf{R}$. Thus, the tracking ability of the RLS algorithm is superior to that of the LMS algorithm for the case of disparate eigenvalues. [Ele86] also shows that the two algorithms have the same steady-state performance, when we assume a first-order Markov time varying model and white noise inputs. In this case, the step size μ must satisfy the following inequalities

$$0 < \mu < \frac{1}{2M+1}. \tag{3.42}$$

For small equalizer lengths, the LMS algorithm is capable of providing tracking behavior similar to that of the RLS algorithm. Thus, the LMS algorithm should be used when the equalizer length is small since it is less complex than the RLS algorithm. However, for large equalizer lengths, the step size μ will violate the stability bound shown in Equation (3.42), if the LMS algorithm is used to such a way as to try to provide the same tracking ability as the RLS algorithm.

Finally, the numerical properties of implementation of the RLS algorithm should also be considered. Since roundoff errors can cause numerical instability for the RLS

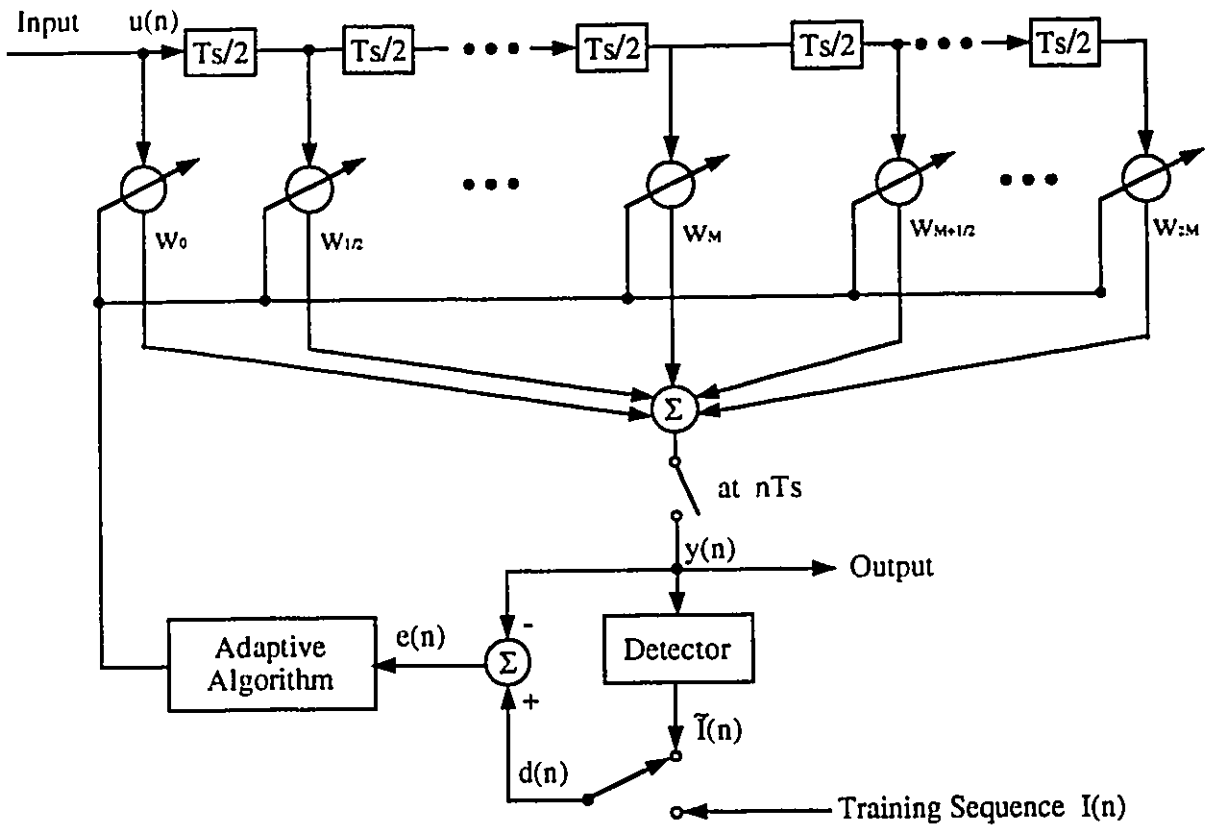

Figure 3.2: A $T/2$ fractionally spaced equalizer.

algorithm, they pose potential problems for implementation. [Lju85] investigated the roundoff error propagation for the RLS algorithm, and proved that the algorithm is exponentially stable with respect to errors when $\rho < 1$. [Ele86] gives the restart procedures for remedying the error caused by numerical roundoff.

3.2 Fractionally Spaced Linear Equalizer

The fractionally spaced equalizer (FSE), which is another type of digital transversal equalizer, provides better performance results as compared to the adaptive linear equalizer. The taps of the FSE are spaced closer than the reciprocal of twice the signaling rate. The FSE can effectively compensate for channel delay distortion, and its performance is unaffected by the receiver timing phase [Git81]. The $T/2$-spaced

equalizer (see Figure 3.2) is the most widely used FSE. The output of the $T/2$-FSE can be expressed as

$$y(n) = \sum_{k=0}^{4M} w_{\frac{1}{2}k} u(n - \frac{1}{2}kT_s), \tag{3.43}$$

where T_s is one symbol duration, $w_{\frac{1}{2}k}$ is the tap weight and $u(n - \frac{1}{2}kT_s)$ is the tap input. The number of taps for the $T/2$-FSE is almost double that of the T-spaced equalizer. In general, if the transmitted signal is shaped by a raised cosine with a rolloff factor α ($0 \leq \alpha \leq 1$), then the signal sampling rate should be $(1 + \alpha)/T_s$. At this sampling rate, the equalizer tap are spaced by $T_s/(1 + \alpha)$.

For a conventional equalizer whose taps are spaced by T, the Fourier transforms of the tap-weights $\{w_l\}$ of the equalizer and the tap input $\{u(n)\}$ are respectively represented by

$$W_T(f) = \sum_l w_l e^{-j2\pi flT} \tag{3.44}$$

and

$$U_T(f) = \sum_k U(f - \frac{k}{T}) e^{j2\pi(f - \frac{k}{T})\tau_0}, \tag{3.45}$$

where τ_0 is the initial sampling delay. Thus the Fourier transform of the T-FSE output is given by

$$Y_T(f) = W_T(f) U_T(f). \tag{3.46}$$

When $|f| > 1/2T$, then $U(f) = 0$, which means that the conventional equalizer can not control the channel distortion inherent in $U(f)e^{j2\pi f\tau_0}$ over both sides of the rolloff region about $|f| = 1/2T$.

For a KT/N-spaced equalizer with $K < N$, the frequency response of the FSE is

$$W_{T'}(f) = \sum_n w_n e^{-j2\pi fnT'}, \tag{3.47}$$

and the equalized spectrum can be expressed by

$$\begin{aligned} Y_{T'}(f) &= W_{T'}(f) U_{T'}(f) \\ &= W_{T'}(f) \textstyle\sum_n U_n(f - nN/KT) e^{j2\pi(f - nN/NT)\tau_0}, \end{aligned} \tag{3.48}$$

where $T' = KT/N$ and $T' \leq T/(1+\alpha)$. When $|f| \leq N/2KT$, the above equation can be presented as

$$Y_{T'}(f) = W_{T'}(f)U(f)e^{j2\pi f\tau_0}. \qquad |f| \leq 1/2T' \tag{3.49}$$

For an FSE receiver, although the equalizer input is sampled at a rate of T', the equalizer output is still sampled at a rate of T. The output is used to make the correct data decision at normal signal intervals. With respect to the output sampling rate of $1/T$, Equation (3.49) shows that the $T/2$-FSE can use $U(f)e^{j2\pi f\tau_0}$ to adjust $W_{T'}(f)$ before aliasing. Thus $W_{T'}(f)$ can effectively compensate for the time phase and the channel distortion in the received signal. Simulation results [Qur77] demonstrate that a mean square $T/2$-FSE has superior performance as compared with a conventional T-spaced equalizer.

3.3 Decision Feedback Equalizer

The decision feedback equalizer (DFE) is one of the nonlinear equalizers, which are believed to be capable of effectively removing the intersymbol interferences (ISI) caused by severe channel distortion. The DFE consists of a feedforward filter (FFF) and a feedbackward filter (FBF). The main function of the DFE is not only to utilize the FFF to estimate and subtract the ISI from the present estimation caused by the equalizer inputs, but also to utilize the FBF to estimate and subtract the ISI from the present estimation caused by previously detected symbols [Aus67] [Mon71]. A DFE is shown in Figure 3.3. Its output can be represented as

$$y(n) = \underbrace{\sum_{k=0}^{N_1} w_k u(n-kT_s)}_{FFF} + \underbrace{\sum_{k=1}^{N_2} w_{N_1+k}\tilde{I}(n-kT_s)}_{FBF}, \tag{3.50}$$

where $\{w_k\}$ are the DFE's tap-weights, $\{u(n)\}$ are the inputs of the FFF, which inherit the ISI, and $\{\tilde{I}(n)\}$ are the detected symbol sequence used for the inputs of the FBF. The length of the FFF is normally chosen to be one longer than the length of the FBF

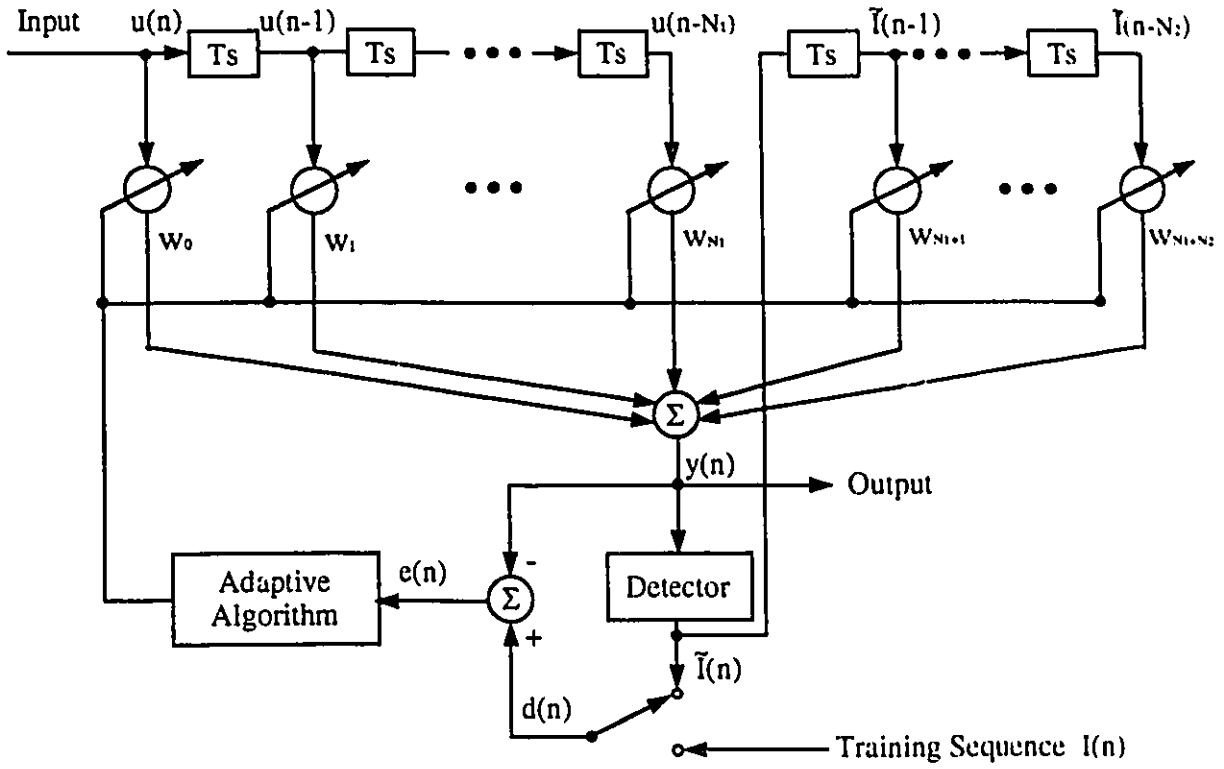

Figure 3.3: A decision feedback equalizer.

(i.e., $N_1 \geq N_2$), so that the DFE can achieve better performance. It has been shown [Mon70] that if correct decisions are made by the detector, a DFE operating over a slow fading channel has superior performance as compared with a linear equalizer. Furthermore, when the channel exhibits a deep selective fade approaching a null, the DFE with correct decisions greatly outperforms the linear equalizer. However, when the decisions are not accurate, the DFE can propagate these errors through the inputs of the FBF causing even worse performance than that of the linear equalizer [Mon74]. Decision errors reduce equalizer performance in two ways. Firstly, they can affect the adaptation process for determining the ideal equalizer tap-weight settings. Secondly, they represent additional errors in the signal path going through the FBF, which results in error propagation. In chapter 5, we will provide simulation results showing the DFE performance. The effects of error propagation can be clearly seen from those results.

Chapter 4

Communication System Description

In this chapter, the block diagram of an indoor wireless communication system used in the simulations is presented. This is followed by a detailed description of each component in the block diagram except for the equalizers and the channel. Equalization techniques were presented in the previous chapter, and indoor wireless channel models were reviewed in Chapter 2. The shaping characteristics of the transmit and receive filters are discussed first. Then, differential quadrature-phase-shift keying (DQPSK) modulation and differential 8PSK-based trellis coded modulation (D8PTCM) are discussed.

4.1 System Model

Figure 4.1 shows the block diagram of an indoor wireless radio system. The data source generates binary information data (a_1 and a_2) with equal probability $p(a_1) = p(a_2) = 1/2$. At the modulator, the information data are mapped into the signal constellation by an encoder, such as an M-ary PSK or a trellis encoder. Then the signal passes through the differential encoder. After being shaped by the transmit filter, the signal is sent through the communication channel. This signal arrives at the

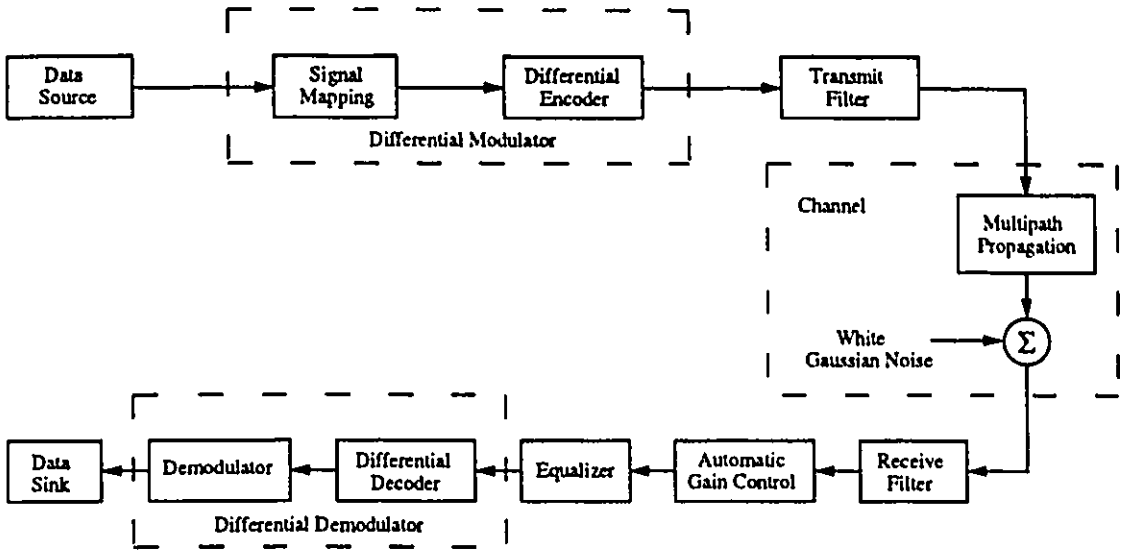

Figure 4.1: Communication system model.

receiving end, after being propagated through the indoor wireless channel, and having white Gaussian noise added to it. In order to combat the intersymbol interference caused by the multipath propagation, an adaptive equalizer is used to process the signal after passing through the receiving filter. An automatic gain control (AGC) device is used in front of the equalizer to amplify the received signal so that it can be restored to its unfaded power level. At the demodulator, the signal is differentially decoded and then further demodulated in an attempt to reconstruct the original signal from the source. The Viterbi decoding technique is employed for the trellis coded signals.

4.2 Transmit and Receive Filters

The digital communication channel is characterized as a band-limited channel. To transmit signals with a symbol duration of T through this channel without inter-symbol interference, a square root raised cosine filter is used for symbol shaping. Its

frequency response has the following form [Proak89]:

$$G(f) = \begin{cases} \sqrt{T} & 0 \le |f| \le \frac{1-\alpha}{2T} \\ \sqrt{\frac{T}{2}\{1 - \sin[\pi\frac{T}{\alpha}(|f| - \frac{1}{2T})]\}} & \frac{1-\alpha}{2T} \le |f| \le \frac{1+\alpha}{2T} \\ 0 & |f| > \frac{1+\alpha}{2T}, \end{cases} \tag{4.1}$$

where α is the raised-cosine roll-off factor whose value is between 0 and 1. The roll-off factor is chosen to be 0.35 in our simulations. The square root raised cosine filter can alternately be shown [Chen91] in terms of its impulse response $g(t)$ expressed as:

$$g(t) = \begin{cases} 1 - \alpha + 4\frac{\alpha}{\pi} & t = 0 \\ \frac{\alpha}{\sqrt{2}}\left[(1 + \frac{2}{\pi})\sin(\frac{\pi}{4\alpha}) + (1 - \frac{2}{\pi})\cos(\frac{\pi}{4\alpha})\right] & t = \pm T/4\alpha \\ \frac{\sin[\pi(1-\alpha)\frac{t}{T}] + 4\alpha\frac{t}{T}\cos[\pi(1+\alpha)\frac{t}{T}]}{\pi\frac{t}{T}[1-(4\alpha\frac{t}{T})^2]} & \text{for all other } t. \end{cases} \tag{4.2}$$

Figure 4.2 shows the frequency response and time impulse response of a square root raised cosine filter. The time axis is normalized to the value of the symbol duration T, and the frequency axis is normalized to the sampling rate $1/T$.

The transmit and receive filters both use the same square root raised cosine filter. The overall transfer function $Hrc(f)$ of the two square root raised cosine filters has a raised cosine spectrum:

$$Hrc(f) = \begin{cases} T & 0 \le |f| \le (1-\alpha)/(2T) \\ \frac{T}{2}\left[1 - \sin\pi T(|f| - \frac{1}{2T})/\alpha\right], & \frac{1}{2T}(1-\alpha) \le |f| \le \frac{1}{2T}(1+\alpha) \\ 0 & |f| > \frac{1}{2T}(1+\alpha). \end{cases} \tag{4.3}$$

The time impulse corresponding to this spectrum is:

$$h_{rc}(t) = \frac{\sin \pi t/T}{\pi t/T}\frac{\cos \alpha\pi t/T}{1 - 4\alpha^2 t^2/T^2}, \tag{4.4}$$

which meets the Nyquist criteria for zero intersymbol interference [Proak89] (i.e., $h_{rc}(t) = 0$ for $t = nT$). The time impulse response of a raised cosine filter with $\alpha = 0.35$ is shown in Figure 4.3. The time is normalized by the symbol duration T.

After being shaped by the transmit filter, the signal is transmitted through an indoor wireless multipath channel and white Gaussian noise is added to it. At

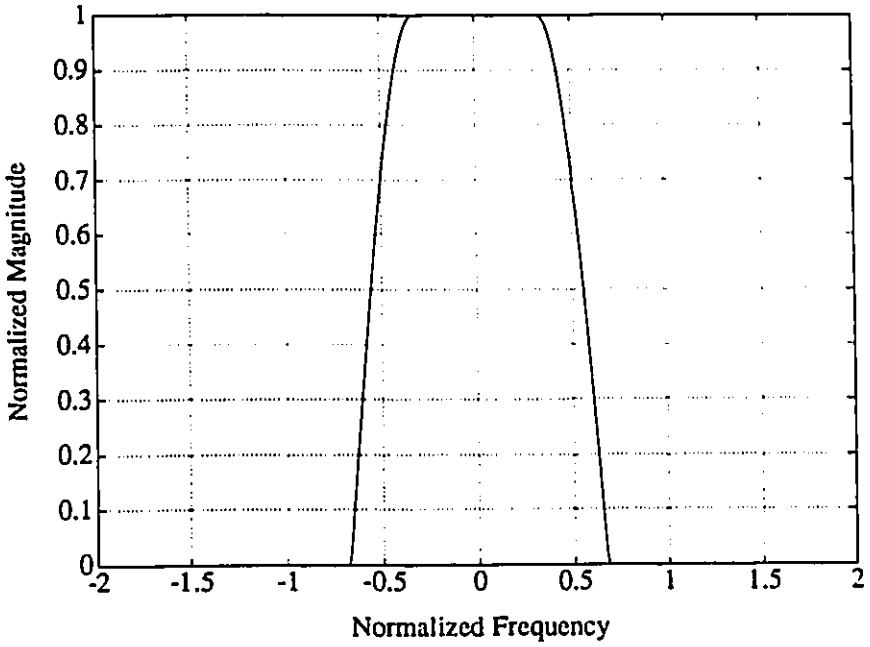

(a)

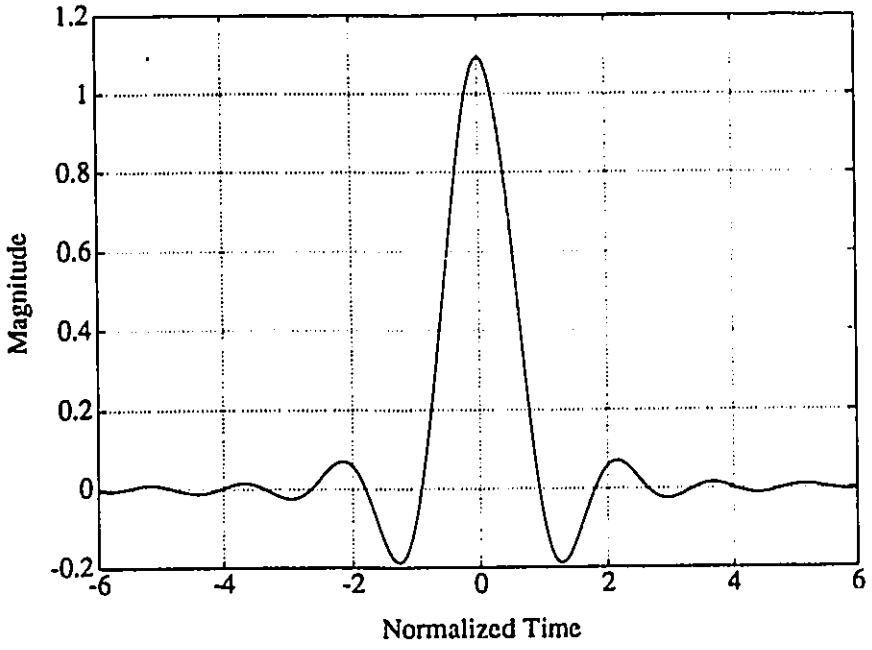

(b)

Figure 4.2: Square root raised cosine filter (roll-off factor $\alpha = 0.35$) (a) frequency response; (b) time impulse response.

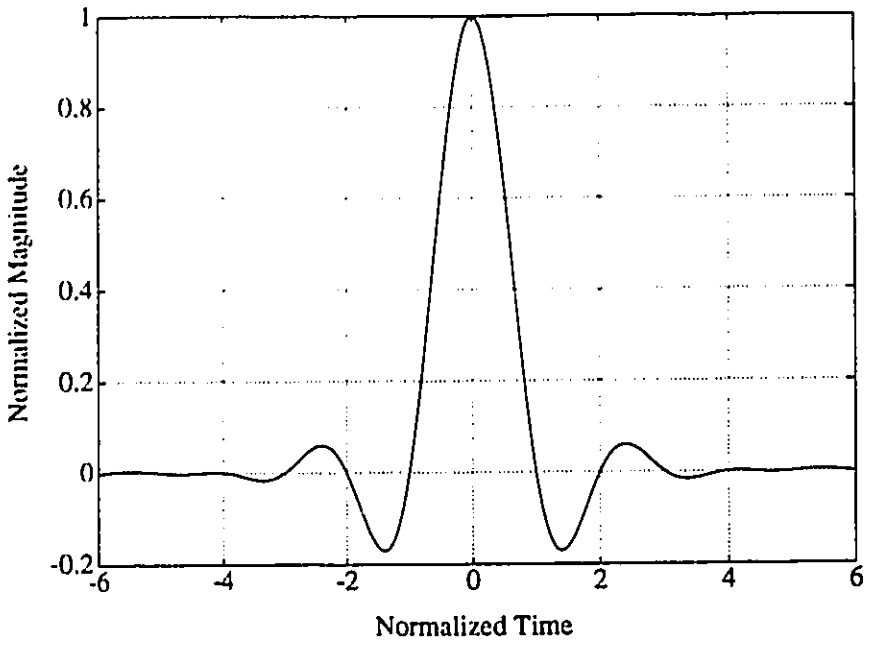

Figure 4.3: Time impulse response of a raised cosine filter (roll-off factor $\alpha = 0.35$).

the receiving end, the signal-to-noise ratio (SNR) which is used in the simulation to calculate the power of the AWGN, is defined as

$$\text{SNR} = \frac{E_s}{E_n}, \tag{4.5}$$

where E_s is the received signal power for each symbol with k information bits, and E_n is the power of the AWGN. E_s is expressed as

$$E_s = E\sum_{l=0}^{L} h_l^2, \tag{4.6}$$

where E is the transmitted signal power per symbol, and h_l represents the complex channel tap coefficients. Since E_s consists of the signal (Eh_0^2) and the set of interferences ($E\sum_{l=1}^{L} h_l^2$), SNR is sometime referred to as the signal plus interference to noise ratio (S+I)/N. However, we will simply use the term SNR instead of (S+I)/N. The average power of the lowpass white noise, with a spectral density of N_0 for $|f| \leq W/2$, can be calculated by

$$\sigma_n^2 = \int_{-W/2}^{+W/2} N_0 df = N_0 W, \tag{4.7}$$

where W is the bandwidth of the bandlimited white noise. W is equal to the reciprocal of twice the signal duration T_s. In the simulations, T_s is set to 1, and therefore

$\sigma_n^2 = N_0/2$, which is equal to the variance given in [Proak89] for each element of the AWGN. Each element of the AWGN is individually added to the corresponding component of the received signal for the simulations. The complex received signal $r(t)$ can be expressed as

$$r(t) = r_I(t) + jr_Q(t). \tag{4.8}$$

Thus, the expression for the AWGN, $z(t)$, can also be written as

$$z(t) = n_I(t) + jn_Q(t). \tag{4.9}$$

Since the power of each component ($n_I(t)$ or $n_Q(t)$) of the noise is $\sigma_n^2 = N_0/2$, the total power of AWGN is $E_n = 2\sigma_n^2 = N_0$. By modifying Equation (4.5), σ_n^2 can be expressed as

$$\sigma_n^2 = \frac{E\sum_{l=0}^{L} h_l}{2E_s/N_0}. \tag{4.10}$$

If we use the bit energy E_b to represent the k-bit information symbol energy, Equation (4.10) can be modified to

$$\sigma_n^2 = \frac{E\sum_{l=0}^{L} h_l}{2kE_b/N_0}. \tag{4.11}$$

In this thesis, the bit error rate (BER) is plotted against the SNR (per bit) in dB for the performance evaluations.

4.3 Differential Quadrature Phase Shift Keying Modulation

4.3.1 DQPSK in Additive White Gaussian Channels

M-ary phase-shift keying (MPSK) is a bandwidth-efficient digital signaling technique. The data rate can increase logarithmically with an increase in the number of signal waveforms, although higher SNRs per bit are needed to maintain the same error rate. The MPSK signal waveforms can be represented [Proak89] as:

$$s_k = Re\{g(t)\ \exp[j(2\pi f_c t + \frac{2\pi}{M}(k-1) + \lambda]\}, \quad k = 1, 2, ..., M, \quad 0 \le t \le T, \tag{4.12}$$

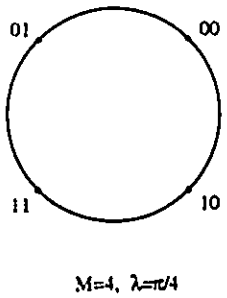

Figure 4.4: QPSK signal constellation.

where the pulse $g(t)$ has a square root raised cosine spectrum, and λ is equal to 0 or $\pi/4$ for QPSK, and 0 or $\pi/8$ for 8PSK.

Using the Gray encoding method, one of $M = 2^k$ combinations of k-bit information data can be mapped onto one of M-ary phase signals. This mapping ensures that adjacent signal phases differ by exactly one binary digit. The QPSK signal constellation with $\lambda = \pi/4$ is given in Figure 4.4.

There are two main demodulation schemes: coherent demodulation and noncoherent demodulation. The former requires a complex carrier synchronization technique for estimating a carrier phase in order to compensate for the channel phase shift. On the other hand, the later does not require estimation of the carrier phase during demodulation of the received signal. With coherent demodulation, a system with QPSK modulation is referred to as a CQPSK system. However, if the system uses noncoherent demodulation, the QPSK signal must be differentially encoded at the transmitting end: this system is called a DQPSK system. In this thesis, noncoherent demodulation is used for communication system analysis.

The following is a description of a simple differential encoder. In contrast with absolute phase encoding, differential encoders utilize phase differences between successive signal transmissions to encode a signal. For a QPSK signal, if the signal bearing information data 00 is transmitted by a zero phase shift relative to the previous signal phase, then the relative phase shifts between successive signals are 90^0,

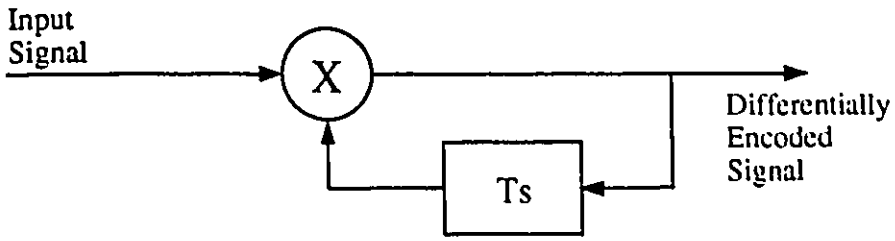

Figure 4.5: Block diagram of a differential encoder.

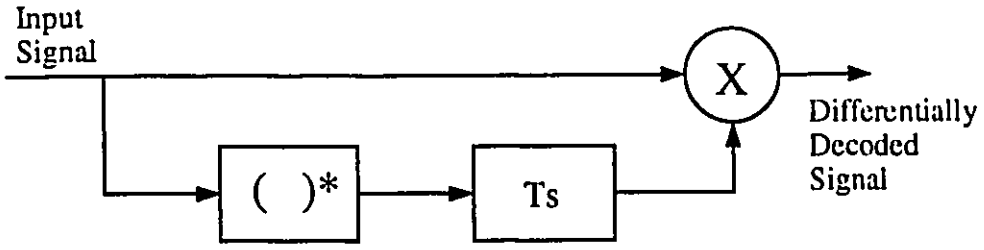

Figure 4.6: Block diagram of a differential decoder.

180^0, and -90^0 corresponding to the signals with the information data 01, 11, and 10, respectively. The implementation of a differential decoder can be realized simply by multiplying the present signal with the complex conjugate of the previous signal. The resulting phase difference can be used to reconstruct the absolute phase of the original signal. Differential encoder and decoder block diagrams are shown in Figure 4.5 and Figure 4.6, respectively.

The average bit error probability for CQPSK is expressed [Proak89] as:

$$P_{eQPSK} = Q\left(\sqrt{2E_b/N_0}\right), \tag{4.13}$$

where E_b/N_0 is the signal-to-noise ratio (SNR) per bit. For a DQPSK system, the average bit error probability is given [Ha90] as:

$$P_{eDQPSK} \approx Q\left(\sqrt{\frac{2E_b}{N_0}(4\sin^2\frac{\pi}{8})}\right), \tag{4.14}$$

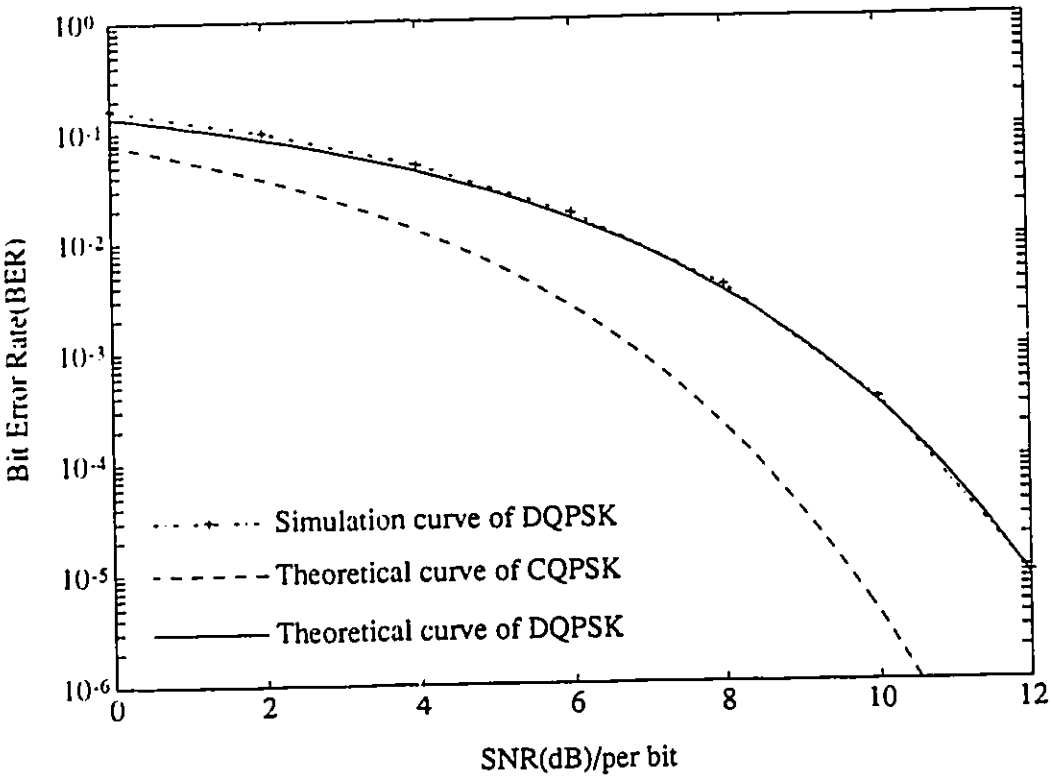

Figure 4.7: Probability of average bit error performance for DQPSK in AWGN channel.

where $Q(x)$ is the Gaussian integral function (Markum function) and is equal to:

$$Q(x) = \frac{1}{2}\text{erfc}\left(\frac{x}{\sqrt{2}}\right). \tag{4.15}$$

Noncoherent demodulation is considered in this thesis for communication system analysis. The results of a simulation for a DQPSK system over the AWGN channel are shown in Figure 4.7. Since these results indicate that the performance is well fitted to the theoretical curve as given in Equation (4.14), therefore the system is properly calibrated. Furthermore, the figure shows that at error probabilities of $P_e \leq 10^{-3}$, the difference in SNR between coherent QPSK and noncoherent QPSK is larger than 2 dB. As expected, the DQPSK system with its relatively simple implementation has worse performance as compared to CQPSK.

4.3.2 DQPSK in Indoor Wireless Channels

The BER performance of a DQPSK system changes with different indoor wireless channel realizations, since the channels have different power profiles that determine distinct maximum delay spreads and rms delay spreads. In this section, it will be shown that the rms delay spread of the channel is one of the main factors affecting the BER performance, as mentioned in [Cox75].

A set of 1000 constant channel impulse responses is used to evaluate BER performance versus rms delay spread (Figure 4.8). The channels are divided into several groups according to their rms delay spreads (in ns). The average BER of each rms delay spread group is calculated by summing the BERs and then dividing by the total number of the channels in the group. Each group covers a range of 5 ns; the first group begins at 12.5 ns and the last group begins at 82.5 ns. The average BER is plotted at the center of each group (i.e. 15 ns, 20 ns ,..., 85 ns). Figure 4.8 shows how the average BER performance at SNR = 6 dB is affected by the rms delay spreads of indoor wireless channels. The BER tends to increase with the rms delay spread, although there are some irregularities on the curve. Since the rms delay spread is not the only factor that affects the BER performance, the curve exhibits non-monotonic behavior.

4.4 Trellis Coded Modulation

In digital communications, error control coding techniques are widely used to provide efficient and reliable signal transmission. If blocks of k-bit information are encoded into blocks of n-bit coded symbols ($n > k$), the code rate is defined as the ratio $R_c = k/n$. For a binary digital information transmission rate of R $bits/s$, the coded bit rate must be R/R_c $bits/s$ in order for the coded system to maintain the same information transmission rate as the uncoded system. In other words, the coded system requires bandwidth expansion by a factor of $1/R_c$ to have the same speed of

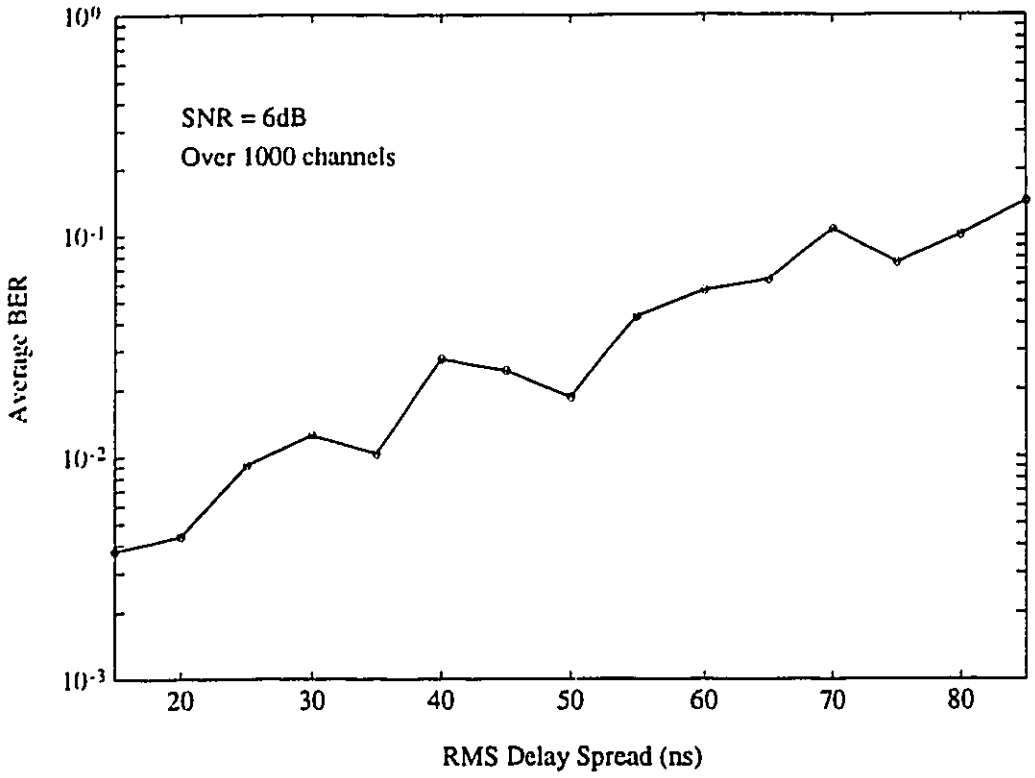

Figure 4.8: Average BER Performance versus rms delay spreads with QPSK over 1000 indoor wireless channel impulse responses.

information transmission as the uncoded system. Trellis coded modulation (TCM), which was introduced by [Ung82], improves error performance without sacrificing data rate or requiring more bandwidth. In this thesis, 4-state and 8-state 8PSK-based TCMs are both used as the coded modulation schemes for communication system performance analysis.

The TCMs use the coded 8PSK waveform that carries the same number of information bits as the 4PSK uncoded waveform without requiring more bandwidth. The innovative aspect of TCM is the concept that convolutional encoding and modulation should not be treated as separate entities, but rather, as a unique operation [Big91]. The TCM system shown in Figure 4.9 is a 4-state 8PSK Ungerboeck code. The information data X_2X_1 is encoded into the coded data $Y_3Y_2Y_1$. This code consists of a linear rate 2/3 convolutional encoder (see Figure 4.9(a)) with $\nu = 2$ binary storages representing 2^ν possible states S_1S_2. The 8PSK signal mapping is shown in

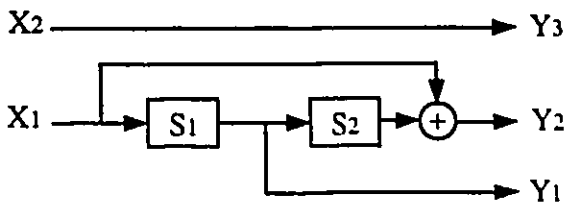

(a)

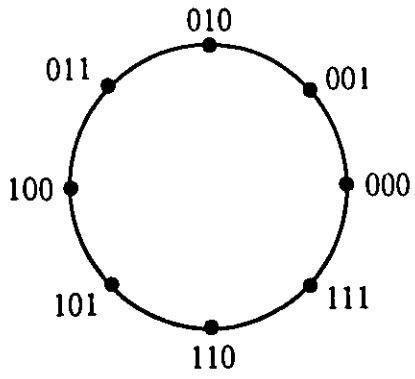

(b)

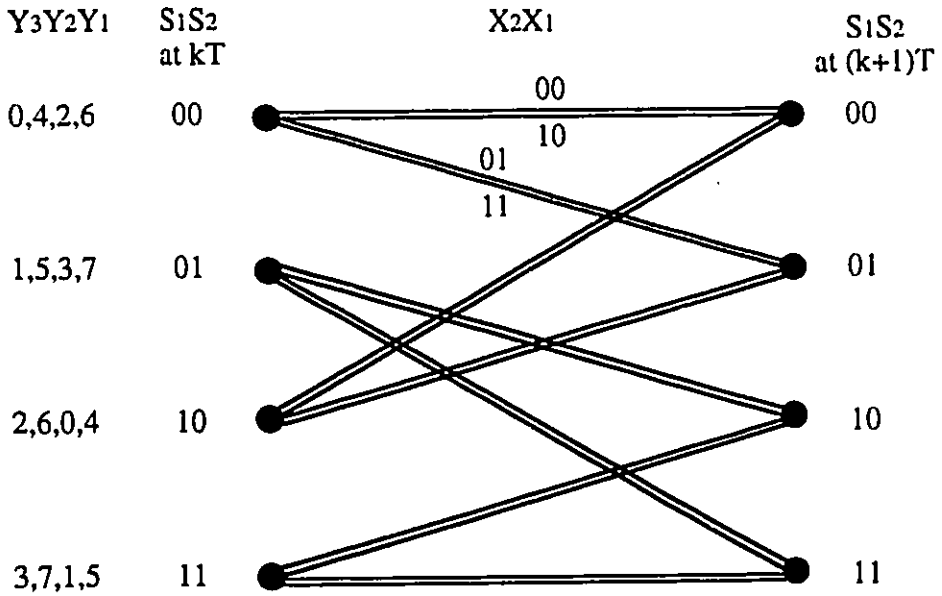

(c)

Figure 4.9: Four-state Ungerboeck code. (a) Encoder; (b) Mapping; (c) Trellis.

Figure 4.9(b) and the trellis diagram is presented in Figure 4.9(c). The parameter ν is also called the code constraint length. For a TCM convolutional encoder with a rate of k/n, the number of possible transitions from each state to a successor state is 2^k in the trellis structure. The 4-state TCM code, which has the trellis structure of parallel transitions shown in Figure 4.9(a), was demonstrated by [Pai91] to have better performance than the 4-state Ungerboeck code with distinct transitions over both AWGN and dispersive channels. Thus, only 4-state 8PSK TCM with parallel transitions is used to evaluate system performance. The 8-state 8PSK trellis code with distinct transitions is shown in Figure 4.10. Figure 4.10 (a) and (b) show a 2/3 convolutional encoder with three storage cells ($\nu = 3$) representing 2^ν states and its trellis structure.

The optimization of the TCM design is based on Euclidean distances rather than on Hamming distances which is the minimum distance between any two code words. TCM increases the free Euclidean distance d_{free} by doubling the coded signals, so that the redundancy enlarges the Euclidean distance $d(a_n, a_n^{'})$ between coded signals $\{a_n\}$ and $\{a_n^{'}\}$. The free Euclidean distance is denoted [Ung82] by

$$d_{free} = \min_{\{a_n\} \neq \{a_n^{'}\}} \left[\sum_n d^2(a_n, a_n^{'}) \right]^{1/2} \tag{4.16}$$

TCM uses the "set partitioning" rule to map coded signals in order to maximize d_{free}. The asymptotic coding gain of TCM can be computed as

$$\gamma = \frac{d_{free}^2 / E}{d_{min}^2 / E^{'}}, \tag{4.17}$$

where E and $E^{'}$ are the average energies spent for transmission of coded and uncoded symbols respectively. In [Ung82], coherent 4-state and 8-state 8PSK TCMs achieve gains of 3 dB and 3.6 dB respectively as compared to the uncoded QPSK modulation scheme over a band-limited AWGN channel.

The purpose of maximum likelihood soft decoding, which is used for the TCMs decoding process, is to find the most likely signal sequence corresponding to the original unaltered information sequence. This decoding process is implemented with the

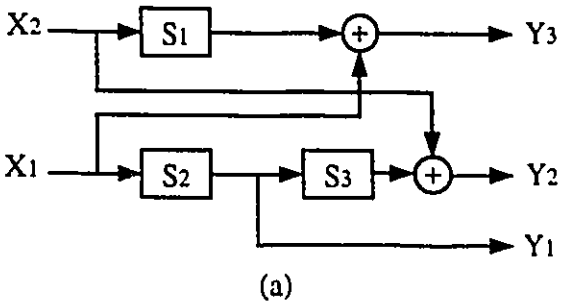

(a)

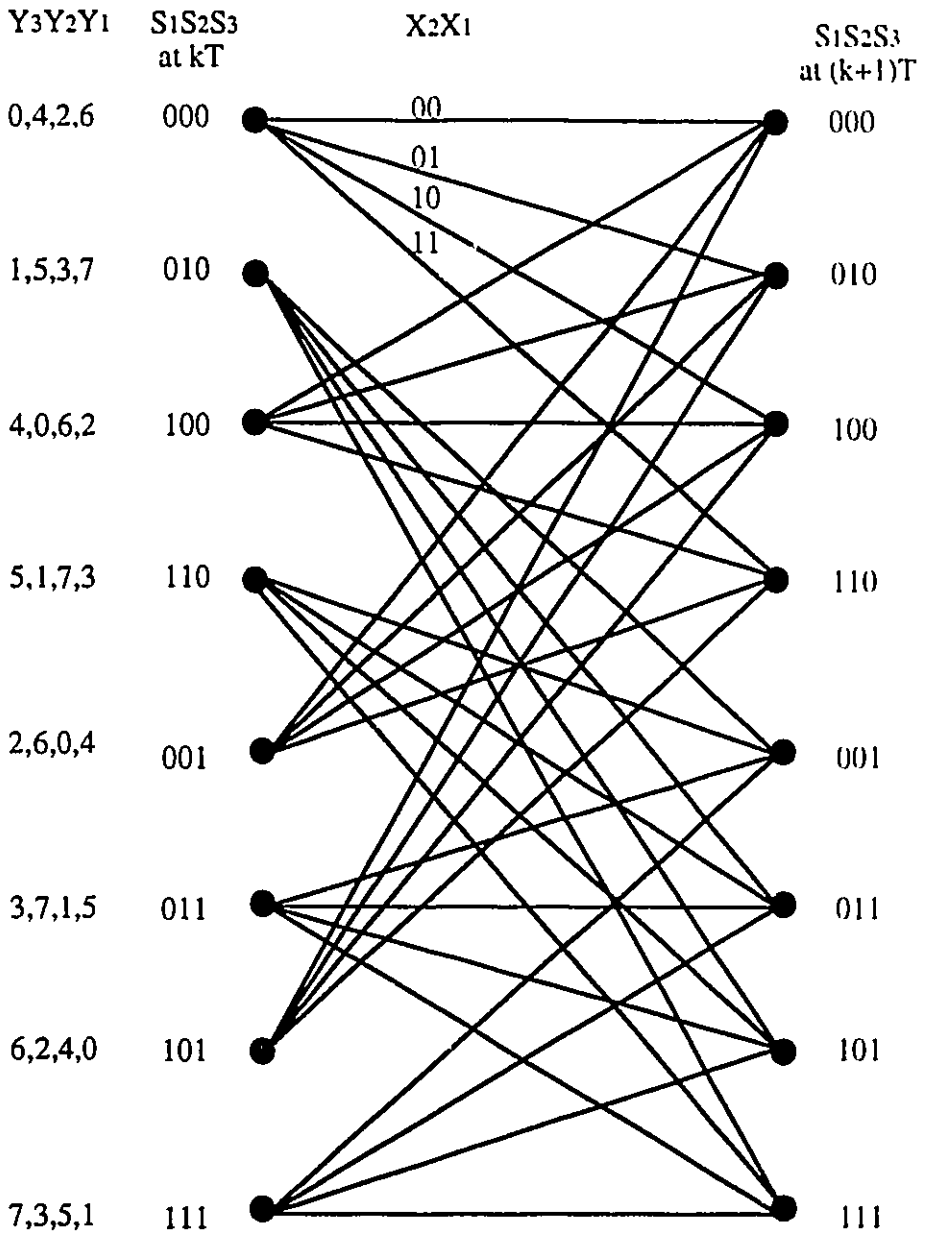

(b)

Figure 4.10: Eight-state Ungerboeck code. (a) Encoder; (b) Trellis.

Viterbi algorithm. The Viterbi decoding algorithm [For73] computes minimum distance metrics, which are optimum metrics for AWGN channels, but are sub-optimum metrics for fading channels [Big91]. Although some work has been done [Zeh92] to explore the optimum metrics for fading channels, we use the sub-optimum metric computation in our simulations for indoor wireless fading channels, since they are easier to implement. The Viterbi algorithm can be summarized as follows:

1. For any state l of 2^ν states, 2^k branch metrics are computed by Euclidean distances between a received signal $\mathbf{r}_j$ and each possible set of transmitted signals $\mathbf{v}_{li_j}$ $(1 \leq i \leq 2^k)$ at time j, expressed as

$$d(\mathbf{r}_j, \mathbf{v}_{li_j}) = \sqrt{|\mathbf{r}_j - \mathbf{v}_{li_j}|^2}, \qquad 1 \leq i \leq 2^k, \quad 1 \leq l \leq 2^\nu. \tag{4.18}$$

2. Choose only a survivor branch with the minimum cumulative metric at each state by

$$\lambda_{lj} = \min_i \{d(\mathbf{r}_j, \mathbf{v}_{li_j}) + \lambda_{(j-1)\xi}\} \qquad 1 \leq i \leq 2^k, \quad 1 \leq l, \xi \leq 2^\nu, \tag{4.19}$$

   where $\lambda_{(j-1)\xi}$ (equal to zero when $(j-1) < 0$) is the cumulative metric at the previous state ξ from which the survivor branch connects to the current working state.

3. Considering a decoding depth $D = 6\nu$, the decoding sequence decision can be made at time $(j - D)$ for $j \geq D$, by choosing the path with the minimum cumulative metric of $\min_l\{\lambda_{lj}\}$ at time j.

The decoding depth $D = 6\nu$ is used for simulations (it was shown in [Pai91] that this value yields a reliable performance).

As for the QPSK modulation scheme, differential demodulation can be used with 8PSK TCM in order to simplify the implementation by ignoring carrier phase estimation. A differential encoder is thus provided following the 8PSK TCM encoder in our communication systems. The simulation results of BER performance over an

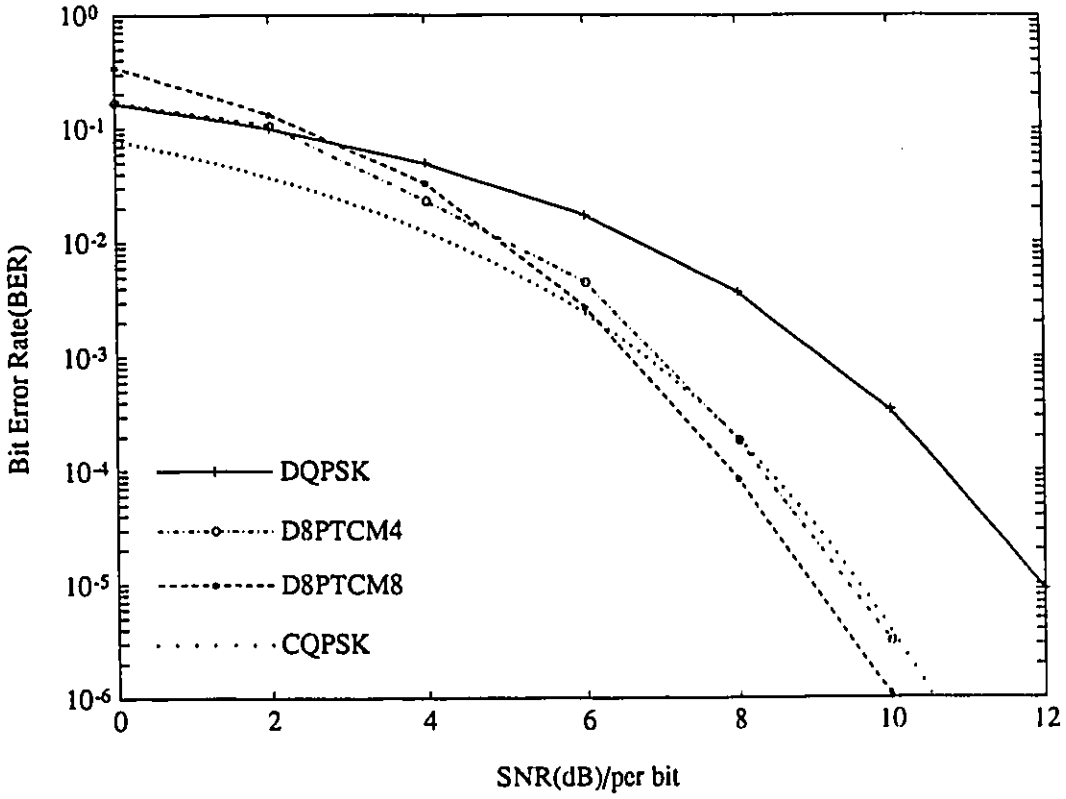

Figure 4.11: BER performance for D8PTCM4 and D8PTCM8 in an AWGN channel.

AWGN channel for both 4-state and 8-state 8PSK TCMs with differential demodulation (D8PTCM4 and D8PTCM8), are shown in Figure 4.11. The figure demonstrates that both D8PTCM4 and D8PTCM8 systems give better BER performances as compared with the DQPSK system when SNRs are greater than 3 dB. When SNRs are greater than 8 dB, the D8PTCM4 system outperforms the CQPSK system, and the D8PTCM8 system also outperforms the CQPSK system when SNRs are greater than 6 dB.

4.5 Conclusion

In this chapter, each component in our communication system block diagram was described. Then, the BER performances for DQPSK and D8PTCM modulation schemes operating over AWGN channels were discussed. It was shown that the rms delay spread causes a significant degradation of the BER performance of indoor wireless communication systems. Finally, it was shown that D8PTCM8 outperforms D8PTCM4, DQPSK, and CQPSK for large SNRs.

Chapter 5

Simulation Results and Discussion

The computer simulation models for the communication systems with quadrature phase shift keying (DQPSK), and 4-state and 8-state 8PSK trellis coded modulations (D8PTCM4, D8PTCM8) using differential encoding have been described in the previous chapter. The performance results of the DQPSK and D8PTCM modulations over both fixed and time varying channels are presented in this chapter.

Three different types of adaptive equalizers (linear equalizer (LE), $T/2$ fractionally spaced linear equalizer (FSE), and decision feedback equalizer (DFE)) are applied to the DQPSK system. For D8PTCM schemes, the performance of both LE and DFE equalizers are investigated. Two algorithms are used for optimizing the tap-weights of equalizers, namely the least-mean-square (LMS) algorithm for all three types of equalizers and the recursive least-squares (RLS) algorithm only for the DFE. The effects of the different equalizers on the two communication systems, DQPSK and D8PTCM, are determined from a comparison of the simulation performance results. Lastly, the convergence properties of the equalizers are examined. In order to obtain reasonable confidence in the results, the simulations run until at least 200 errors have been detected.

Here, we use confidence intervals to describe the accuracy of our simulation results. According to the normal approximation in [Jer92], the total number of the

transmitted bits should be $10^n/P_b$, $n = 1, 2, 3, \ldots$ In the following example, $n = 2$. For a given signal-to-noise-ratio with a bit error probability P_b of 10^{-4}, the total number of bits sent should be at least 10^6 in order to achieve a 95% confidence interval of about $(0.8P_b, 1.25P_b)$. However, if $n = 1$, then the total number of bits sent is 10^5, and the resulting 95% confidence interval is about $(0.55P_b, 1.8P_b)$ for the same bit error probability as in the previous example. Since the total number of bits sent for the DQPSK modulation scheme is 10^7, and for the D8PTCM modulation schemes, 2×10^6 bits are sent, a 95% or better confidence interval of $(0.8P_b, 1.25P_b)$ is achieved for $P_b = 10^{-4}$.

This analysis provides only approximate confidence intervals because errors did not occur randomly in our simulations. For a more accurate set of confidence intervals, correlated error estimation should be used.

5.1 Performance of DQPSK with Adaptive Equalizers

The adaptive linear equalizer, the T/2 fractionally spaced equalizer and the decision feedback equalizer are used in the simulations to determine their effectiveness in negating the intersymbol interference (ISI) in the DQPSK communication system. The simulations include both the fixed and time varying channels. Generated according to Saleh & Valenzuela's channel model [Sal87(2)] with different random generator seeds, the impulse responses of the channel are truncated to the tapped delay line channel. The tap-coefficients for the fixed channel do not change during the simulation. For the time varying channel, the amplitudes of the tap-coefficients change as a function of time and follow a Rayleigh distribution. The corresponding phases are uniformly distributed.

The bit error rate (BER) for the simulation is computed by

$$P_e = \frac{\text{total number of received bits in error}}{\text{total number of sent bits}} \tag{5.1}$$

Two methods can be used to count the total number of bit errors during the simulations. For the first method, the program terminates for each chosen signal-to-noise ratio, when the total number of bit error events being counted at the output of the equalizer reaches 200. Obviously, the total number of bits sent at the transmitting end for each SNR is different, since higher SNRs require more transmitted bits to obtain the same number of receiving end errors as for the case of lower SNRs. For the second method, the total number of bits that are sent for each SNR is identical. Thus, simulations that use the second method will not be stopped until all the transmitted bits have passed through each stage of the simulation. The first method is used for the simulation of fixed channels, since it greatly reduces the simulation time for low SNRs while yielding simulation results that are almost identical to those produced by the second method. On the other hand, the time varying channel requires the second method so that the simulation process can cover at least one whole fade of the channel. These two simulation methods are compared further using simulation results in Section 5.1.1.

5.1.1 DQPSK Performance with Adaptive Linear Equalizers

Figure 5.1 shows BER versus SNR (per bit) of the DQPSK modulation system using the adaptive linear equalizer (LE) with the LMS algorithm over three fixed channels with channel seeds: 52, 55 and 45; as well as the corresponding time varying channels. The notation DQPSK_LE7_F4(55) is used to represent a communication system in which DQPSK is the modulation scheme, LE7 is a linear equalizer with seven taps, and F4 or T4 indicates the presence of either a fixed channel or a time varying channel, respectively, with four taps. The channel seed appears inside the parentheses. The channel seed, the rms (root mean square) delay spread σ, and the maximum delay

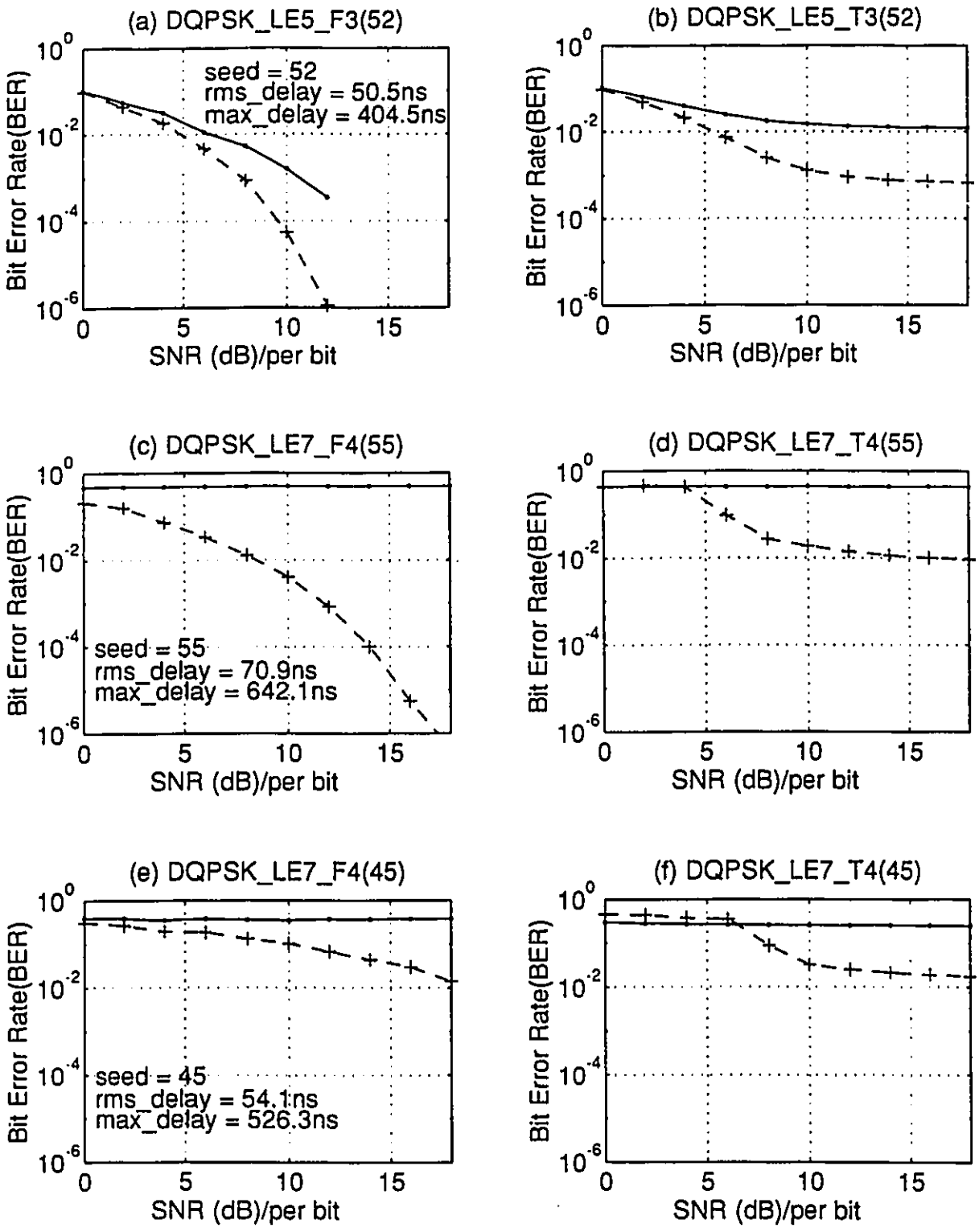

Figure 5.1: Performance of the DQPSK system with the LE (a) (c) (e) over fixed channels and (b) (d) (f) over the corresponding time varying channels (the dashed and solid lines represent the performance with and without the equalizer, respectively).

spread for each channel are individually represented as *seed*, *rms_delay* and *max_delay* in the figure. The total number of the transmitted bits for the simulation over the time varying channels is 10^7.

The channel having the seed 52 yields the best performance results as compared to the two other channels with different seeds regardless of the presence of the adaptive LE. In contrast, the systems with a channel seed of 45 consistently show the worst performance. Without using an LE, the channels with seeds of 55 and 45 are unacceptable since the BERs for these channels are about 0.3. The results for the time varying channels shown in Figures 5.1 (b), (d) and (f) are consistly worse than the corresponding fixed channels given in Figures 5.1 (a), (c) and (e).

In Figures 5.1 (e) and (f), we notice that the BER for the system with an LE is worse than that for the system without an LE over the time varying channel at lower SNRs, but not for the fixed channel. The main reason for this result is that the LE using the LMS algorithm cannot track the changes of the time varying channel, even if the value of step size is changed. This inability to track the changes results in the large error floors in Figures 5.1 (b), (d) and (f)). The number of equalizer taps is equal to the number of channel taps plus two in order to obtain the best performances. Since the time varying channel model more accurately represents the practical transmission medium than the fixed channel model for indoor wireless communications, therefore the simulation results shown in Figure 5.1 (b), (d) and (f) are considered to be more accurate than those of Figure 5.1 (a), (c) and (e) for indoor wireless communications.

As mentioned earlier, simulations for the fixed channel use the first simulation method, whereas the time varying channel uses the second method; in the first simulation method, named SM1, simulations are stopped when the number of errors is greater or equal to 200, while the second method SM2 allows simulations to continue until all of the transmitted bits are received and detected after the equalizer. Figures 5.2, 5.3 and 5.4 compare the simulation results of both methods for each channel and equalizer combination. For SM2, the total number of transmitted bits

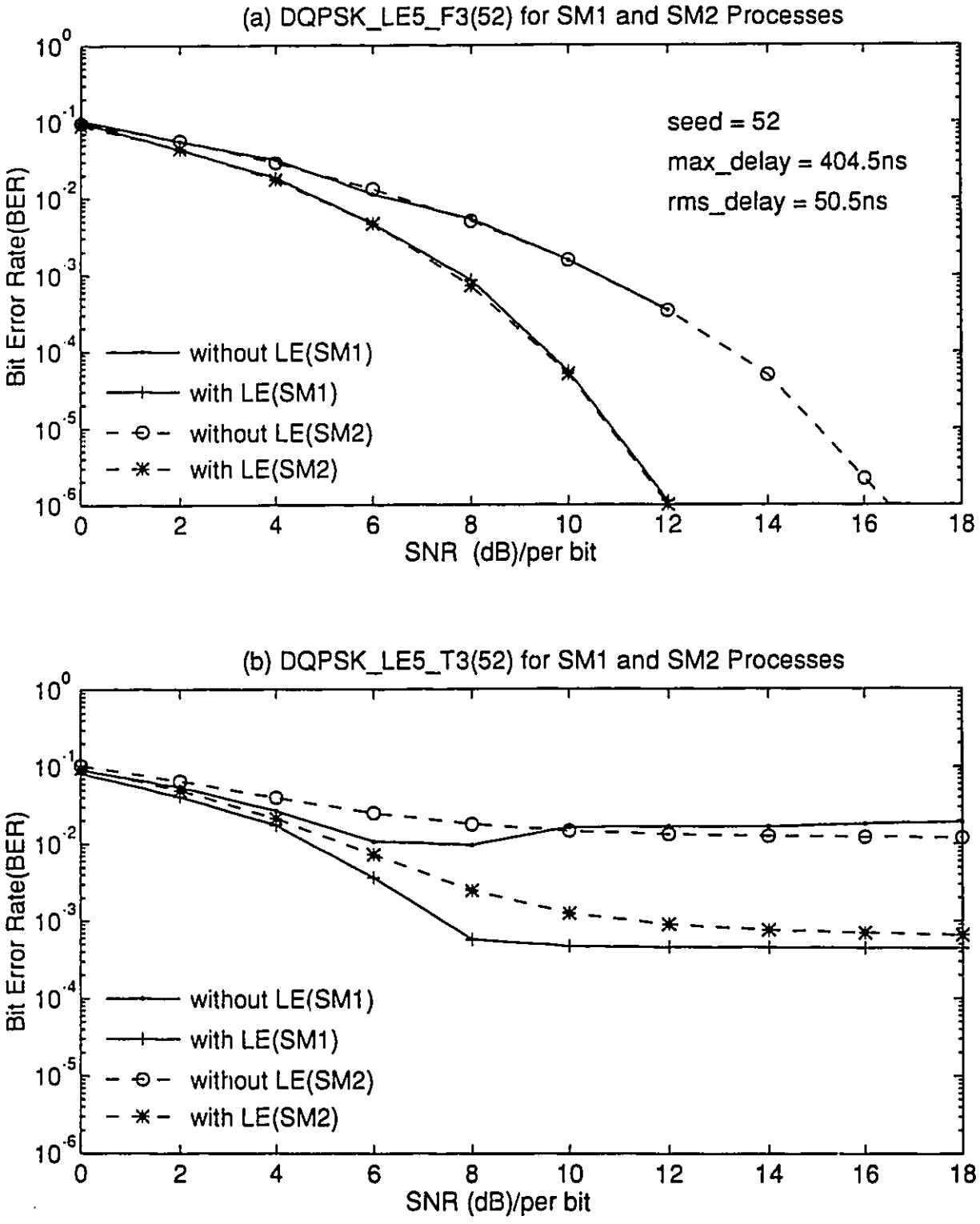

Figure 5.2: Performance of the DQPSK system with the LE for two kinds of simulation methods SM1 (solid line) and SM2 (dashed line) over (a) a fixed channel and (b) the corresponding time varying channel.

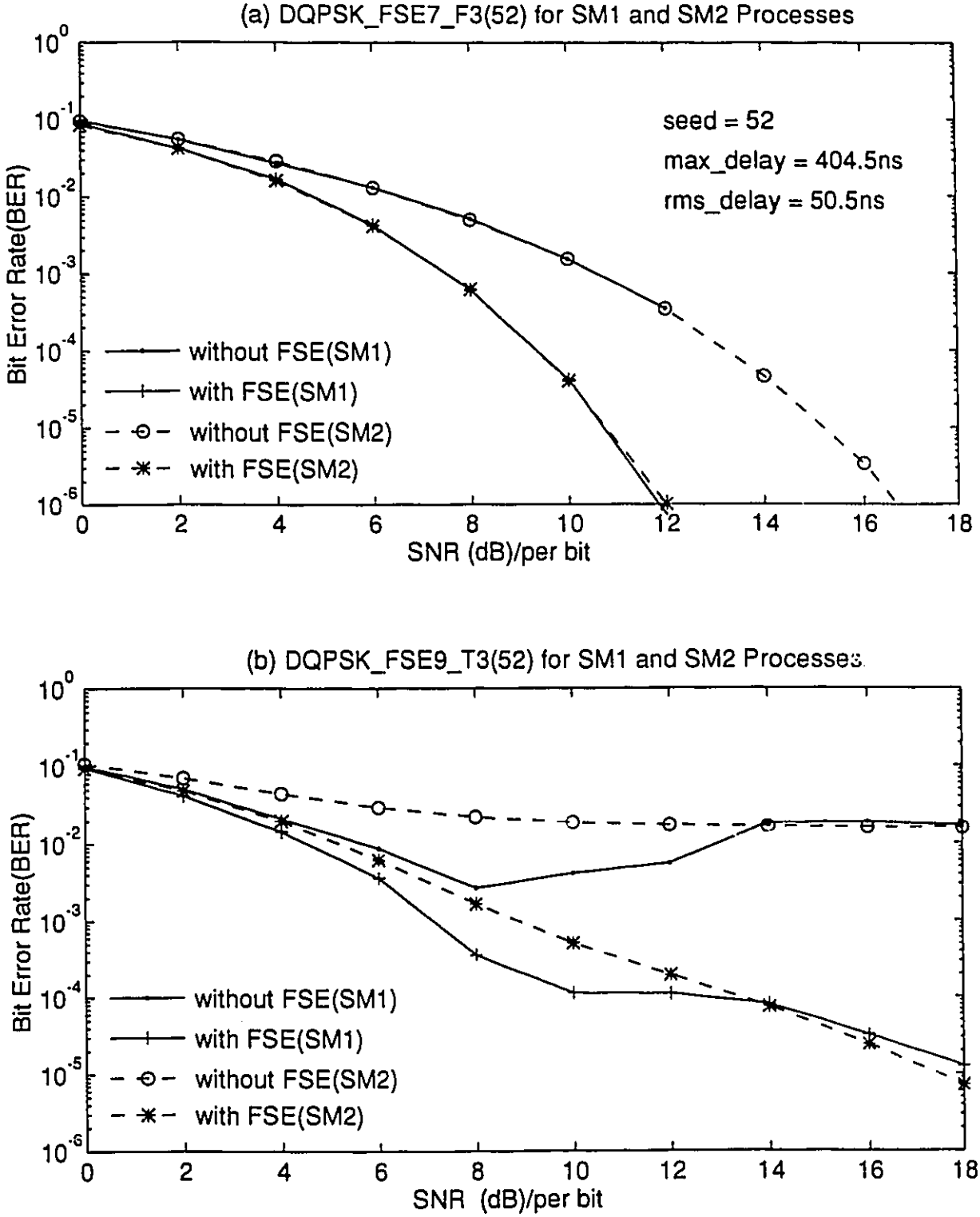

Figure 5.3: Performance of the DQPSK system with the FSE for two kinds of simulation methods SM1 and SM2 (dashed line) over (a) a fixed channel and (b) the corresponding time varying channel.

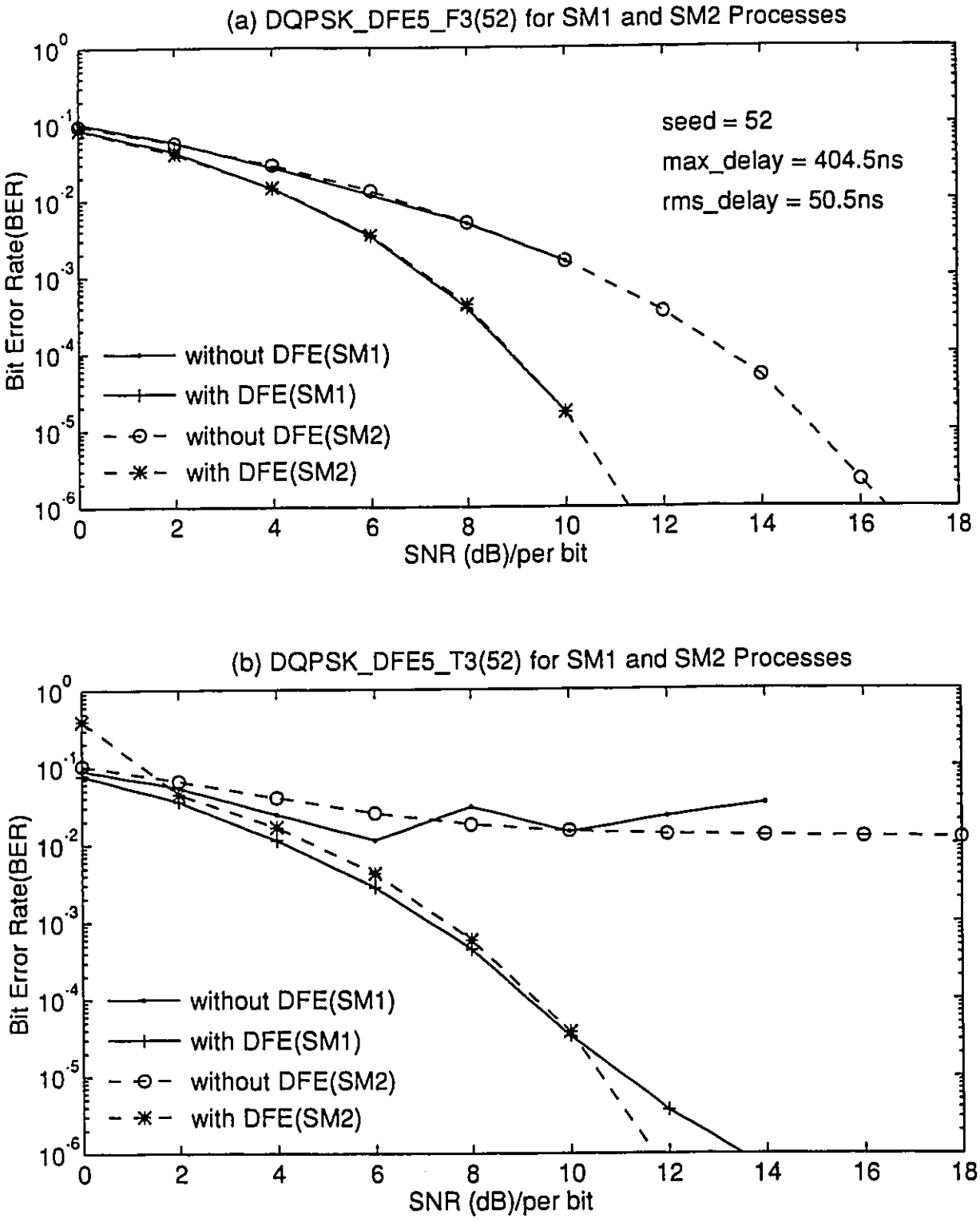

Figure 5.4: Performance of the DQPSK system with the DFE for two kinds of simulation methods SM1 (solid line) and SM2 (dashed line) over (a) a fixed channel and (b) the corresponding time varying channel.

is 10^7.

When we consider a user walking at a regular pace of 5 km/h, the Doppler frequency is about 7 Hz for DQPSK/D8PTCM systems at carrier frequency of 1.5 GHz. In other words, the total number of fades encountered during the simulation process is only seven using the SM2 method. In this thesis, the minimum value for the number of transmitted bits in SM2 has been chosen so that the simulation process covers at least one whole channel fade.

Figure 5.2 shows the results of DQPSK with LE over the (a) fixed channel and (b) time varying channel. Little difference exists between the results from SM1 and SM2 over the fixed channel. On the other hand, large differences can be seen for the results from the corresponding time varying channel. Figures 5.3 and 5.4 show the results for a $T/2$ fractionally spaced equalizer (FSE) and a decision feedback equalizer (DFE), respectively. Again both simulation methods show almost identical results for the fixed channel and results that do not match for the time varying channel. Based on these findings, simulations over a fixed channel are carried out with the first method SM1 and simulations over a time varying channel are carried out with the second method SM2.

5.1.2 DQPSK Performance with $T/2$ Fractionally Spaced Linear Equalizers

In Section 3.2, it was mentioned that a $T/2$ fractionally spaced linear equalizer (FSE) leads to better performances than a conventional linear equalizer (LE), since the FSE can eliminate phase distortion. Another advantage obtained by using the FSE is that data transmission can begin with an arbitrary sampling phase, since the FSE synthesizes the correct delay during adaptation.

Figure 5.5 shows the performance of the DQPSK system with the FSE over three different fixed channels (with seeds 52, 55 and 45) and their corresponding

time varying channels. The channel parameters are also shown in the figure. The total number of transmitted bits is 10^7 for the SM2 process. DQPSK_FSE7_F3(52) represents the DQPSK modulation system with a 7-tap FSE simulated over a fixed (F) channel with three taps and the seed 52. The conventional LE taps are spaced at the symbol rate, and those of the $T/2$ FSE are spaced at half the symbol period. In general, if the number of LE taps is 2L+1, then the number of FSE taps is $2 \times (2L+1)-1$. In order to have better performance, we can add either two or four more taps to the total calculated number of taps for the FSE depending on the practical situation.

Figure 5.6 shows the performance of the DQPSK system with different numbers of taps for the FSE. The simulations are executed using the SM2 process. In general, the equalizer with the largest number of taps yields the best performance. However, this is not always true; equalizers with too many taps may contribute noise causing the equalizers performance to degrade.

Figure 5.7 provides a performance comparison of the DQPSK system with the LE and the FSE over three different fixed channels (seeds of 52, 55 and 45) and their related time varying channels. LE7/FSE13_F4(55) represents an LE with 7 taps and an FSE with 13 taps those performances are being compared over a fixed channel (F) having four paths and a seed of 55. As shown in the figure, the FSE outperforms the symbol rate equalizer LE in each channel (especially in the worst channel with seed 45). This result is due to the FSE, which is not sensitive to the choice of sampling phase, and therefore it can compensate for channel distortion in the received signal before the effects of aliasing. However, the FSE requires about twice as many taps as the LE.

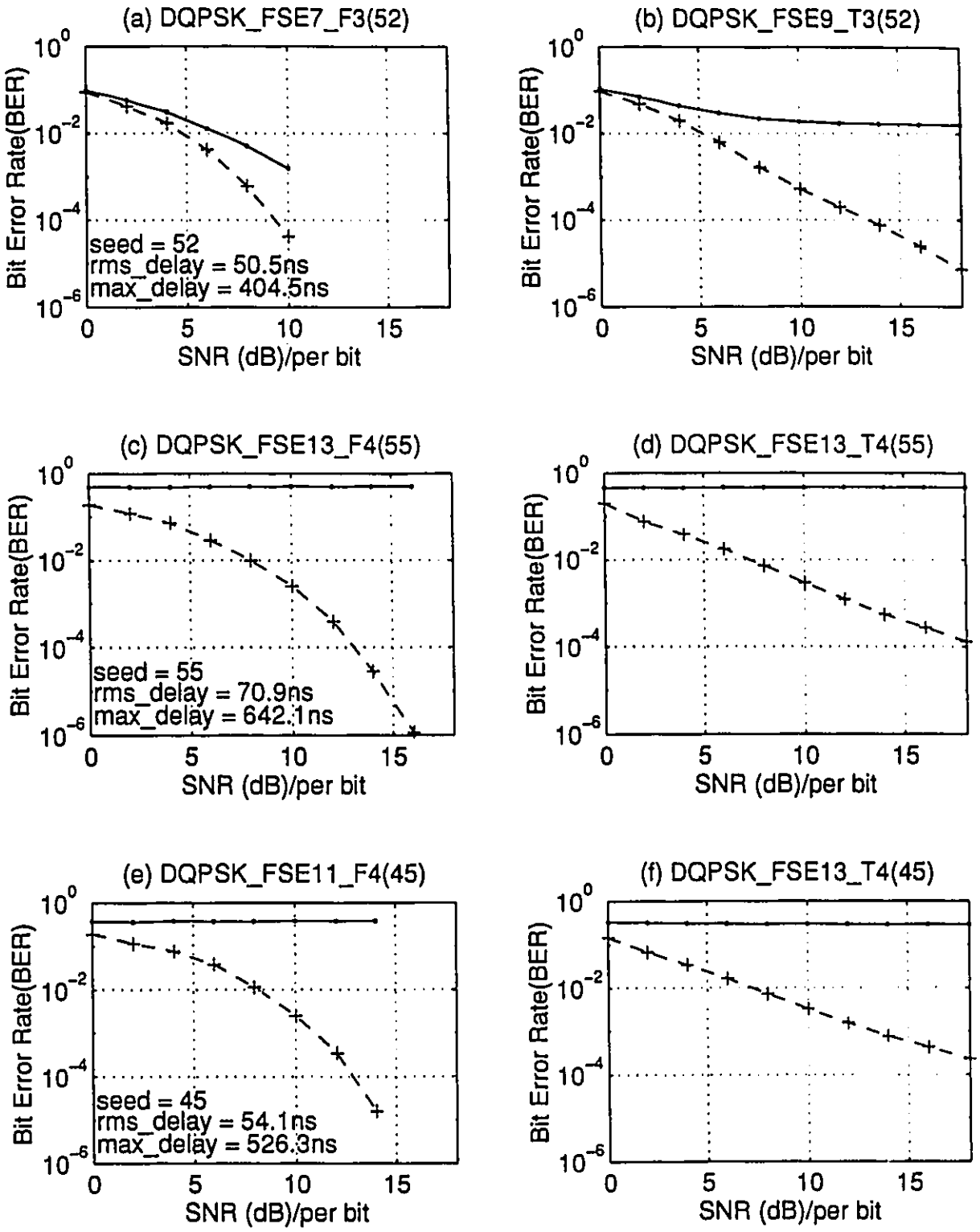

Figure 5.5: Performance of the DQPSK system with the FSE (a) (c) (e) over fixed channels and (b) (d) (f) over the corresponding time varying channels (dashed and solid lines represent the performance with and without the equalizer, respectively).

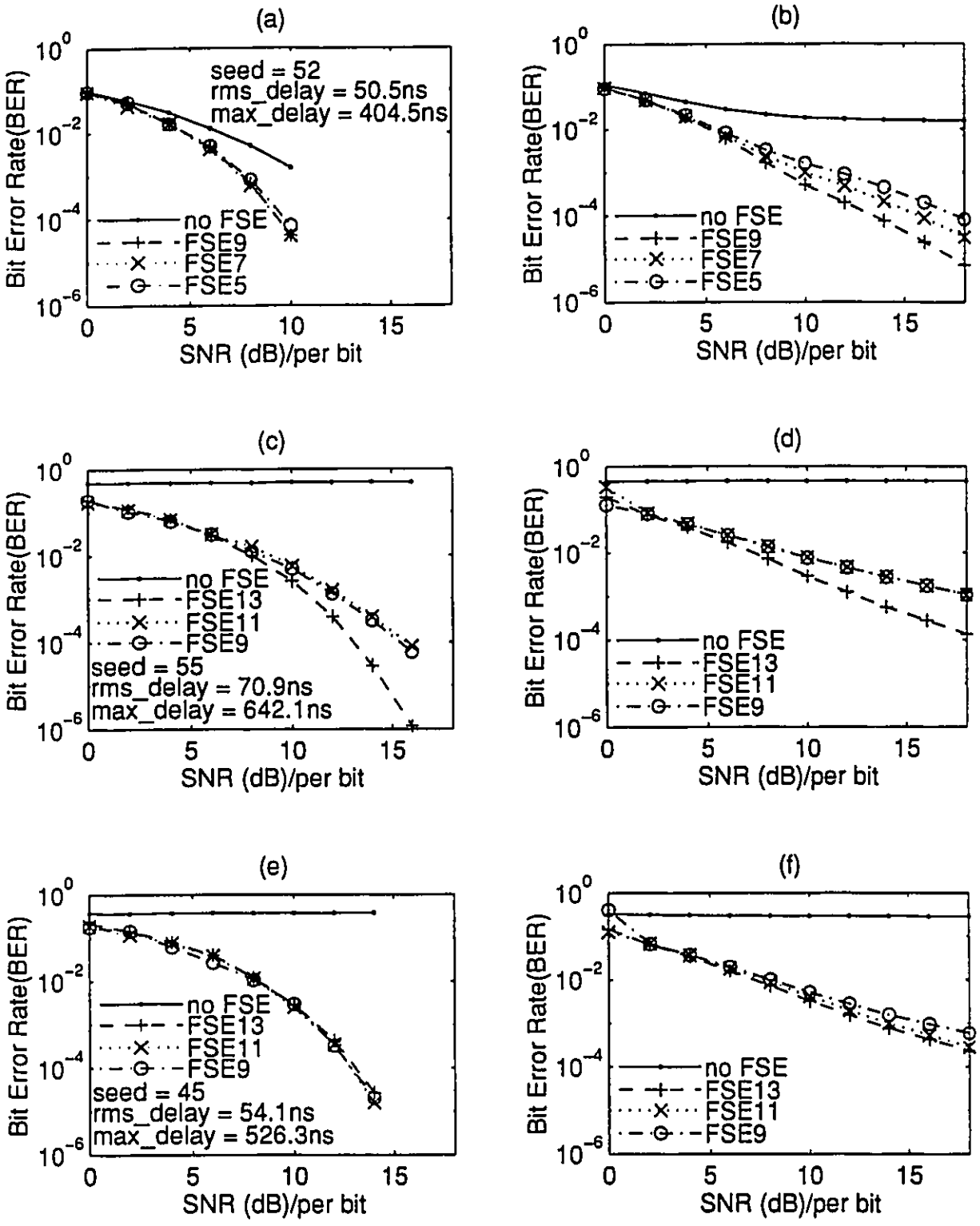

Figure 5.6: Performance comparison of the system having the $T/2$ FSE with different tap numbers (a) (c) (e) over fixed channels and (b) (d) (f) over the corresponding time varying channels.

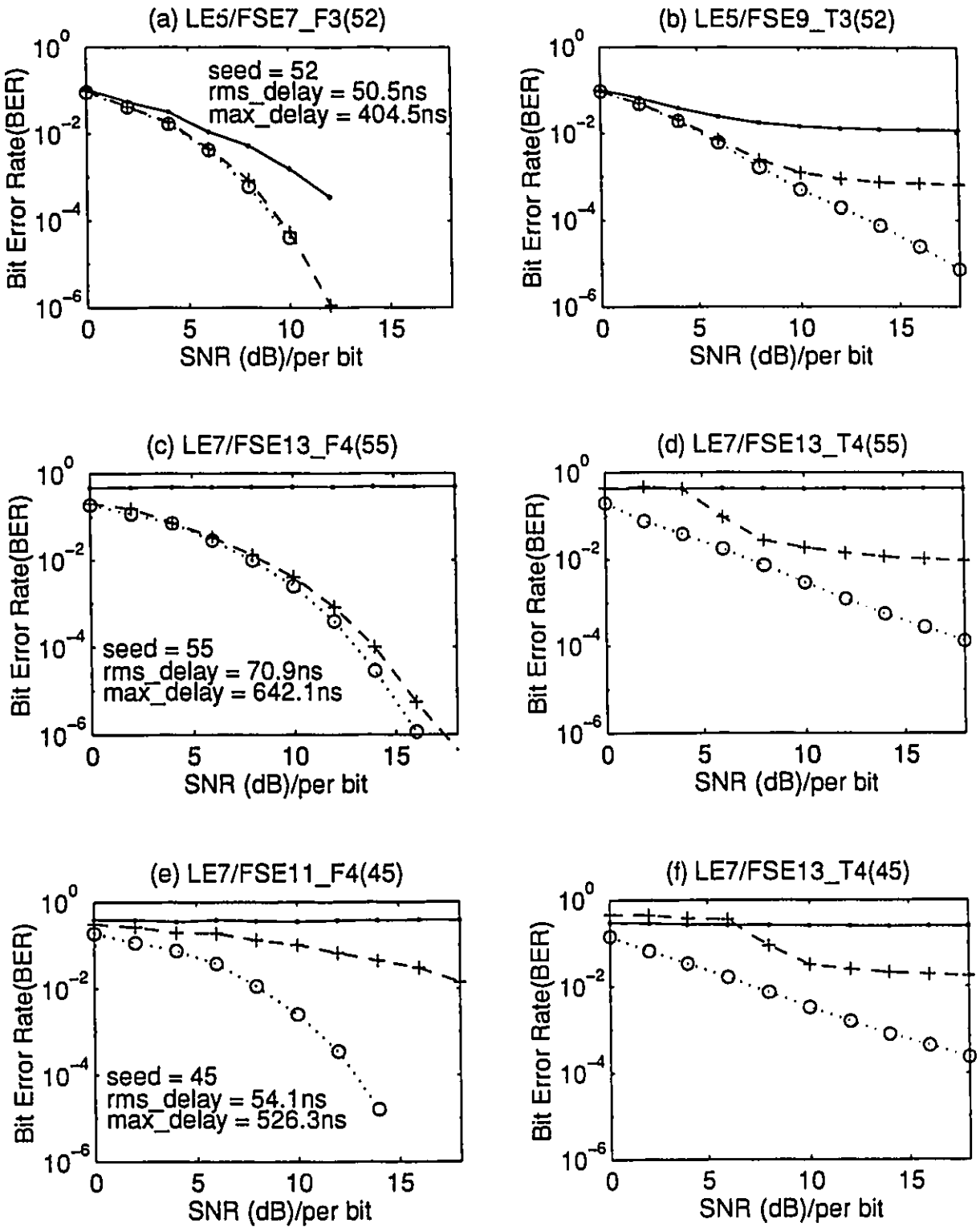

Figure 5.7: Performance comparison of the DQPSK system with the LE and the FSE (a) (c) (e) over fixed channels and (b) (d) (f) over the corresponding time varying channels (solid, dashed and dotted lines for the performance with no equalizer, LE and FSE respectively).

5.1.3 DQPSK System Performance with Decision Feedback Equalizers

With the feedforward and especially the feedback filters, the DFE can have much better performance than the other two equalizers (LE and FSE) since the feedback filter of the DFE can eliminate the intersymbol interference from the current estimate caused by previously detected symbols.

For the three fixed channels (seeds 52, 55 and 45) and the corresponding time varying channels, the BER performances of the DQPSK system with the DFE are shown in Figure 5.8. The total number of transmitted bits is 10^7 for the SM2 process. DQPSK_DFE7_T4(55) represents a DQPSK system with a 7-tap DFE that is simulated over the time varying channel (T) with seed 55 consisting of four taps. For Figure 5.8, the structure of the DFE with $2L + 1$ taps consists of an $(L + 1)$-tap feedforward filter and an L-tap feedback filter. The curves shown in Figure 5.8 (b), (d) and (f) for the time varying channels have worse performance when the SNR is low. In Figure 5.8, the result from each simulation is yielded with the same equalizer step size μ that is used to adjust convergence of the iterative procedure. In fact, the step size μ must be adjusted slightly depending on the SNR to provide optimum performance over the whole SNR range (0 to 18 dB).

By changing the number of taps between the feedforward and feedback filters, we will see that the best structure for the DFE, in order to achieve optimum performance, has a feedforward filter with one more tap than the feedback filter for the equalizer structure of $2L + 1$ taps. The performance comparison of the DQPSK system with the DFE by changing the feedforward and feedback filter tap numbers is given in Figure 5.9. The channel seed is 55 and the number of channel taps is four. Figure 5.10 shows a similar performance comparison for the channel with seed 45. The results of Figure 5.9 and Figure 5.10 are simulated through the SM1 process for the fixed channels, and SM2 for the time varying channels. The notation of F3B4 means that

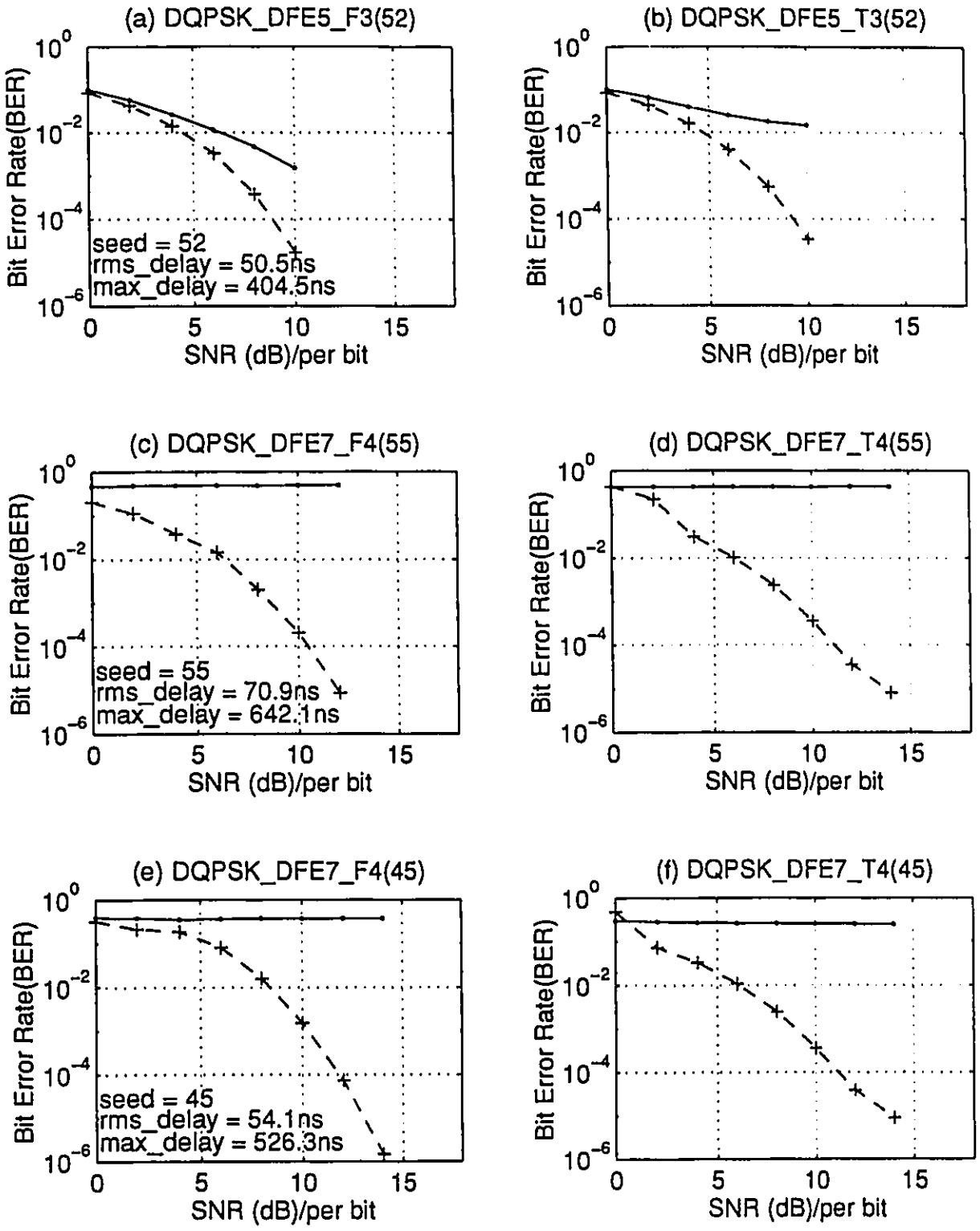

Figure 5.8: Performance of the DQPSK system with the DFE (a) (c) (e) over fixed channels and (b) (d) (f) over the corresponding time varying channels (dashed and solid lines represent the performance with and without the equalizer, respectively).

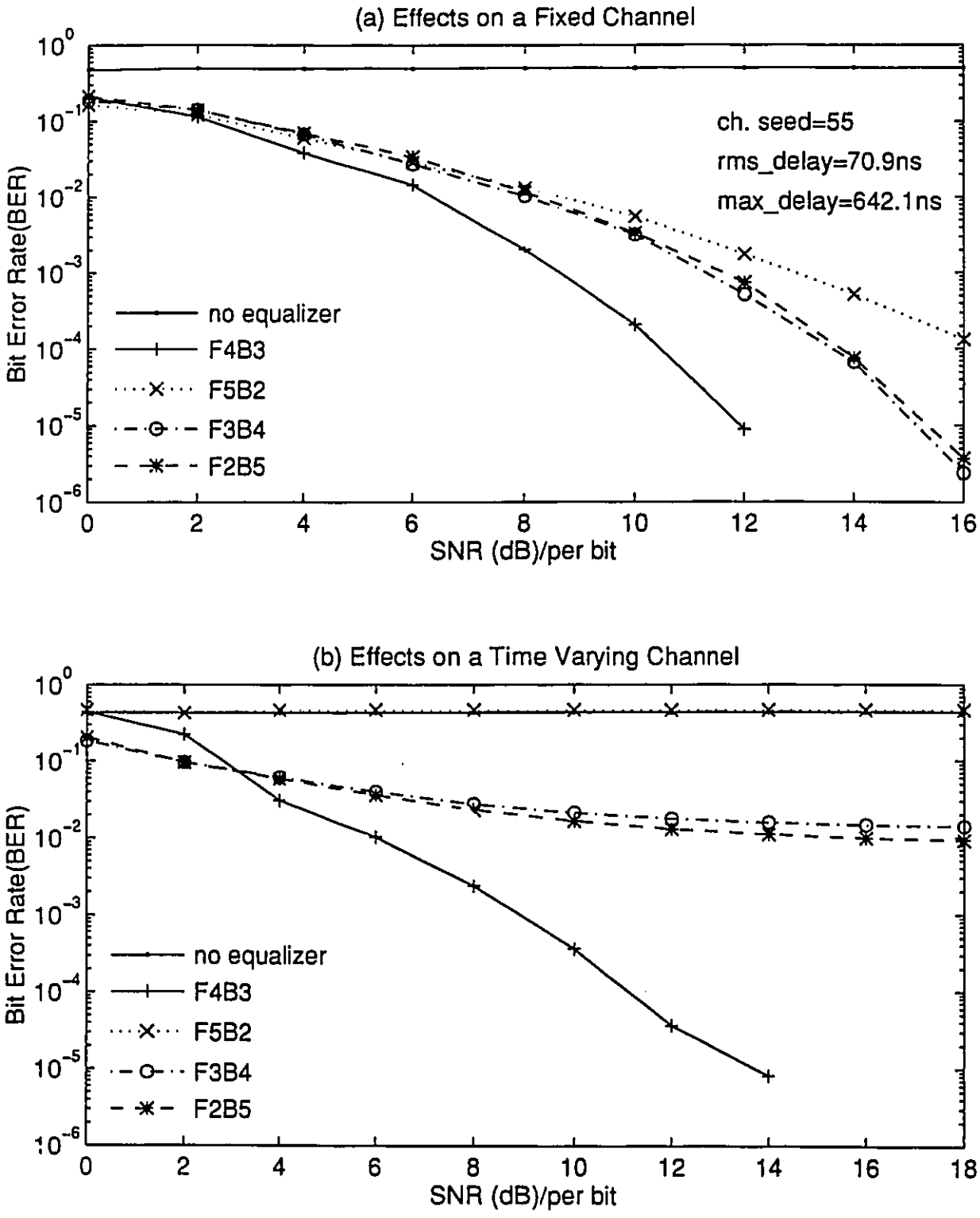

Figure 5.9: Performance comparison of the DQPSK system with the DFE by changing the feedforward and feedback tap numbers (a) over a fixed channel with a seed 55 and (b) the corresponding time varying channel.

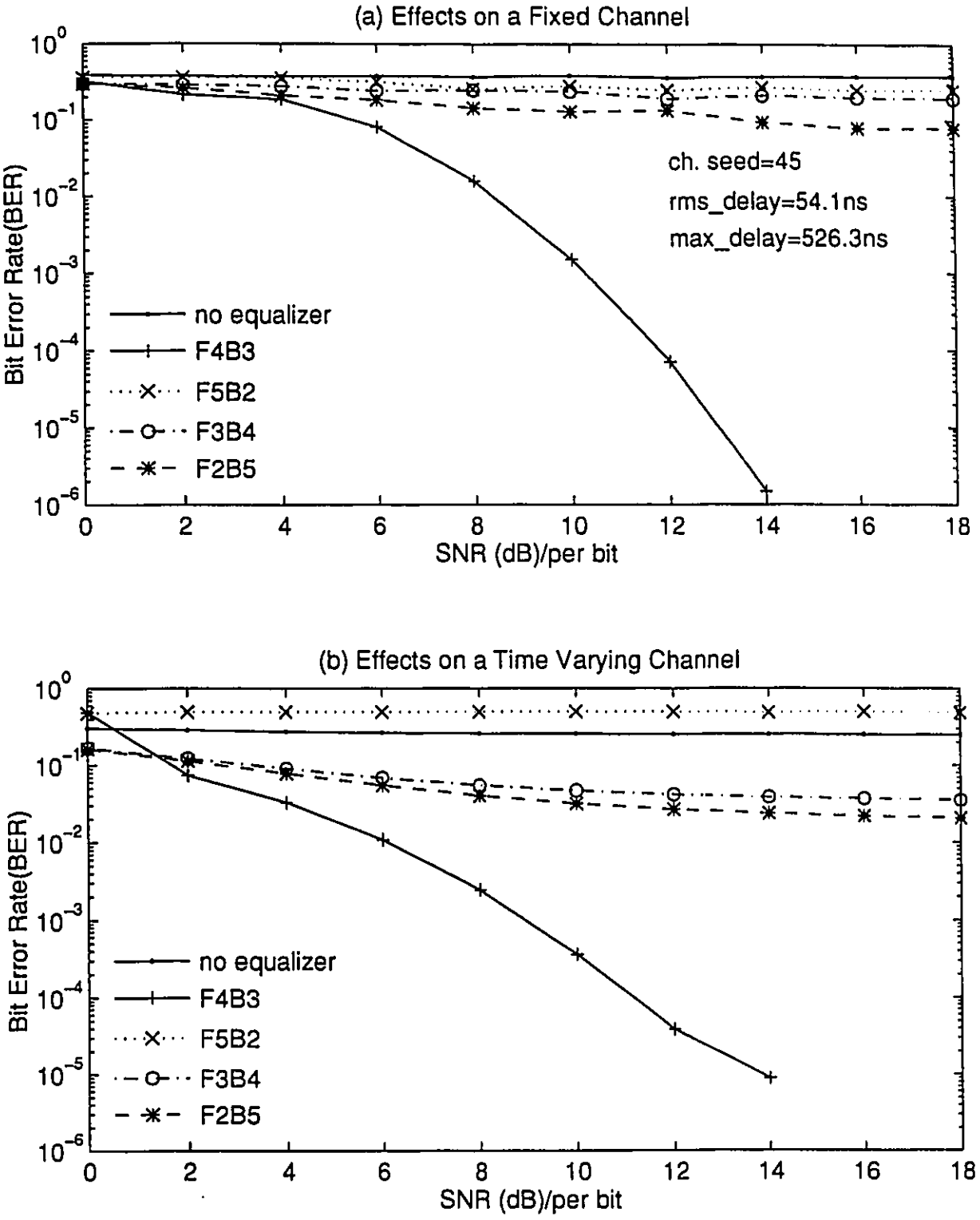

Figure 5.10: Performance comparison of the DQPSK system with the DFE by changing the feedforward and feedback filter tap numbers (a) over a fixed channel with a seed 45 and (b) the corresponding time varying channel.

the DFE consists of a 3-tap feedforward filter and a 4-tap feedback filter. The figures show that the DFE with the F4B3 structure has the best performance compared to the other structures (F3B4 and F2B5). The BER performance curve of the DFE with F5B2 is not shown because it exhibits worse performance than the DFEs with F3B4 and F2B5.

From Figure 5.11 to Figure 5.13, the LE, FSE and DFE performances are compared for the DQPSK system over three fixed channels of seeds 52, 55 and 45 and the corresponding time varying channels. The results illustrates the superiority of the DFE over the FSE and the LE. The DFE yields a significant improvement in performance relative to the LE having the same number of taps and the FSE having about twice as many taps. However, the results indicate that there is still a significant degradation in performance for the DFE due to the residual intersymbol interference (ISI), especially on channels with severe distortion. Another phenomena of DFEs having error propagation can be observed in Figure 5.13. The FSE shows better performance than the DFE for low SNRs. The crosspoint for the two BER curves occurs at SNR = $6dB$. The feedback filter of the DFE not only removes the part of the ISI from the present estimate caused by previously detected symbols, but also enhances the ISI from it. When the pre-detected symbols are not accurate, the errors from them are fed back through the DFE feedback filter, causing worse performance than for the FSE. With lower SNRs, pre-detected symbols have high probability of being invalid. Thus the feedback filter of the DFE actually propagates the errors. But the DFE still shows its strong capability of combatting the ISI for higher SNRs.

5.2 Performance Analysis of D8PTCM with Adaptive Equalizers

The advantage of using trellis coded modulation (TCM) is that a performance gain is desired without expanding the signal bandwidth. As shown in Chapter 4, BER

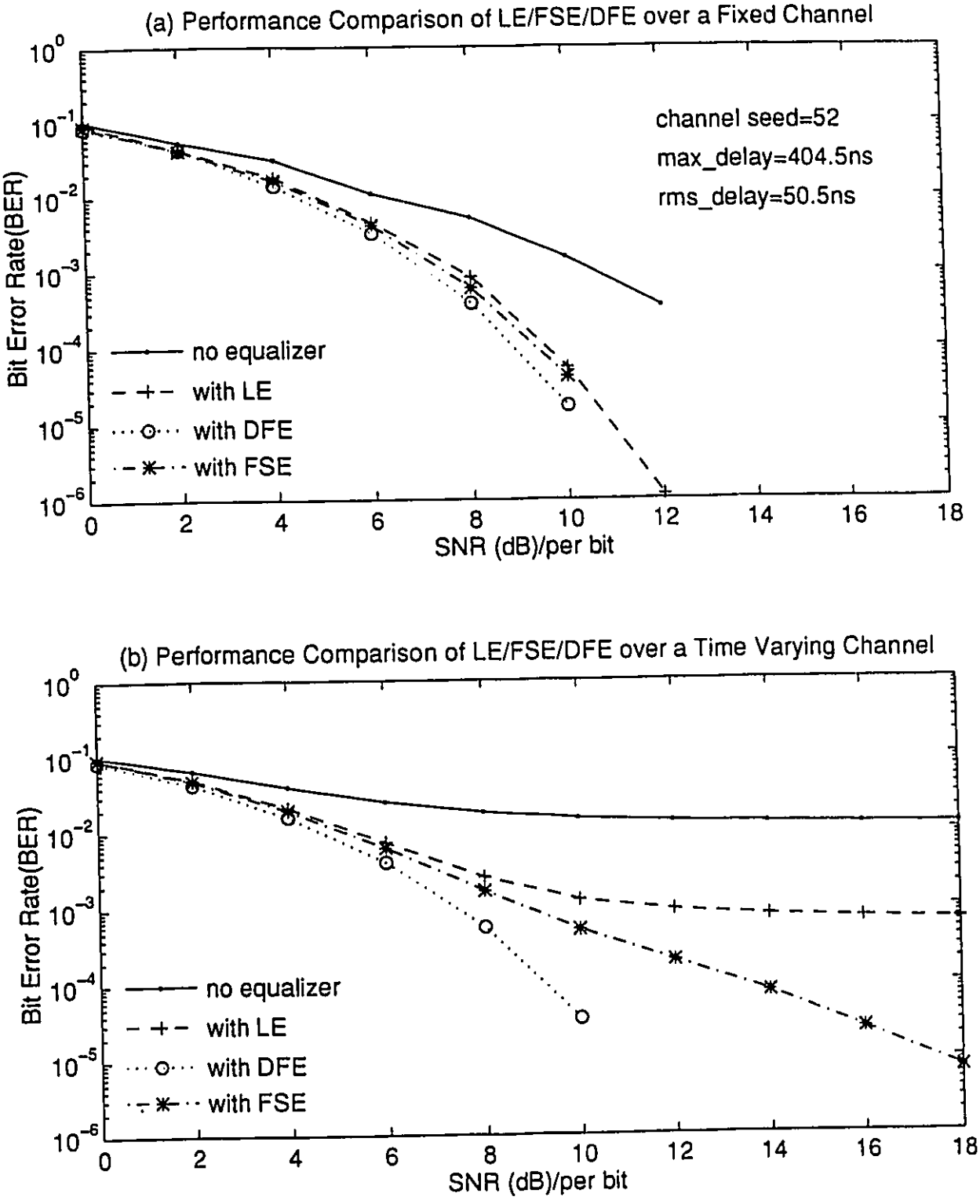

Figure 5.11: Performance comparison for the DQPSK system among the LE, FSE and DFE (a) over a fixed channel with the seed 52 and (b) over the corresponding time varying channel.

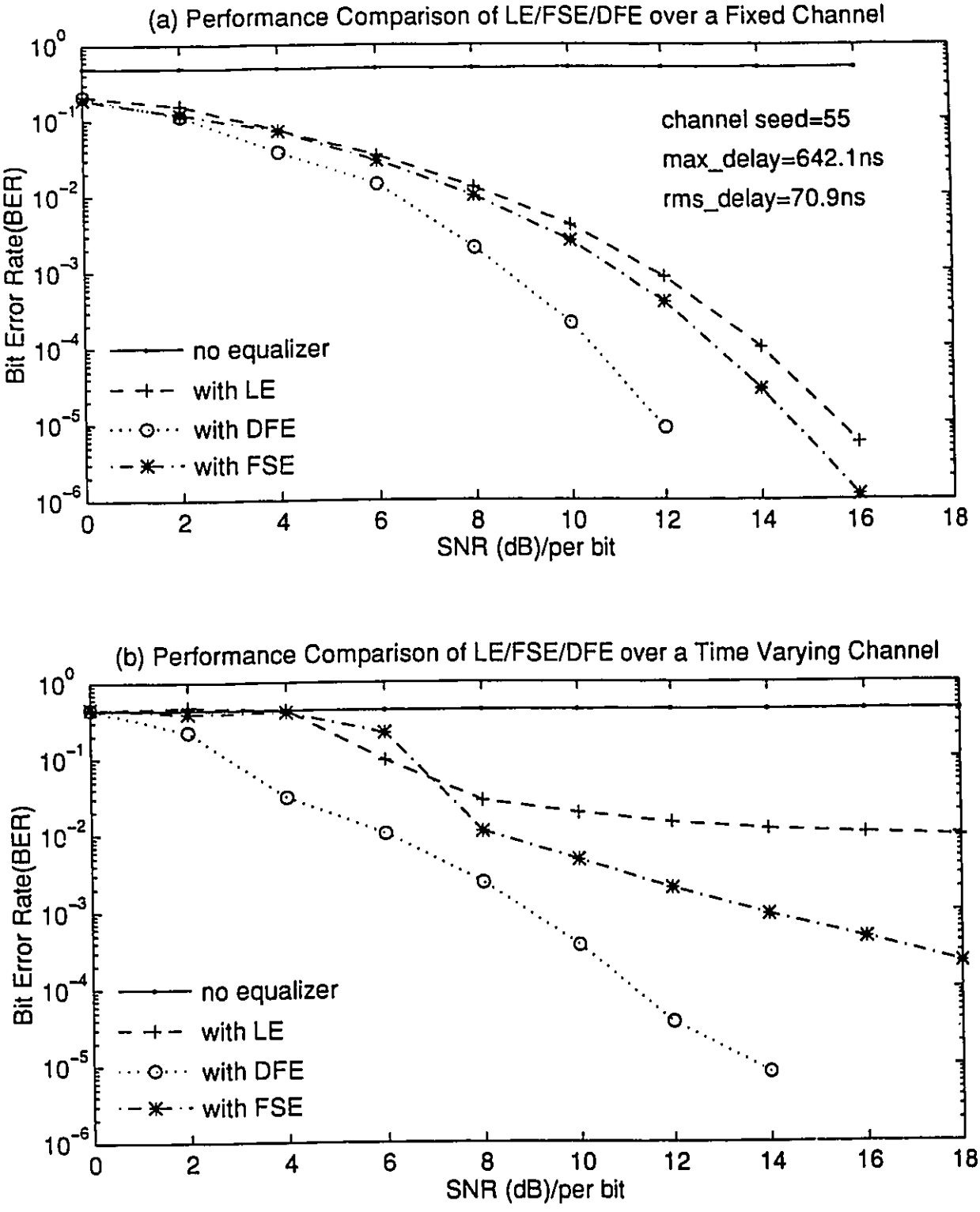

Figure 5.12: Performance comparison for the DQPSK system among the LE, FSE and DFE (a) over a fixed channel with the seed 55 and (b) over the corresponding time varying channel.

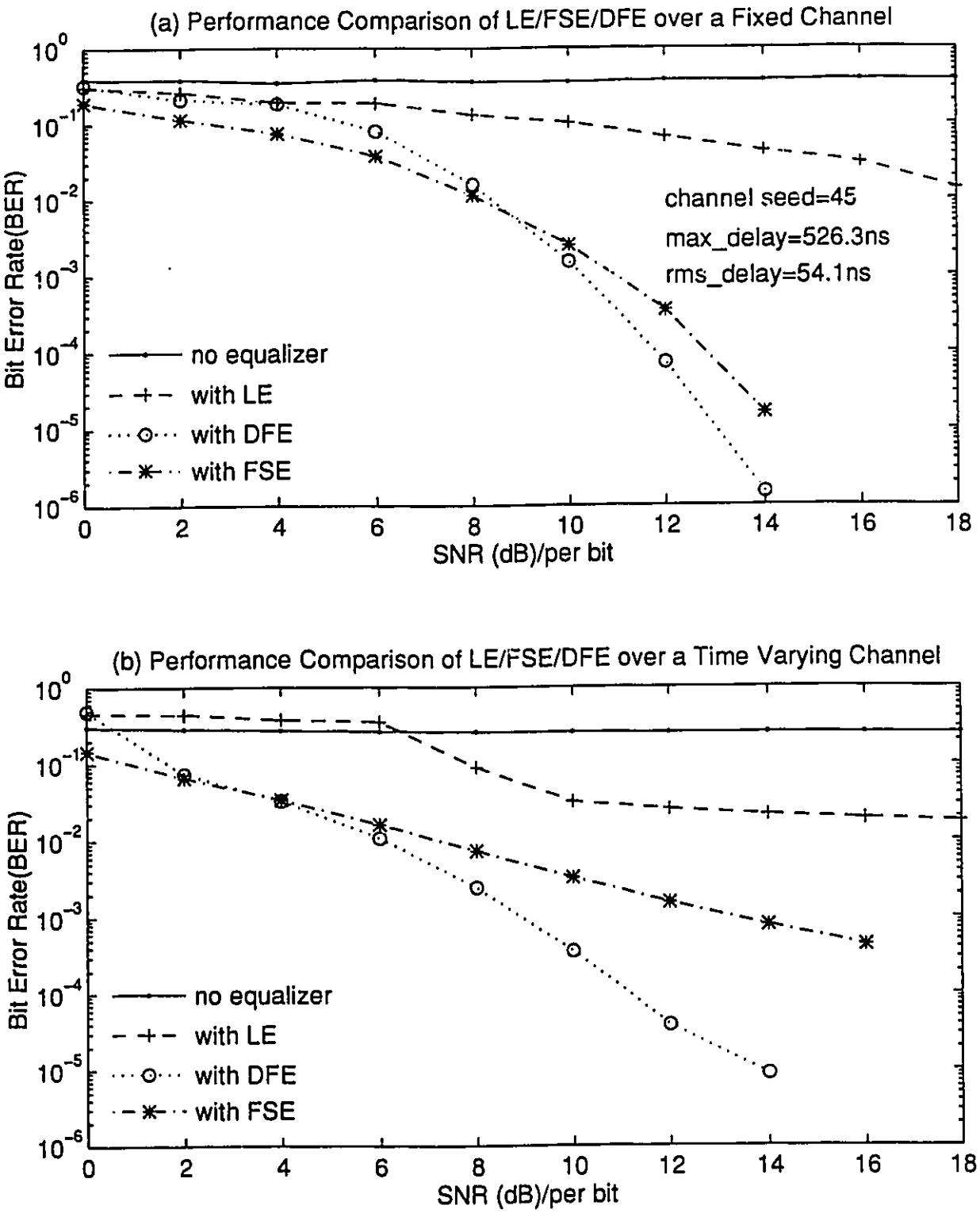

Figure 5.13: Performance comparison for the DQPSK system among the LE, FSE and DFE (a) over a fixed channel with the seed 45 and (b) over the corresponding time varying channel.

performance improvement has been achieved over the AWGN channel. In this section, the performances of 4-state and 8-state D8PTCM systems using differential encoding with LE and DFE are examined over both fixed and time varying indoor wireless channels (IWC). The performance comparison of two different D8PTCM with the equalizers is presented. Both DQPSK and D8PTCM systems with different equalizers are compared to determine their effectiveness over the IWC.

5.2.1 Performance of 4-State D8PTCM with Adaptive Equalizers

The 4-state D8PTCM named D8PTCM4, which has parallel transitions, is used to evaluate adaptive linear equalizers (LE) and decision feedback equalizers (DFE). The Viterbi decoding technique is applied to decode the trellis coded modulation symbols in the simulation, due to its simplicity. Although the Viterbi algorithm which computes the Euclidean distance metric to decode the coded symbols is optimum for the AWGN channel, it is not the case for fading channels. An optimum decoding method for fading channels was explored in [Chev89].

The simulation results of D8PTCM4 with both the LE and DFE over fixed and time varying channels are shown in Figure 5.14. For the fixed channels, the simulation method SM1 is used. The simulation method SM2 is applied to the time varying channels. The total number of sent bits in SM2 is $2x10^6$. The notation of LE7/DFE7_T4(45) means that both LE with 7 taps and DFE with 7 taps are evaluated over a 4-tap time varying channel (T) with a seed 45. Again F is used instead of T for a fixed channel. The simulation results with the DFE has not much difference from that with the LE for fixed channels. For the time varying indoor wireless channels, the DFE shows its better capability of tracking a time variant channel than the LE. It is also noticed that the BER performance of D8PTCM4 with the LE is slightly better than that of D8PTCM4 with the DFE shown in Figure 5.14(e). As mentioned earlier, the DFE will yield worse BER performance than the LE, if pre-detected sym-

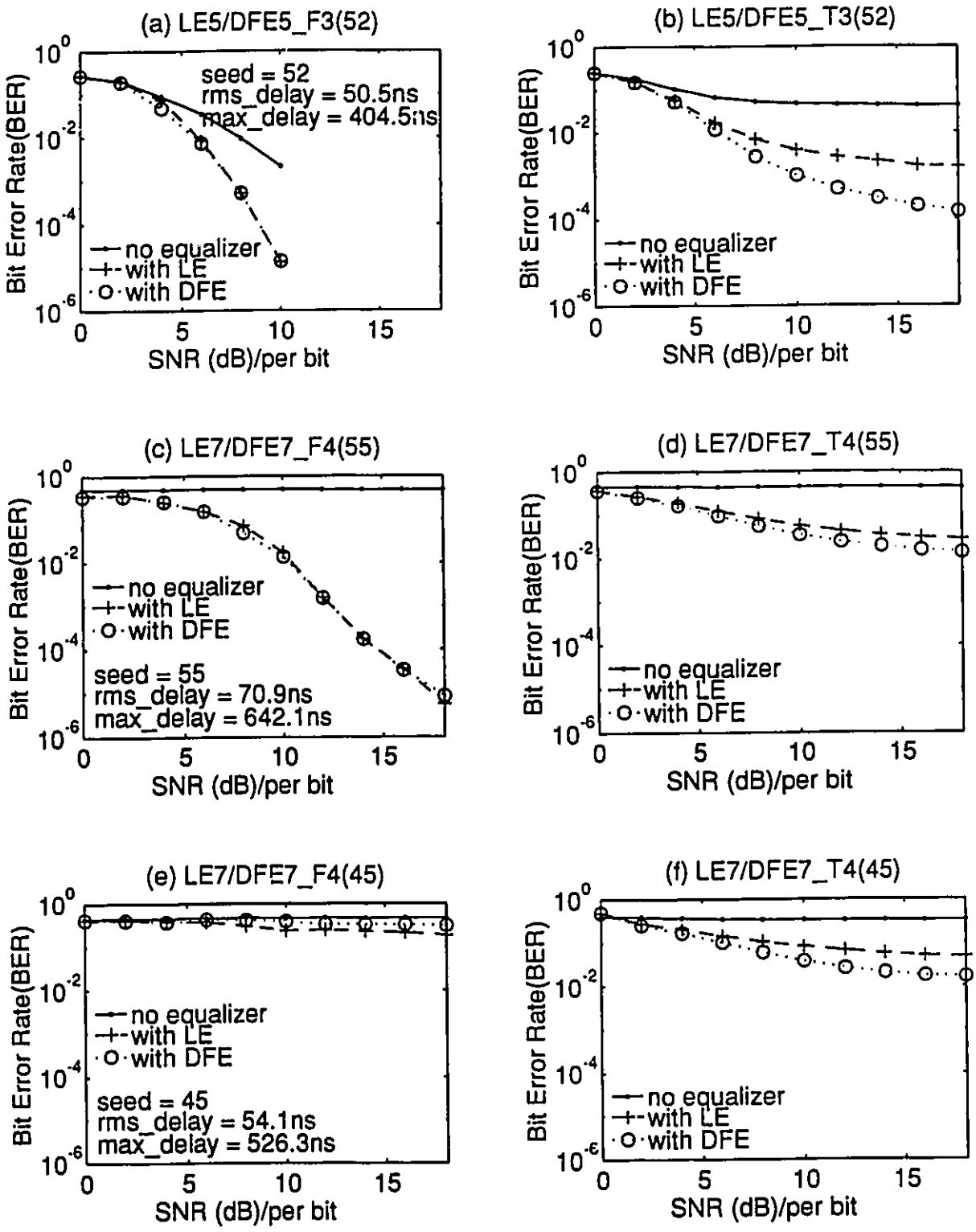

Figure 5.14: The simulation results of the D8PTCM4 system with the LE and DFE (a) (c) (e) over fixed channels and (b) (d) (f) over the corresponding time varying channels.

bols for the DFE are not accurate due to noisy transmission medium or low SNRs. Thus, the channel with a seed 45 is corrupted severely due to multipath propagation (first two paths having almost same amplitude). When the channel (seed 45) is simulated as a time invariant channel, it represents a worse transmission medium than one as a time variant channel. Since the amplitudes of first two paths for the time varying channel gradually change with time, and they become different. But those for the fixed channel do not change during whole simulation. Therefore, the BER performance shown in Figure 5.14(f) is better than that shown in Figure 5.14(e). For the time varying channels with seeds 55 and 45, the BERs of the system with both the LE and the DFE are in order of 10^{-2} for SNR greater than 8dB. Although the performance improvement of the DFE can be seen, it still cannot compensate the severe intersymbol interference. When SNR is greater than 10dB, the DFE outperforms the LE by one order of magnitude (10^{-4} vs. 10^{-3}) for the channel with a seed 52. The channel is believed to be not severely distorted.

5.2.2 Performance of 8-State D8PTCM with Adaptive Equalizers

The performances of a 8-state D8PTCM (D8PTCM8) with both LE and DFE are evaluated in this section. The results are compared to those from the 4-state D8PTCM with both the LE and the DFE. The performance effectiveness between the D8PTCM and the DQPSK modulation systems combined with the DFE are then examined.

First, the simulation results of a D8PTCM8 with the LE and the DFE are compared to those of the D8PTCM4 with the LE and the DFE over a fixed channel of a seed 52 and the corresponding time varying channel in Figure 5.15. Without the equalizer, D8PTCM4 has better performance than D8PTCM8 over the fixed channel, when SNR is less or equal to 8 dB. But when SNR is greater than 8 dB, the D8PTCM8 appears to provide better performances than the D8PTCM4. The D8PTCM systems with the LE and the DFE have the same behavior as without the equalizers. But the

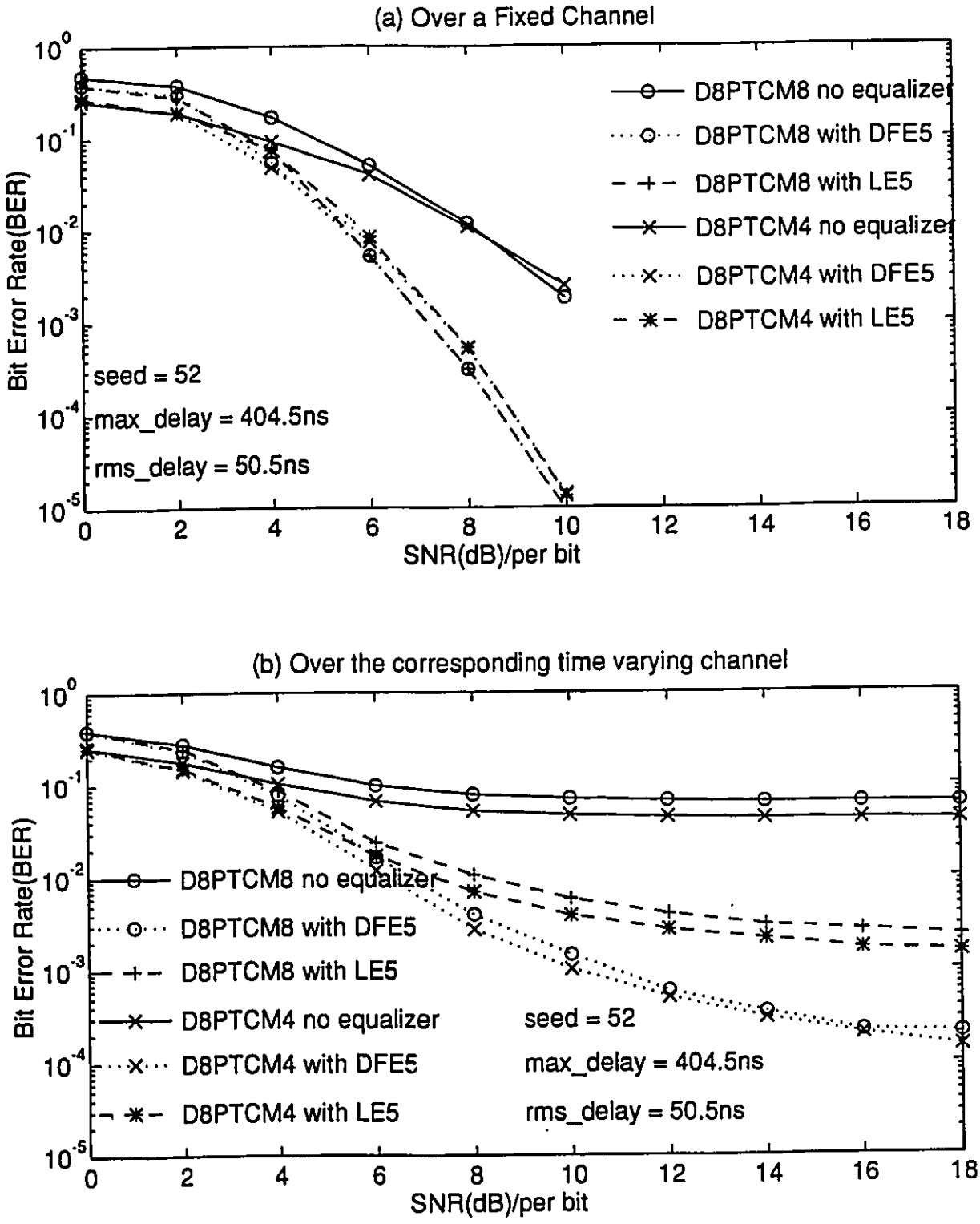

Figure 5.15: Performances comparison of the D8PTCM4 and D8PTCM8 systems with the LE and the DFE over a fixed channel (seed 52) in (a) and over the corresponding time varying channel in (b).

equivalent point moves from 8 dB to 4 dB.

For the time varying channel, the performances of the D8PTCM4 with and without both the LE and the DFE are better than those of the D8PTCM8 respectively in the range of SNRs from 0 dB to 18 dB. The D8PTCM systems with the DFE outperform the systems with the LE by about one order of magnitude. Figure 5.16 and Figure 5.17 show the simulation results over both fixed and time varying channels of seeds 55 and 45. Again the results show that the performances of the D8PTCM4 system, without the equalizers and with both the LE and the DFE, are respectively better than those of the D8PTCM8 system with the same combination as the D8PTCM4 system over the time varying channels.

The DFE exhibits the best performances in all channels in the simulations. The performance comparison of the DQPSK and D8PTCM modulations with the DFE over both fixed and time varying channels with seeds 52, 55 and 45 are given in Figures 5.18, 5.19 and 5.20 respectively. The number of DFE taps used for different modulation schemes in those three figures are the same, and two more taps than that for the channel models to enhance the capability of combatting the intersymbol interference. In Figure 5.18(a) the DQPSK modulation scheme has the best performance among three modulation schemes when SNRs are less than 8 dB. The D8PTCM8 individually shows better performance than the DQPSK for SNRs greater than 8 dB and the D8PTCM4 for SNRs greater than 9 dB. With DFE, D8PTCM8 respectively provides better performance than D8PTCM4 for the critical point of SNR = 4 dB and the DQPSK for SNR = 8 dB. D8PTCM4 has better performance than the DQPSK when SNR > 10 dB.

On the other hand, the DQPSK with/without the DFE significantly outperforms the D8PTCM4 and the D8PTCM8 with/without the DFE over the time varying channel in Figure 5.18(b). In Figures 5.19 and 5.20, the same conclusion is reached for the two other time varying channels.

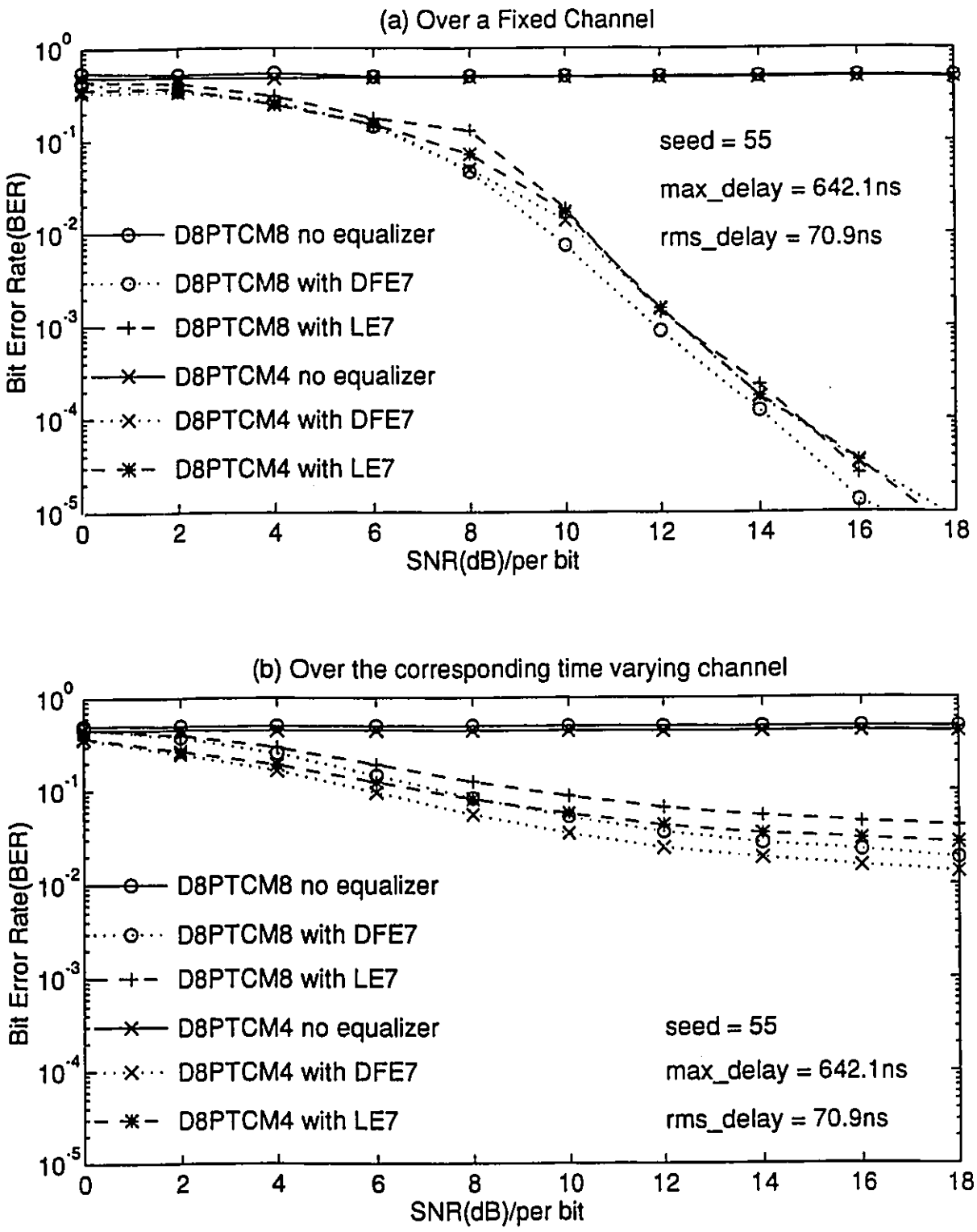

Figure 5.16: Performances comparison of the D8PTCM4 and D8PTCM8 systems with the LE and the DFE over a fixed channel (seed 55) in (a) and over the corresponding time varying channel in (b).

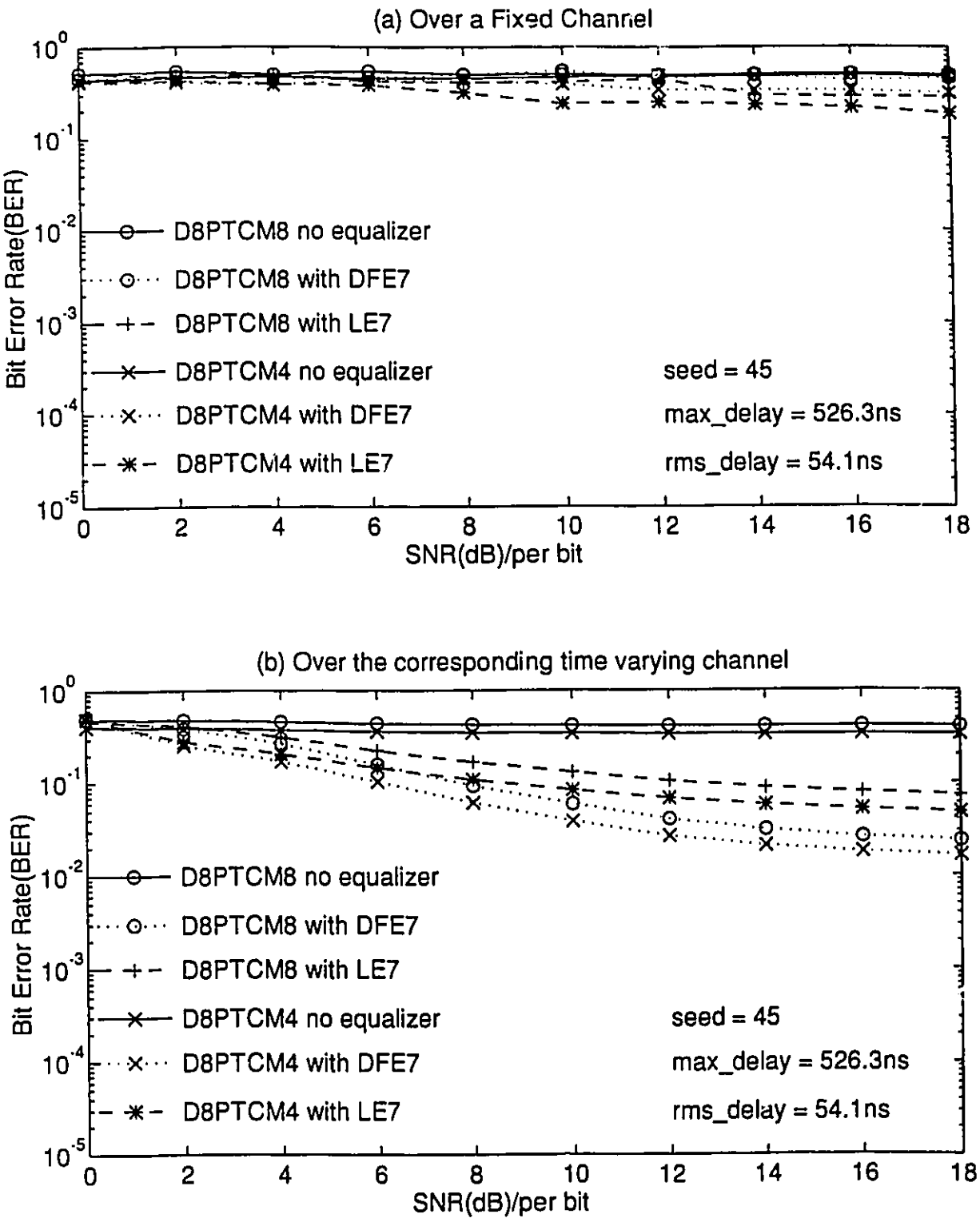

Figure 5.17: Performances comparison of the D8PTCM4 and D8PTCM8 systems with the LE and the DFE over a fixed channel (seed 45) in (a) and over the corresponding time varying channel in (b).

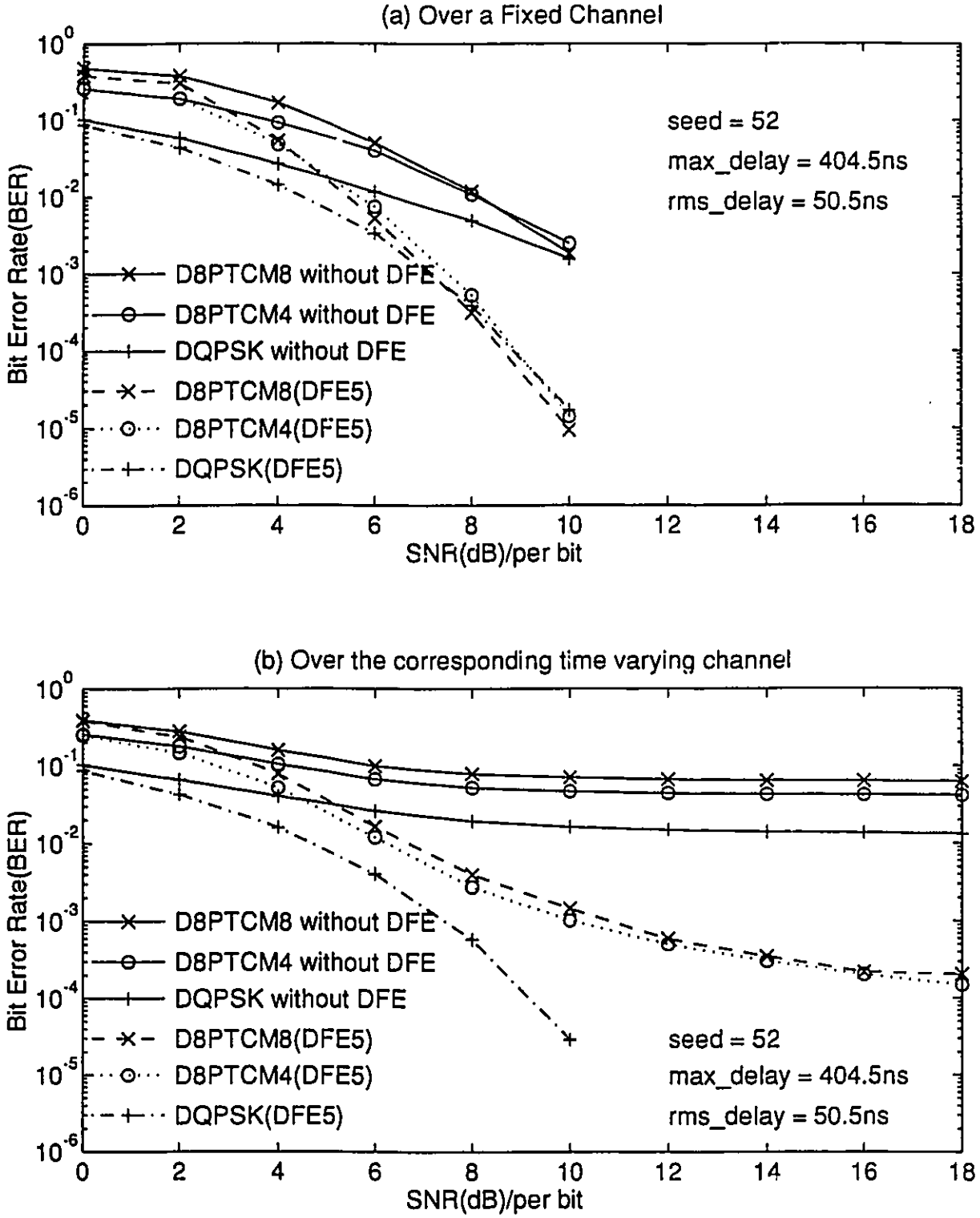

Figure 5.18: Performances comparison of the DQPSK/D8PTCM4/D8PTCM8 system with the DFE over a fixed channel (seed 52 and 3 taps) in (a) and over the corresponding time varying channel in (b).

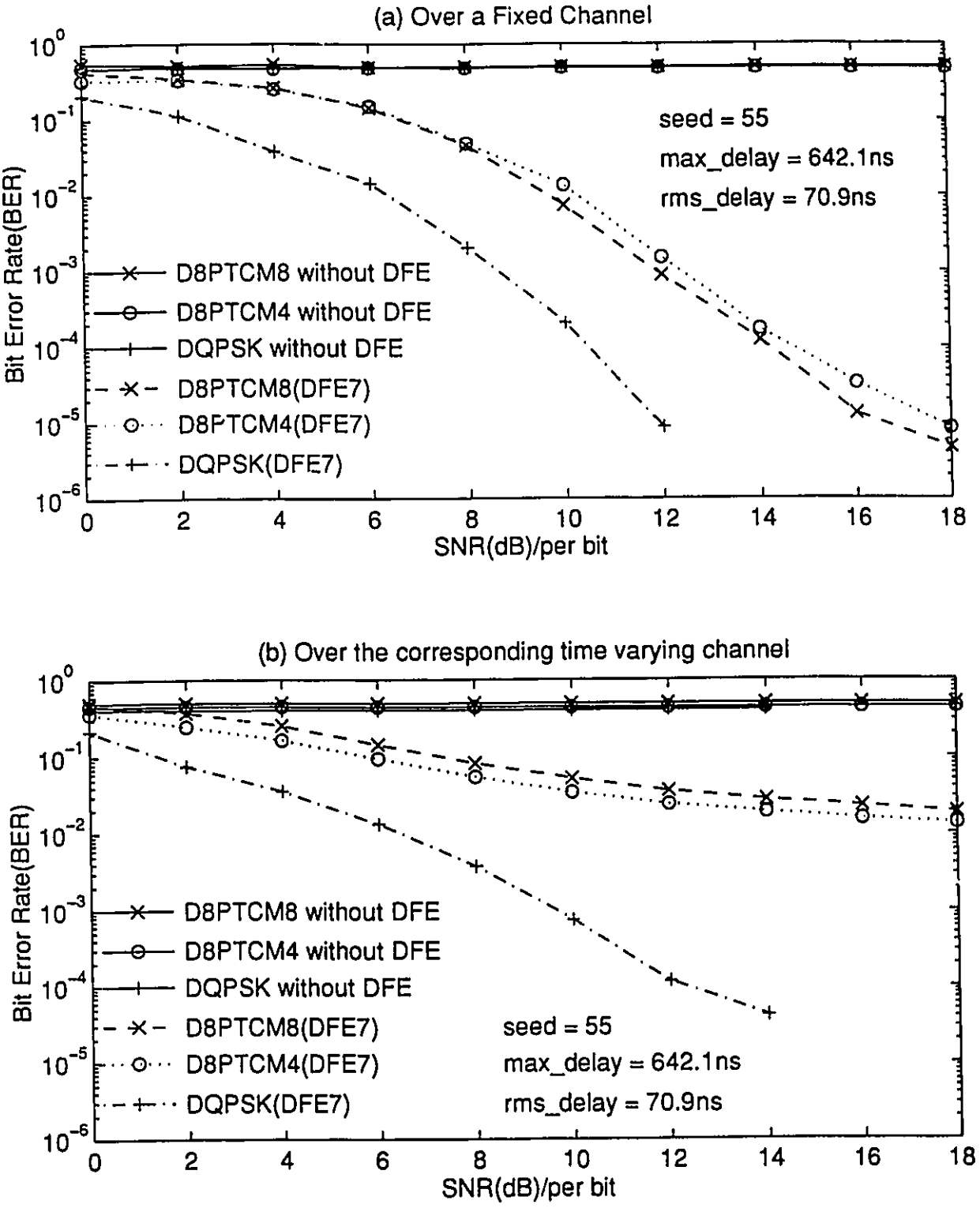

Figure 5.19: Performances comparison of the DQPSK/D8PTCM4/D8PTCM8 system with the DFE over a fixed channel (seed 55 and 5 taps) in (a) and over the corresponding time varying channel in (b).

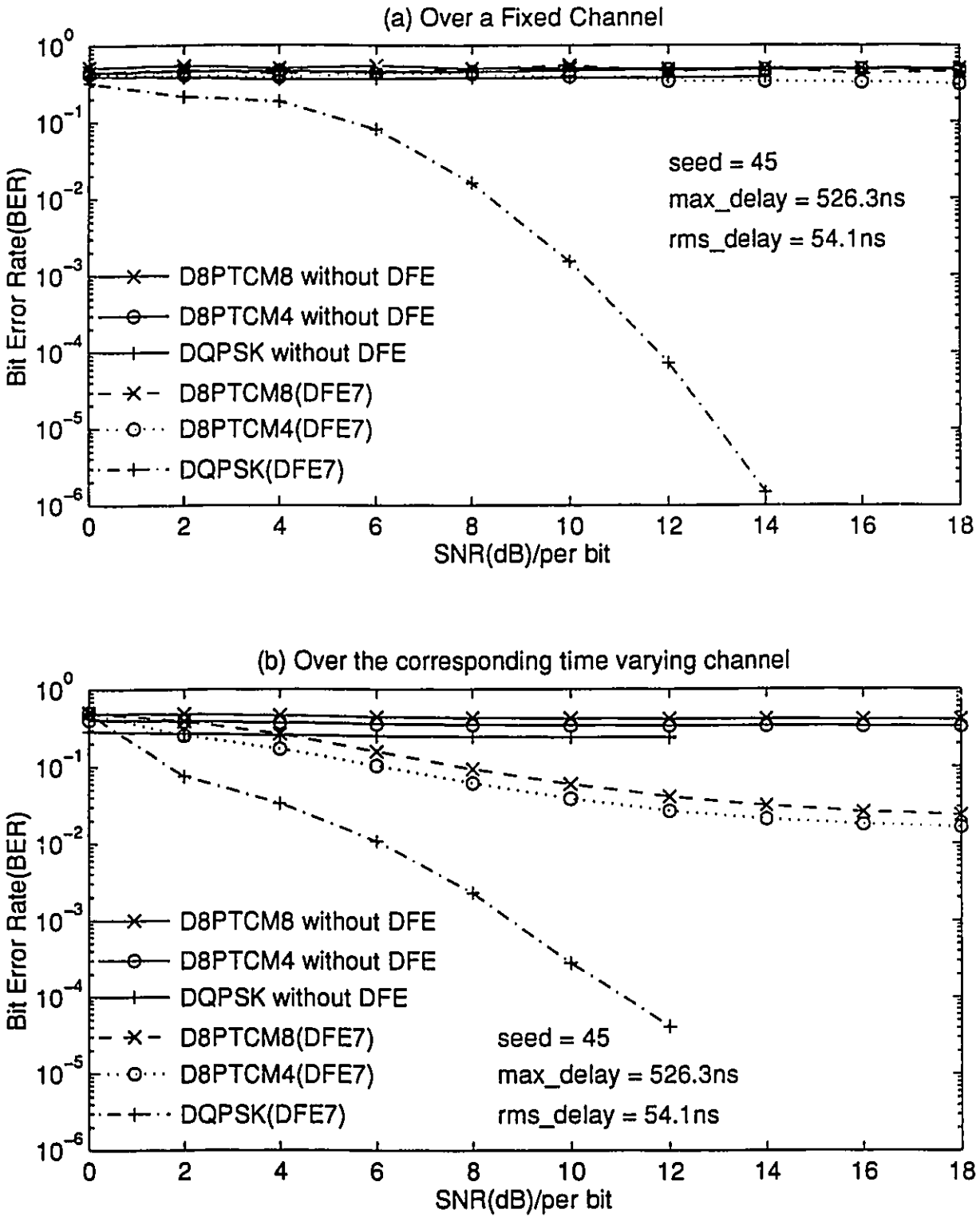

Figure 5.20: Performances comparison of the DQPSK/D8PTCM4/D8PTCM8 system with the DFE over a fixed channel (seed 45 and 5 taps) in (a) and over the corresponding time varying channel in (b).

5.3 Performance Comparison of DFE with LMS and RLS for DQPSK and D8PTCM

Figure 5.21 presents the BER performance comparison of the LMS and RLS algorithms applied to the DFE for DQPSK, D8PTCM4, and D8PTCM8 communication systems over a time varying channel (TCHNL2). It is clearly shown that the DQPSK modulation schemes with the DFE (7 taps) of both the LMS and RLS algorithms, named DQPSK_LMS and DQPSK_RLS, have better BER performance than D8PTCM4 and D8PTCM8 with the same equalizer combinations. The RLS algorithm slightly improves the BER performance of the DFE as compared with the LMS algorithm. As mentioned in [Ele86], the LMS algorithm is capable of providing tracking behavior similar to that of the RLS algorithm only for small equalizer lengths. Thus, the LMS algorithm should be used when the equalizer length is small since it is less complex than the RLS algorithm.

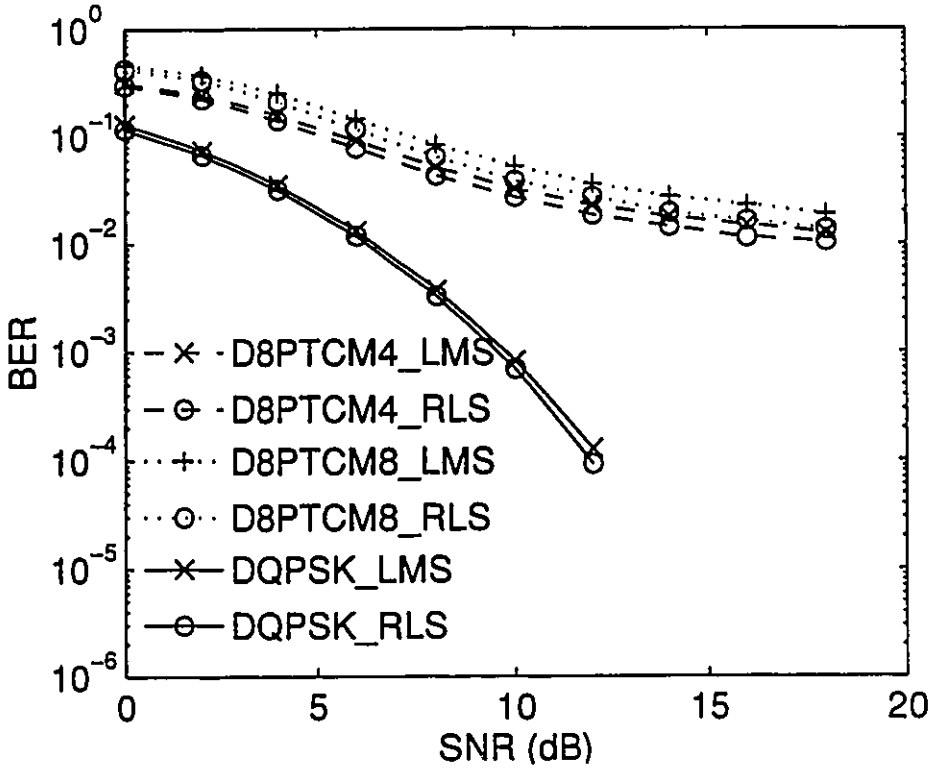

Figure 5.21: Performance comparison of DFE with LMS and RLS algorithms for D8PTCMs and DQPSK modulation schemes over a time varying channel (CHNL2).

5.4 Convergence Analysis of DFELMS and DFERLS

In this section, the transient behaviors of the mean-squared error (MSE) of adaptive decision feedback equalizers (DFE) with the least-mean-squared (LMS) and the recursive least-square (RLS) algorithms are discussed and compared for both DQPSK and D8PTCM4 modulation schemes. The convergence speeds of DFEs with both algorithms (DFELMS and DFERLS) are also presented. All simulations are run over time varying channels. The influence of different channels on both DFELMS and DFERLS is also explored.

A common and obvious measure of performance for a digital communication system is the bit error rate for a given signal-to-noise ratio (SNR): the BER is measured at the output of the receiver decision device. In addition, the mean-squared error (MSE) at the output of equalizer, but before the decision device, is also a good measure of the convergence rate of different receivers. Since the measurement locations of the MSE and BER measurements are separated by a nonlinear decision device, the relationship between the MSE and BER is highly nonlinear. Despite their non-trivial relationship, the MSE and BER are sufficiently correlated so that the MSE can also provide a somewhat indirect, but meaningful, measure of system performance.

In Section 3.1.2, we discussed the LMS algorithm (gradient estimation process) and the RLS algorithm. Both algorithms introduce noise into a tap-weight vector of an equalizer. The second noise source, which also causes an additional misadjustment of the tap-weight vector, occurs when the equalizer cannot accurately track a nonstationary channel. This noise is caused by the difference between the ensemble mean of the tap-weight vector and unknown optimum solution $\mathbf{w}_o(n)$. In this section, we will show that the MSE in DFELMS and DFERLS is affected by the algorithm parameters and the type of channel.

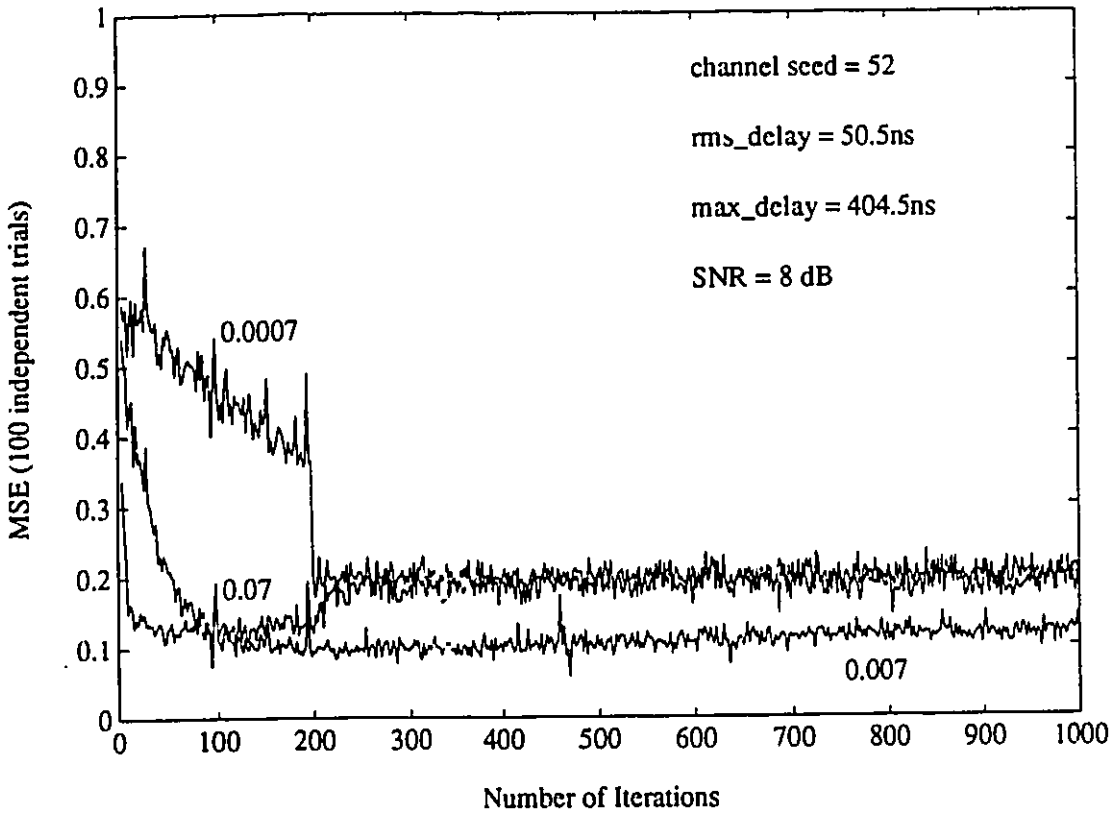

Figure 5.22: Transient behavior of MSE in DFELMS with different step sizes μ for D8PTCM4 modulation scheme over a time varying channel (CHNL1).

5.4.1 Transient behavior of MSE in DFELMS for D8PTCM4 and DQPSK

The computer simulation learning curves of DFELMS, which represent the MSE in DFELMS over a time varying channel of seed 52 (CHNL1), are given in Figure 5.22. Three curves are shown in the figure representing three values (step size parameter μ = 0.07, 0.007 and 0.0007). The differential 4-state trellis coded modulation scheme (D8PTCM4) is used for the digital communication system. The corresponding plots of the mean-squared error are obtained by ensemble averaging over 100 independent trials of the experiment. For each trial, a different computer realization of the input data and noise is used, but the time varying channel is kept the same. The simulation results show that transient behavior of the DFELMS is highly sensitive to variations in the step size parameter μ. For large step size values, the DFELMS converges

quickly and the MSE stays in a steady state after 150 iterations. As mentioned in section 3.1.2, the convergence time is inversely proportional to the step size parameter μ. On the other hand, the steady state value of the MSE increases with μ. This steady state value can also be affected by the training sequence. In most of the simulations, the total number of training sequence bits used is 100. For a properly chosen step size μ, the steady state value of the MSE will not increase significantly after the training sequence is stopped, unless the channel is severely corrupted by intersymbol interference (ISI). In Figure 5.22, the value of the MSE for the learning curve of $\mu = 0.07$ increases after a training sequence of 200, but the learning curve with $\mu = 0.007$ does not have obvious changes. In order to clearly show the influence of varying step size μ on learning curves, a training sequence of 200 is used instead of 100. Figure 5.23 gives the MSE learning curves of different step sizes for DQPSK modulation scheme over the same channel as Figure 5.22. Again, the value of the MSE with step size $\mu = 0.007$ is the smallest. After a training sequence of 200, the learning curves continue to converge without increasing as was the case for $\mu = 0.07$ in Figure 5.22.

From these ensemble statistics, a useful measure of equalizer performance is computed as the average MSE. The average MSE performance criteria can be used to select a near-optimum value for the simulation parameter μ (step size) that gives the smallest value of the MSE in the DFELMS.

5.4.2 Comparison of MSE in DFELMS and DFERLS for D8PTCM4

In section 3.1.3, the characteristics of the recursive least-squares (RLS) algorithm are discussed. The main advantage of the algorithm is that it makes the DFE converge quickly. On the other hand, the RLS algorithm may give the DFE better tracking ability over a time varying channel. In this section, we will compare the MSE of both the RLS and LMS algorithms for DFE, to determine the better of the two algorithms

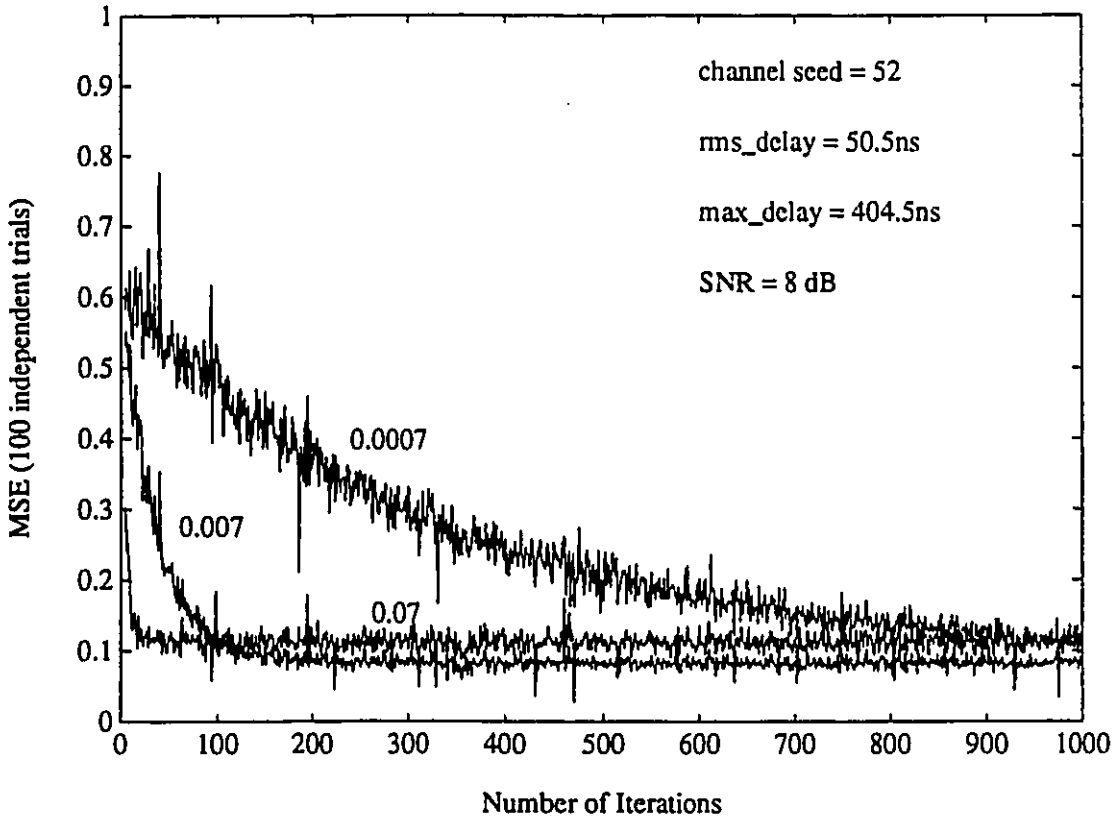

Figure 5.23: Transient behavior of MSE in DFELMS with different step sizes μ for DQPSK modulation scheme over a time varying channel (CHNL1).

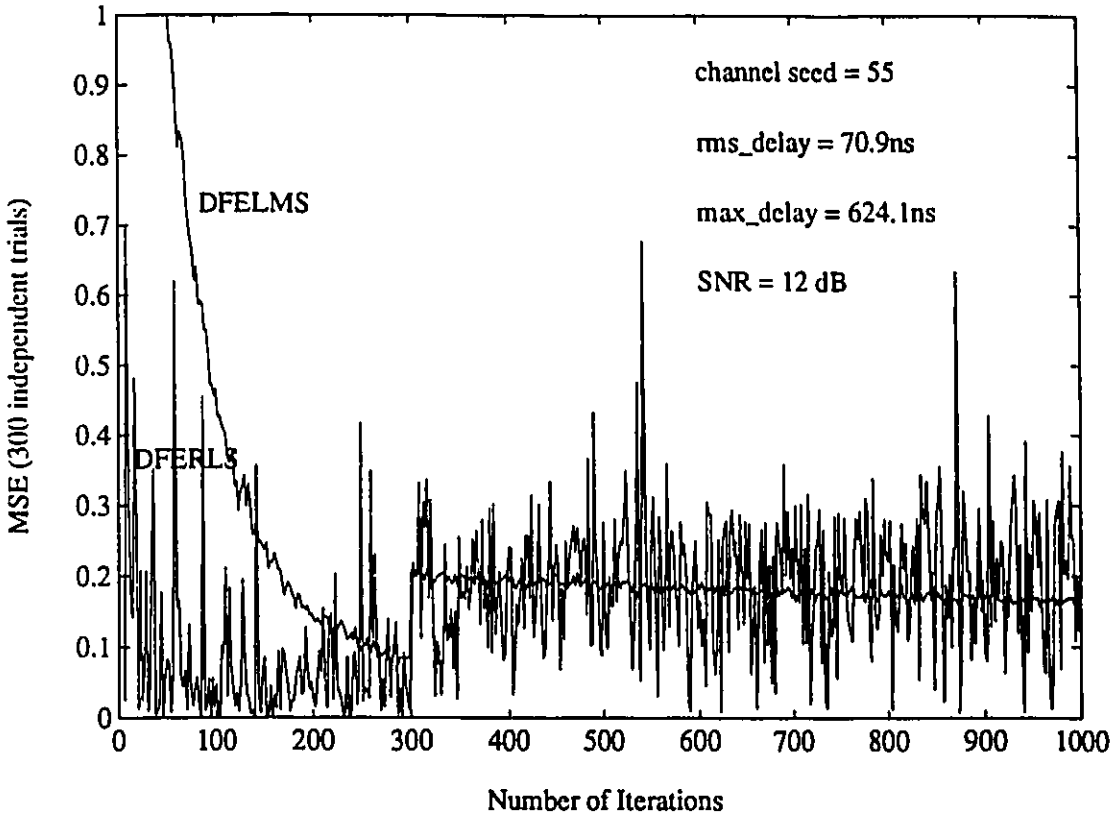

Figure 5.24: Transient behavior of MSE in DFELMS and DFERLS for D8PTCM4 modulation scheme over a time varying channel (CHNL2).

for the DFE in D8PTCM4 system.

Figure 5.24 shows the comparison of the transient behavior of the MSE between the DFELMS and DFERLS for the D8PTCM4 modulation scheme over the time varying channel of seed 55 (CHNL2). The MSE of the corresponding curves are calculated individually by averaging over 300 independent trials. The SNR is 12 dB, and the exponential weighting factor ρ is 0.995. It is obviously shown that the DFE with the RLS algorithm has a faster convergence speed than the DFELMS. In order to compare the learning curves of the MSE over both fixed channel and time varying channels, Figure 5.25 shows the transient behavior of MSE in DFELMS and DFERLS over a fixed channel. Figure 5.24 and Figure 5.25 are similar in that the plot of the MSE in the DFERLS converges faster than that in the DFELMS, and the values of the MSE in steady state are almost identical for both the DFELMS and DFERLS in

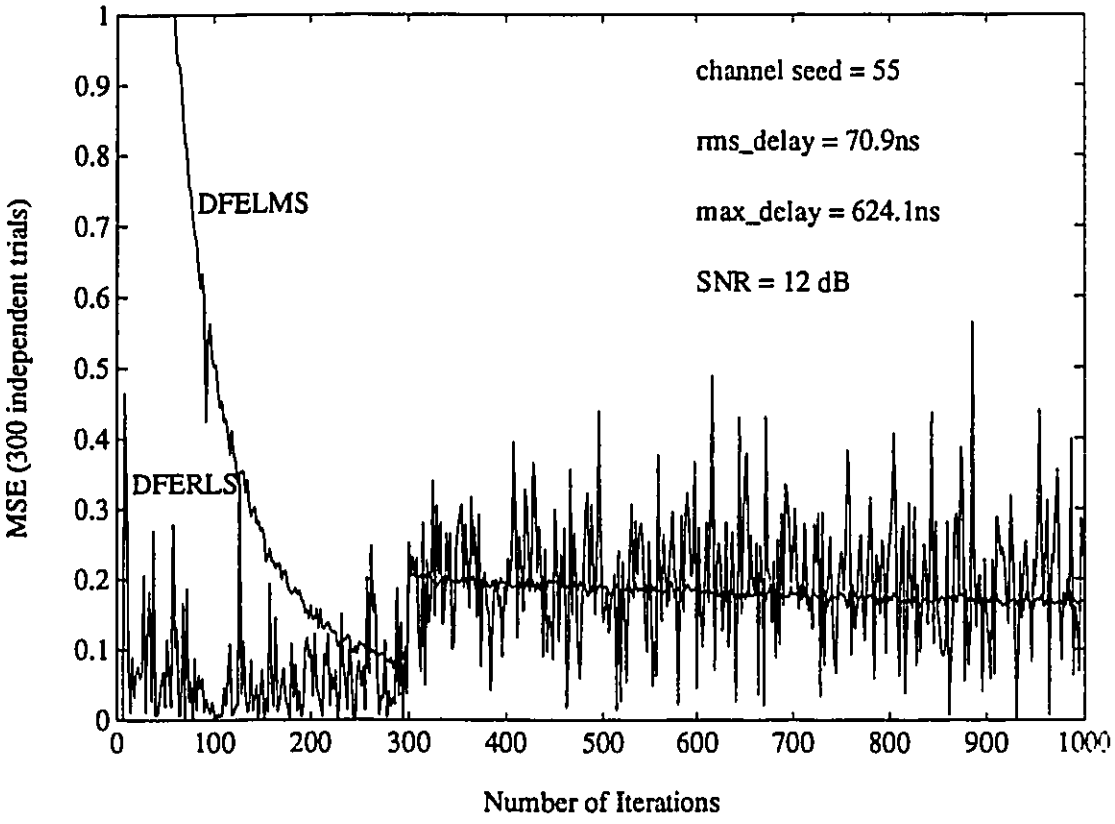

Figure 5.25: Transient behavior of MSE in DFELMS and DFERLS for D8PTCM4 modulation scheme over a fixed channel with seed 55.

each figure.

However, the plots of the MSE for the DFERLS in both figures are very noisy, even though the DFERLS plots are obtained by ensemble averaging over 300 independent trials. But the curve for the DFERLS over the fixed channel in Figure 5.25 is less noisy than that over the time varying channel in Figure 5.24. The most likely reason for this behavior is that the RLS algorithm uses time averages, but the LMS algorithm uses a statistical average. The estimates of equalizer tap weights for the RLS algorithm are updated on a sample-by-sample basis, so the value of the MSE changes throughout these estimates. The amount of change in the MSE value is based on a specific channel. It is expected that a channel with high ISI will have an MSE value that experiences greater fluctuations than the MSE value for a channel with lower ISI.

The number of training sequence bits used for both Figures 5.24 and 5.25 is 300, and thus an increase of the MSE value can clearly be seen after the training sequence has ended. Since CHNL2 is severely corrupted by ISI, both the DFELMS and DFERLS provide an inaccurate desired response that causes a large estimation error during temporary decision making in the equalizer. Thus, there is an increase in the MSE value on both curves at the 300th iteration.

5.4.3 MSE in DFELMS and DFERLS for DQPSK Modulation Scheme

In this section, we will discuss the performance (MSE) difference between DFELMS and DFERLS, when they are used with different modulation schemes (DQPSK and D8PTCM4).

Figure 5.26 gives the learning curves of MSE in DFELMS and DFERLS for the DQPSK modulation scheme over a time varying channel (CHNL2). The figure shows two clear plots of the MSE in the DFELMS and the DFERLS for the DQPSK modu-

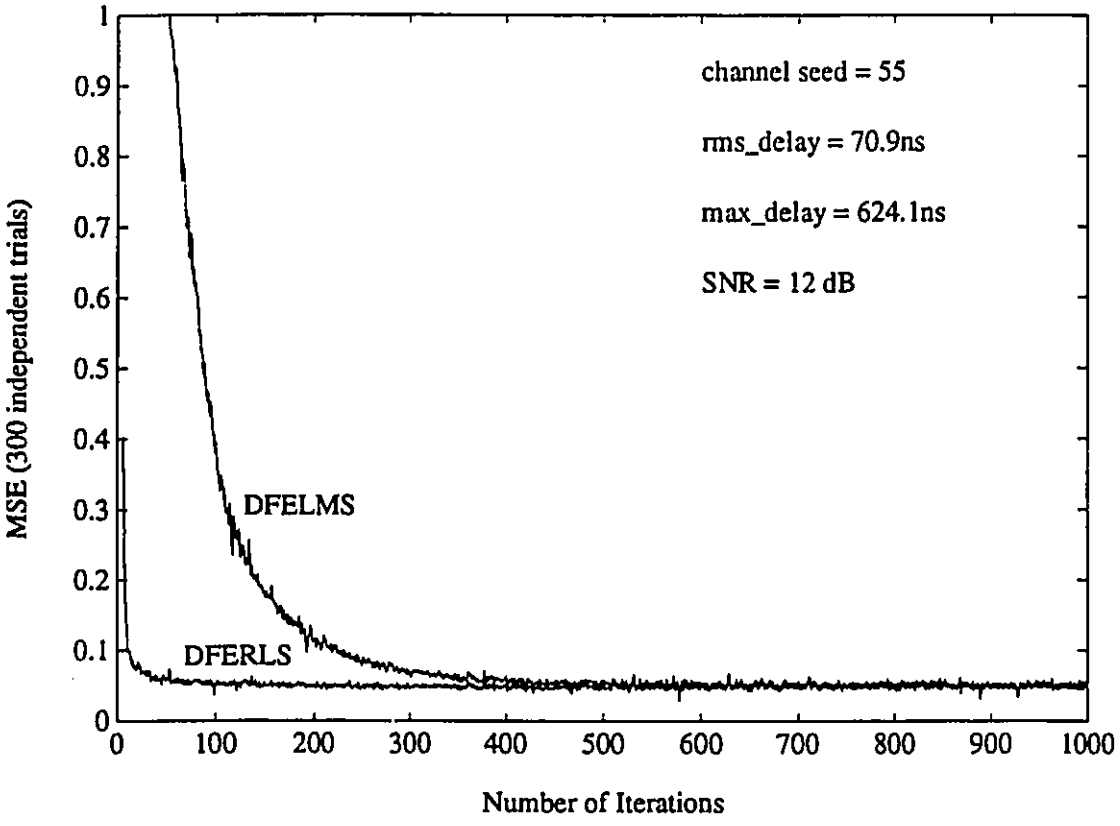

Figure 5.26: Transient behavior of MSE in DFELMS and DFERLS for DQPSK modulation scheme over a time varying channel (CHNL2).

lation scheme as compared to those for the DSPTCM4 modulation scheme shown in Figure 5.24. The MSE in the DFERLS takes no more than 50 iterations to converge to a steady state value less than 0.1, but for the DFELMS, more than 300 iterations are required to approach this value. Time constants are used to express how fast an equalizer converges. The time constant is the time required for each tap-weight of an equalizer to approach its optimum value by decaying to $1/e$ of its initial value, which is the difference between the tap-weight and its optimum value. As discussed in Section 3.1.2, the time constant for the DFELMS given in Equation 3.18 is larger than that for the DFERLS shown in Equation 3.38.

It is also shown that the MSE curves for both the DFELMS and DFERLS eventually overlap, which means that the DFERLS has almost the same tracking ability as the DFELMS over the time varying channel (CHNL2). As proven by [Ele86], for a small equalizer length, the LMS algorithm is able to provide almost the same tracking behavior as that of the RLS algorithm. A detailed discussion is provided in Section 3.1.3.

In the nonstationary case, an algorithm used for optimizing an equalizer must continuously follow (track) the time varying statistics of the input. Hence, the adaptive algorithm must pass from a transient mode of operation (convergence) to a steady state mode with permanent adjustment. [Ele86] suggests that the RLS algorithm be used for an equalizer at the beginning of the tracking process, so as to fully take advantage of the high convergence speed of the RLS algorithm. Thus, after the equalizer reaches its steady state mode, the RLS algorithm can be replaced by the LMS algorithm. In doing so, the complex computation of the RLS algorithm for the DFE can be avoided without reducing performance. For relatively short equalizers, where the LMS step size μ that guarantees similar tracking behavior does not violate the stability bound of Equation 3.42, there is no tracking advantage in using the more complex RLS algorithm.

Thus, the MSE provides as good a measure of system performance as the BER,

and it shows that a system with the DQPSK modulation scheme combined with DFERLS gives better performance than the D8PTCM4 modulation scheme combined with the same equalizer.

5.5 Conclusion

In this chapter, the simulation results for various indoor wireless communication systems were presented. Three modulation schemes (DQPSK, D8PTCM4, and D8PTCM8). two types of channels (fixed and time varying), and three equalizers (LE, FSE, and DFE) were used for the simulations. Table 5.1 summarizes the required SNR to achieve a BER of 10^{-2} for each modulation scheme with a DFE over the three time varying channels each having a different level of ISI. The effects of two equalizer opti-

Table 5.1: SNRs for BER = 10^{-2} over three time varying channels

		low ISI	medium ISI	high ISI	
seed		52	55	45	
SNR (dB)	DQPSK	4.5	6	6	BER=10^{-2}
	D8PTCM4	6.3	-	-	
	D8PTCM8	6.7	-	-	

mization algorithms (RLS and LMS) were also discussed. It was shown that the RLS algorithm exhibits slightly better tracking ability than the LMS algorithm. However, RLS involves a higher degree of complexity than LMS. For a small equalizer length, the performance of LMS approaches that of RLS.

Chapter 6

Conclusions

6.1 Summary of Thesis

In this chapter, we provide a summary of the thesis. The results of the simulations are highlighted, and some suggestions for further research are enumerated and explained.

The purpose of this thesis is to study the performance of LE, FSE, and DFE equalizers used in conjunction with DQPSK, D8PTCM4 and D8PTCM8 modulation schemes for fixed and time varying indoor wireless channels. Performance results were obtained from the output of our computer simulations. For these simulations, software modules representing each part of an indoor wireless communication system (including the channel) were developed.

In Chapter 2, two indoor wireless channel models are described, namely the fixed and time varying channel models. Since the time varying channel is the more realistic of the two models for representing indoor wireless communications, therefore, three realizations of the time varying channel, which are used in the simulations, are presented. The three channels have different levels of ISI.

Chapter 3 provides a review of LE, FSE and DFE equalizers. The least-mean-square (LMS) and the recursive least-square (RLS) algorithms, which guide the equalizers in combatting ISI, have also been described. While the RLS algorithm involves

a higher degree of complexity, it provides better performance.

In Chapter 4, a general description of the components of an indoor wireless communication system is presented. After detailing the characteristics of the shaping filters, three modulation schemes are considered: DQPSK, D8PTCM4 and D8PTCM8.

Chapter 5 presents the simulation results for the various indoor wireless communication system configurations. The simulation results show that, for a fixed channel, D8PTCM4 and D8PTCM8 with DFE perform better than DQPSK with DFE only when ISI is low. For time varying channels, DQPSK modulation with the DFE leads to better BER performances than both the D8PTCM4 and D8PTCM8 with the DFE under both mild and severe ISI conditions. The LMS algorithm provides adequate channel tracking capability, compared with the RLS algorithm, when the equalizer length is small.

6.2 Contribution

In this thesis, we present a time varying indoor wireless channel. As shown, time varying channels are better than fixed channels for comparing the tracking performance of equalizers.

While most of the research in the area of equalizer performance evaluation in indoor wireless communications has been done with fixed channels, we have used the time varying channel in our simulations to compare the adaptive linear, $T/2$ fractionally spaced, and decision feedback equalizers.

We have also presented our simulation results to evaluate the performance of two modulation schemes, namely DQPSK and D8PTCM, under the same time varying IWC conditions.

6.3 Suggestions for Further Research

The simulation results obtained for the DFE combined with the DQPSK and DSPTCM modulation schemes leave many profitable areas for continuing research. Attention should be focused on providing more accurate decoding and more reliable temporary decision making for the DFE.

In order to provide effective detection with the Viterbi algorithm for TCM, modified branch metrics for fading channels should be used instead of minimum metrics that are optimal only for the AWGN channel. Modifying branch metrics is achieved by a Viterbi decoder operating on both the combined ISI and code trellis. Then the metric that takes into account the ISI due to past symbols is minimized. In [Chev89], this method is incorporated into the maximum likelihood estimation. Similar research has been conducted [Eyu88] to simplify the Viterbi algorithm by modifying branch metrics with reduced state sequence estimation.

To efficiently improve DFE performance over indoor wireless channels, temporary decisions made in the DFE, which are used to adjust the DFE's tap weights, have to be made more accurately. Similar work has been done [Eyu88] by using decision feedback noise prediction with interleaving.

Lastly, diversity can also be considered a good research subject. Diversity is used to provide the DFE with a better signal that has less deep fades. In [Char92], space diversity is introduced as a compound strategy by combining it with coding and equalization, to eliminate dispersive fading, ISI, and co-channel interference.

Bibliography

[Abend70] K. Abend, B. D. Fritchman, "Statistical detection for communication channels with intersymbol interference," *Proceedings of the IEEE*, pp. 779-785, May 1970.

[Aus67] M. E. Austin, "Decision-feedback equalization for digital communication over dispersive channels," *MIT Lincoln Laboratory, Lexington, Mass. Technology Report*, No. 437. August 1967.

[Big91] E. Biglieri, D. Divsalar, P. J. McLane M. K. Simon, *Introduction to Trellis-Coded Modulation with Applications*, New York, Macmillan Publishing Company, 1991.

[Bult87] R. J. C. Bultitude, "Measurement, characterization and modeling of indoor 800/900 MHz radio channels for digital communications," *IEEE Communication Magazine*, Vol. 25, No. 6, pp. 5-12, June 1987.

[Chen94] X. Chen, J. Y. Chouinard "Adaptive Equalization of Frequency Selective Indoor Wireless Communication Channels," *1994 Canadian Conference on Electrical and Computer Engineering*, September 1994.

[Chen91] S. Chennakeshu, G.J.Saulnier, "Differential detection of $\pi/4$-shifted-DQPSK for digital cellular radio," *Proceedings of the IEEE Vehicular Technology Conference*, pp. 186-191, July 1991.

[Chev89] P. R. Chevillat, E. Eleftheriou, "Decoding of trellis-encoded signals in the presence of intersymbol interference and noise," *IEEE Transactions on Communications*, Vol. COM-37, pp. 669-676, July 1989.

[Cox72] D. C. Cox "Delay doppler characteristics of multipath propagation at 910 MHz in a suburban mobile radio enviroment," *IEEE Transactions on Antennas Propagation*, Vol. AP-20, pp. 625-635, Sept. 1972.

[Cox75] D. C. Cox, R. P. Leck, "Correlation bandwidth and delay spread multipath propagation statistics for 910-MHz urban mobile radio channels," *IEEE Transactions on Communications*, Vol. COM-23, pp. 1271-1780, Nov. 1975.

[Char92] C. L. B. Despins, D. D. Falconer, S. A. Mahmoud "Compound strategies of coding, equalization, and space diversity for wide-band TDMA indoor wireless channels" *IEEE Transactions on Vehicular Technology*, Vol. 41, No. 4, pp. 369-379, November 1992.

[Duel89] A. Duel-Hallen, C. Heegard "Delayed decision-feedback sequence estimation" *IEEE Transactions on Communications*, Vol. 37, No. 5, pp. 428-436, May 1989.

[Ele86] E. Eleftheriou, D. D. Falconer, "Tracking properties and steady-state performance of RLS adaptive filter algorithms," *IEEE Transactions on Acoustics, Speech, and Signal Processing*, Vol. ASSP-34, No. 5, October 1986.

[Eyu88] V. M. Eyuboglu "Detection of coded modulation signals on linear, severely distorted channels using decision-feedback noise prediction with interleaving" *IEEE Transactions on Communications*, Vol. 36, No. 4, pp. 401-409, April 1988.

[Eyu88] V. M. Eyuboglu, S. U. Quereshi "Reduced-state sequence estimation with decision feedback and set partitioning," *IEEE Transactions on Communications*, Vol. 36, No. 1, pp. 13-20, January 1988.

[For73] G. D. Forney, Jr., "The Viterbi algorithm", *Proceedings of the IEEE*. Vol. 61, No. 3, pp. 268-278, March 1973.

[Fri82] B. Friedlander, "Lattice filters for adaptive processing," *Proceedings of the IEEE*, Vol. 70, pp. 829-867, August 1982.

[Git81] R. D. Gitlin, S. B. Weinstein, "Fractionally-spaced equalization: an improved digital transversal equalizer", *The Bell System Technical Journal*, Vol. 60, No. 2, pp. 275-296, February 1981.

[Good91] D. J. Goodman "Second generation wireless information networks," *IEEE Transactions on Vehicular Technology*, Vol. 40, No. 2, May 1991, pp. 366-374.

[Ha90] T. T. Ha, *Digital Satellite Communications*, Second Edition, McGraw-Hill communications series, 1990.

[Hay91] S. Haykin, *Adaptive Filter Theory*, Second Edition, Prentice-Hall, Englewood Cliffs, 1991.

[Jakes74] W. C. Jakes, Ed., *Microwave Mobile Communications*, New York: Wiley, 1974.

[Jer92] M. C. Jeruchim, P. Balaban, K. S. Shanmugan, *Simulation of Communication Systems*, Plenum Press, New York, 1992.

[Lin83] S. Lin, D. J. Costello, *Error Control Coding Fundamentals and Applications*, Prentice-Hall, Englewood Cliffs, 1983.

[Lju85] S. Ljung, L. Ljung, "Error propagation properties of recursive least-squares adaptation algorithms," *Automatica*, Vol. 21, No. 2, pp. 157-167, 1985.

[Mon70] P. Monsen, "Linear equalization for digital transmission over noisy dispersive channels," *Eng. Sc.D. thesis*, Columbia University, New York, N. Y., June 1970,

[Mon71] P. Monsen, "Feedback equalization for fading dispersive channels," *IEEE Transactions on Information Theory*, Vol. IT-17, pp. 56-64, January 1971.

[Mon74] P. Monsen, "Adaptive equalization of the slow fading channel," *IEEE Transactions on Communications*, Vol. COM-22, No. 8, pp. 1064-1075, August 1974.

[Pai91] R. V. Paiement, J. Y. Chouinard, "Simulated application of trellis coded modulation to the the indoor wireless channel," *41st IEEE Vehicular Technology Conference*. pp. 216-221, St-Louis, Missouri, May 19-22, 1991.

[Proak89] J. G. Proakis, *Digital Communications*, Second Edition, New York: McGraw-Hill, 1989.

[Proak91] J. G. Proakis, "Adaptive equalization for TDMA digital mobile radio," *IEEE Transactions on Vehicular Technology*, Vol. 40, No. 2, pp. 333-341, May 1991.

[Qur77] S. U. H. Qureshi, G. D. Forney, Jr, "Performance and properties of a $T/2$ Equalizer," *Conference Record, NTC 1977*, pp. December 1977.

[Sal87(1)] A. A. M. Saleh, A. J. Rustako, JR., R. S. Roman, "Distributed antennas for indoor radio communications," *IEEE Transactions on Commununications*, Vol. COM-35, pp. 1245-1251, Dec. 1987.

[Sal87(2)] A. A. M. Saleh, R. A. Valenzuela, "A statistical model for indoor multipath propagation," *IEEE Journal on Selected Areas in Communications*, Vol. Sac-5, No. 2, pp. 128-137, Feb. 1987.

[Ung72] G. Ungerboeck, "Theory on the speed of convergence in adaptive equalizers for digital communication," *IBM J. Res. Dev.*, Vol. 16, pp. 546-555, 1972.

[Ung82] G. Ungerboeck, "Channel coding with multilevel/phase signals," *IEEE Transactions on Information Theory*, Vol. IT-28, No. 1, pp. 55-67, January 1982.

[Verm74] F. L. Vermeulen, M. E. Hellman "Reduced state Viterbi decoders for channels with intersymbol Interference," *Proceeding of 1974 IEEE International Conf. Commun.*, pp. 37B-1-37B-4.

[Wid60] B. Widrow, M. E. Hoff, JR., "Adaptive switching circuits," *IRE WESCON Conv. Rec.*, PT. 4, pp. 96-104, 1960.

[Wid71] B. Widrow, "Adaptive filters," in *Aspects of Network and System Theory*, R. E. Kalman and N. DeClaris, Eds. New York: Holt, Rinehart, and Winston, pp. 563-587, 1971.

[Wid76] B. Widrow, J. M. McCool, M. G. Larimore, C. R. Johnson, "Stationary and nonstationary learning characteristics of the LMS adaptive filter," *Proceeding IEEE*, pp. 1151-1162, August, 1976.

[Zeh92] E. Zehavi, "8-PSK trellis codes for a Rayleigh channel," *IEEE Transactions on Communications*, Vol. 40, No. 5, pp. 873-884, May 1992.

[Zig92] A. Zigic, R. Prasad, "Bit error rate of decision feedback equalizer for indoor wireless communications," *Electronics Letters*, Vol. 28, No. 21, 1992.

[Zhou90] K. Zhou, J. G. Proakis, F. Y. Ling, "Decision-feedback equalization of time dispersive channels with coded modulation," *IEEE Transactions on Communications*, Vol. 38, No. 1, pp. 18-24, January 1990.